European Commission

technical steel research

Reduction of iron ores

Reductions in dust and gaseous emissions from sinter strands

A. M. W. Briggs

Corus UK

Swinden Technology Centre, Moorgate, Rotherham S60 3AR, United Kingdom

F. Garcia Carcedo

CENIM

Avda. Gregorio del Amo 8, E-28040 Madrid

J. Vega Sedeño

CSI-Planos

Apartado 93, E-33480 Aviles

M. A. Estrela

ISQ

Estrada Nacional 249 — Km 3, Cabanas, Leião (Taguspark), P-2781 Oeiras

7210-AA/824, 942, 943, 944

1 October 1996 to 31 March 2001

Final report

Directorate-General for Research

2004

EUR 21146 EN

Europe Direct is a service to help you find answers to your questions about the European Union

Freephone number:

00 800 6 7 8 9 10 11

A great deal of additional information on the European Union is available on the Internet. It can be accessed through the Europa server (http://europa.eu.int).

Cataloguing data can be found at the end of this publication.

Luxembourg: Office for Official Publications of the European Communities, 2004

ISBN 92-894-8110-2

Printed in Belgium

PRINTED ON WHITE CHLORINE-FREE PAPER

ABSTRACT

The production of sinter is economically important for the integrated steelmaking route, and sinter plants also serve an environmentally useful function in allowing the convenient reprocessing of revert materials. However, sinter plant main stacks typically account for up to 30% of the mass of airborne pollutants from an integrated steelworks, largely because emissions are continuous and are associated with very large gas flows. Sintering operations are therefore the focus of considerable interest and effort in attempts to improve environmental performance, and are subject to environmental pressures for improved abatement of pollutants, both internationally and from national permitting authorities.

Throughout Europe, sinter plant main stack emissions are controlled mainly by electrostatic precipitators. Typically these clean particulate material to around 100 mg/m^3, and exceptionally to levels as low as 30 mg/m^3. A step change is needed to achieve lower particulate emission levels and to mitigate other pollutants such as heavy metals and trace organic species. Best Available Techniques are currently centred on very expensive wet scrubbing technology or the use of bag filters.

Although bag filters can provide enhanced dust removal, generally to levels of 10-20 mg/m^3, and are suitable for the use of additives for control of other pollutants, they have drawbacks in terms of temperature performance and susceptibility to damage from moisture, sticky hydrocarbon components and abrasive particles. The problems are attributable to the properties of fabrics available at reasonable cost.

A new technology, the KN Filter, offers the possibility of bag filter performance whilst avoiding the problems of fabrics. This device operates in a similar manner to the pulse jet bag filter but employs metallic filter screens of relatively coarse mesh, with apertures many times the size of the dust particles to be filtered. A cake can be built on this mesh from the particulate contaminants themselves, and this cake then acts as the filtration medium. The robust screens can be vigorously cleaned, have a long life, and are far less subject to the problems which can affect fabric media.

In this project a specially designed KN Filter has been tested at small pilot scale (~1 m^3/s flow) in industrial conditions. The device was a 4 chamber unit, with 3 chambers filtering at any particular time. Filter screens were of 316 grade stainless steel mesh.

Initial tests on the direct (or 4th hole) extraction duct of an electric arc furnace confirmed the ability to give good filtration performance with very fine particles (largely sub-micron). Outlet dust concentration was ~10 mg/m^3 stp during periods of intense furnace activity, and as low as 3 mg/m^3 stp over a full operating cycle. Inlet dust loading averaged 8 g/m^3 stp, so filtration efficiency was about 99.9%. Inlet gas temperatures of up to 270°C were accommodated, and substantially higher temperatures should not be problematic. Filtration velocity at 1.4 m/min and the pressure drop of 16 - 22 mbar were not dissimilar to the values encountered on fabric filters in EAF applications.

Subsequent tests were performed on a side stream of the wind main of an operating sinter strand at the Scunthorpe Works of Corus UK. Following resolution of some problems with

the valves which direct gas either to the filter outlet or to the recirculation duct for cake building in the off-line chamber, filtration performance was good. For inlet dust loadings of 0.5 - 1 g/m^3 stp, the outlet concentration was generally 5 - 6 mg/m^3 stp. Filter pressure drop was 15 mbar, again similar to that expected for a fabric filter. The filtration velocity, at 2.3 m/min, was superior to that which would normally be chosen for a fabric filter in this application.

Concurrent work in Spain, using a much smaller test unit inserted in sinter pot equipment, gave little extra information, as it proved difficult to present simulated industrial gas conditions to the test filter. Later tests with the same small filter on an industrial sinter stand suffered from condensation problems due to excessive heat loss, but succeeded in demonstrating some filtration in adverse conditions.

The pilot filter operated without difficulty during a cold start of the sinter strand. Although considerable condensation of water was evident, the screens did not become blocked and cake built at a normal rate. These conditions would have been expected to cause severe difficulties with fabric bags.

Analysis of the dust collected in the hoppers and from the filter screens indicated that smaller particles, relatively rich in alkali chlorides, lead, zinc, and sulphur compounds, predominated on the screens. The larger particles, more typical of sinter bed material and so well-suited to recycling, tended to settle out of the gas stream before the screens. A combination of a cyclone or settling chamber and a KN Filter may therefore offer an effective combination, allowing segregation of less desirable components for separate treatment or disposal.

The enhanced filtration performance when compared with an electrostatic precipitator also led to improved capture of heavy metals. Measured outlet concentrations were ¼ of those in the main stack after the precipitator. A reduction of 95% in the small quantities of radioactive species which normally pass to the stack from the feedstock was also achieved.

Tests in which steam activated carbon and lignite coke powders were injected into the inlet manifold illustrated the potential for enhanced abatement of emissions of trace organic micropollutants. Although the effect of dosing rate was not established, injection rates of these powders in the range 50 - 250 mg/m^3 stp of inlet gas were associated with outlet concentrations of polychlorinated dibenzo-p-dioxins and polychlorinated dibenzofurans (PCDD/F) of 0.1 - 0.2 ng I-TEQ/m^3 stp, compared with a typical level in the main stack of 1 ng I-TEQ/m^3 stp. Emissions of polycyclic aromatic hydrocarbons (PAH) were reduced by about 75%, and of polychlorinated biphenyls (PCB) by about a half.

Samples of candidate mesh materials (grades of stainless steel) exposed to wind main conditions for a year showed little evidence of corrosive attack.

A basic design for a full scale unit has been provided. Capital costs are similar to those expected for a fabric filter. Operating costs should be less in view of the potential life of the filter elements, but this might be offset by the running cost of the recirculation fans.

The potential of the filtration device has therefore been demonstrated when applied to raw wind main gas. The question remains as to whether it is suitable for operation in series with an electrostatic precipitator (as might be the case in a retrofit application) where the inlet dust characteristics would be different. Although there is little doubt that cake building can be accomplished, it would be necessary to test whether acceptable pressure drop at reasonable filtration velocity can be achieved.

CONTENTS

LIST OF TABLES

LIST OF FIGURES

27. SEM Image of Outlet Dust

28. SEM Image of Outlet Dust

29. EDA Spectrum of 4 μm Particle

30. EDA Spectrum of 12 μm Particle

31. EDA Spectrum of 20 μm Particle

32. Dust Sampling Positions and Carbon Injection Point

33. Corrosion Test Coupons

34. 304 Stainless Steel Mesh Coupon After 6 Months Exposure

35. 316 Stainless Steel Mesh Coupon After 6 Months Exposure

36. Side Elevations of Large Scale Plant

37. Plan of Large Scale Plant

38. Isometric Impression of Large Scale Plant

39. Underside View of Large Scale Plant

40. End View of Large Scale Plant

FINAL TECHNICAL REPORT

1. INTRODUCTION

Sinter plant main stacks typically account for up to 30% of the mass of airborne pollutants from an integrated steelworks, largely because emissions are continuous and are associated with very high gas flows. They are therefore a focus of considerable interest and effort in attempts to improve environmental performance. The environmental background to the project, applicable at the start in 1996, is outlined in Appendix 1. Legislative moves to reduce sinter plant emissions, previous work on improved measures for the abatement of emissions, and specified Achievable Release Levels are summarised. It is concluded that alternative economic technologies should still be sought to meet these release levels.

Since then, the European Commission instigated the production of a series of Best Available Techniques (BAT) Reference Documents (BREFs) through the Directorate General Joint Research Centre. One of these relates to the production of iron and steel[1]. This lists techniques to be considered in the determination of BAT for abatement of releases from sinter plants. The extract given in Appendix 2 summarises BAT for the gaseous and particulate emissions relevant to this project. It can be seen that a number of techniques are specified, most importantly those based on expensive wet scrubbing systems or fabric filtration (especially where low dust emission is required).

National Governments are embodying the information in the BREF into legislation for Integrated Pollution Prevention and Control (IPPC) and associated guidance. As an example, in the UK draft guidance for IPPC[2], the benchmark release level of particulate material from sinter plant main stacks is given as < 10 mg/m^3 (annual average) on the basis of a bag filter. Similarly, for dioxin and furan compounds (PCDD/F) a benchmark release level of 0.1 - 0.5 ng I-TEQ/m^3 stp is given, based on a bag filter with injection of a sorbent such as lignite coke powder.

Very low dust emissions such as these cannot reliably be achieved by electrostatic precipitators (ESPs), and these devices are less suited to the injection of sorbents than bag filters. Bag filters, however, have some drawbacks when applied to sintering off-gas.

- The gas temperature is usually higher than the 120 - 130°C tolerated by economic polyester-based fabrics.
- The high water vapour levels cause hydrolysis of polyester at normal sintering off - gas temperatures, and condensation (e.g. during start up from cold) can cause wetting of the bags.
- The dust contains hard, angular, abrasive particles which can damage the bags in time.
- Sticky components arising from hydrocarbons in the off-gas can cause blinding of the bags.

All these drawbacks are attributable to the properties of fabrics available at reasonable cost.

The KN Filter, as developed on a relatively small scale by AFI Ltd. (now defunct) and now marketed by Parftec Ltd., uses metallic filter screens on which the cake built from the contaminants themselves acts as the filtration medium. The robust screens are far less subject to the problems listed above which can adversely affect fabric media. The advent of the technology offered the steel industry an opportunity to compare the performance of such filters with the conventional ESP, with a view to reducing sinter plant emissions.

In this project, Corus UK Ltd. provided a test site for a small pilot scale filter. CENIM and Aceralia (formerly CSI Planos) in Spain and ISQ (Portugal) provided analytical support, tests involving a smaller unit and some determinations of relevant operational data on Spanish plants. Some theoretical work on possible design improvements was also carried out by the Iberian partners.

2. OBJECTIVES

The primary objective of this ECSC Research Project was to evaluate the applicability of the KN metallic mesh filter for use on sinter plant wind main gas.

The chief subsidiary objectives were to evaluate:

- the operational characteristics of the filter;
- the potential to introduce sorbents upstream of the filter for gas cleaning purposes;
- the potential for installing a full scale KN Filter to replace or complement an electrostatic precipitator.

It was also intended to consider characteristics of dust and gaseous emissions from British and Spanish sinter plants, with a view to judging the applicability of the technology to a range of off-gas conditions.

If the technology could be made to work effectively it could provide a future option for a cost-effective technique, based on the well proven principles of a pulse jet filter (and with similar performance) for improved environmental performance of sintering operations. This would help maintain the viability of sintering operations which make an important contribution to the economy of integrated steelmaking whilst offering a route for recycling revert materials.

3. FILTER CONCEPT

3.1 Rationale and Early Design

Note: In this and subsequent Sections the term 'filtration velocity' is used. This parameter (also known as air:cloth ratio for fabric filters) is the filter flow (m^3/min) divided by the surface area available for filtration (m^2), giving a mean velocity (m/min) for the gas stream at the filtration surface. It is important in that it represents the flow per unit filtration area, which is the major factor in determining the size of filter required for a given application. For a given filtration medium the value of filtration velocity will vary with the nature of the dust, and the frequency of cleaning.

Conventional bag filters employ a sufficiently fine fabric medium so that gas-borne particles can be filtered from the flow stream by the clean bags. Filtration efficiency tends to be reduced until a cake of the particles has built up, which then acts as a superior filter. The cake is removed when its thickness dictates that the pressure drop has become too great, and the building process is repeated. The filtration efficiency varies during the process of cleaning and establishing a cake. Strategies to increase efficiency include the use of heavier and finer fabrics (increasing operating costs) and reduced filtration velocities (increasing required filter area and hence capital costs).

If a full cake of the contaminant alone could be used as its own filter during the whole of the filtration cycle, the problems would be greatly reduced or eliminated. Experiments by the suppliers had shown that it is readily possible to build a cake on a mesh with apertures many times the size of the particles in the gas stream. Indeed, within quite wide limits, the mesh size simply changed the time required to build a complete cake. The filtration efficiency of the cake is self-adjusting to its own particle size range. Fine particles build fine filter cake and coarse particles build a more open filter cake.

The KN Filter employs two stages. In one stage a filter cake is built up on a metal mesh screen (although other materials such as plastic meshes are possible), whilst in the other an established cake performs the filtration. The thickness of the cake, and hence filtration efficiency, can be selected by choosing an appropriate pressure drop.

The first embodiment of the concept employed a two chamber configuration to allow off-line cake build up in one chamber whist simultaneously filtering in the other.

The process is illustrated schematically in Fig. 1. In Fig. 1(a), the contaminated gas stream enters Filter A which is in cake building mode. The largest particles are trapped first on the relatively coarse metal screen, and progressively finer particles are then trapped on and between the coarser particles. Until the cake is fully established on the screens in Filter A, some of the finer dust will pass through and enter with the gas into Filter B, where it is filtered by the established cake. The desired filtration efficiency through Filter A is reached when a sufficient cake has accumulated on the screen, at which time the gas can exit directly from Filter A. Chamber B is then taken off line for cleaning (Fig. 1(b)). After cleaning (generally by a pulse of compressed air) Filter B is switched on stream ahead of Filter A (Fig. 1(c)), and cake building progresses whilst Chamber A performs the bulk of the filtration, until the cake is fully formed in Filter B and Filter A can be cleaned (Fig. 1(d)). This cycle continues sequentially.

Filter screens are generally of stainless steel, allowing high temperature operation (up to 600°C in present designs) and more vigorous cleaning than in fabric filters. Moist gases can be handled without fear of fabric blinding, as can sticky particulate materials. The screens can last indefinitely, unlike fabric bags. A typical filter screen is shown in Fig. 2 where the use of a coarse mesh cylinder supporting the finer mesh filtration screen can be seen.

Although the filter applications to date have served small plants (e.g. foundries), the design lends itself to modular construction so that high volume applications are feasible.

3.2 New Design Employed for this Project

The two chamber design had been shown to be effective but there were some drawbacks. When switching between series operations (cake building plus filtering) to single chamber operation (filtering only) there is a rapid change in resistance to flow which can in some cases cause a shock to the cake, leading to partial removal and/or short term bleed-through

of dust. Also it was recognised that the need to provide two chambers for filtration by only one chamber (i.e. 50% utilisation of filtration area) had implications for size and cost.

A new design was therefore developed to improve economy and smoothness of operation.

The principles of operation are similar to those for the original two chamber design but the design incorporates four chambers, three of which are on-line at any particular time, thus maximising available filter area. Another important change is the incorporation of a recirculating fan which pulls filter inlet gas through the off-line chamber, and returns this chamber's outlet to the filter inlet manifold. This allows cake build-up in the off-line chamber to be accomplished with simpler valve arrangements than in the earlier design. The arrangement is illustrated in Fig. 3 and the operation is described in Fig. 4.

A novel (and experimental) feature of the design was the use of air curtain sealing in the diverter valves which direct the filtered gas either to the filter outlet or to the recirculation circuit. A sketch of a section through one of these valves is shown in Fig. 5. Air is inspired by the normal system suction through the hollow valve shafts. This is distributed to slots around the edges of the valve blade, producing a curtain which opposes fume transfer across the blade to housing gap. A proportion of the air also feeds into the gap between the valve shaft and its mounting tube, serving a similar function. This arrangement was designed to give a non-contact seal which, in the absence of touching surfaces, should eliminate wear.

4. INITIAL RESEARCH ACTIVITIES

Early work was aimed at characterising the dusts from a number of sinter plants as an aid to filter design. Although it subsequently transpired that the filter appears insensitive to variations in dust loading, type and chemistry, these results are incorporated into this report for reference as they may be of interest in other studies relating to sinter plant operation and the recycling of materials. Some results were also relevant when considering how the collected dust might be treated when more undesirable components are present, as would be the case with improved collection in a filter.

It had been agreed that the Scunthorpe sinter plant of Corus UK would host the experimental unit. Measurements were therefore made of off-gas parameters to enable design of the offtake and return from the wind main to and from the filter, and sizing and siting of the filter etc. Some measurements were also made in the wind main of the Veriña G-7 sinter strand at Gijon, to confirm that a filter design for conditions at Scunthorpe would be applicable elsewhere.

4.1 Characterisation of Dusts

The results of chemical, microstructural and granulometric analysis for the Spanish ESP dust are given in Appendix 3, including the outcome of some water washing tests, heating tests and magnetic separation tests.

In the washed samples, as might be expected, sodium and potassium compounds were reduced substantially, indicating a possible way of improving properties for recycling the dust, particularly as the proportion of alkali chlorides in dust emitted from ESPs is high. However, such treatment may be undesirable as it produces its own disposal/treatment issues.

Heat treatment had little effect on the dust until, at temperatures over 800°C, S, Na and K compounds began to volatilise with increasing temperature. Simply recycling these compounds (which would be expected to be captured more effectively by improved filtration) via the sinter feed would therefore lead to increasing concentration. Further comments on this effect are made in Section 7.8.

Magnetic separation had little effect other than to segregate some CaO, C and SiO_2 into the non-magnetic fraction, so there would be little benefit from such a technique.

The results of microstructural, physical and chemical characterisation of ESP dusts from two Corus plants, plus a further sample from Spain (as carried out by analysts at CENIM) are given for archival purposes in Appendix 4.

The composition of dusts from the KN Filter is discussed in Section 7.8

4.2 Industrial Off-Gas Conditions

ESP entry box measurements made at the Corus sinter plant at Scunthorpe are summarised in Table 1, and concurrent information on particle size distribution as measured using an Andersen cascade impactor is given in Figs. 6 and 7. The gas velocity at the precipitator inlet of about 8 m/s, when translated to the 4.6 m diameter off-gas main, is equivalent to 12 m/s. The sampling offtake for the pilot filter was sized, in relation to the design flow, to give a similar velocity so that approximately isokinetic conditions should apply during filter operation. The results also indicated that the filter design should accommodate inlet dust concentrations of ½ to 1 g/m^3 stp, with around 10-15% of the dust as PM_{10} and below.

Note: stp (standard temperature and pressure) is defined as 237K and 1013.25 mbar.

Initial attempts by ISQ to measure dust concentrations in the wind main on the M5 sinter strand at Aviles were unsuccessful owing to an inability to provide sufficient sampling suction to generate isokinetic conditions. NO_x was measured at 157 mg/m^3 and SO_2 at 228 mg/m^3 (uncorrected to a specific oxygen level).

Later measurements on the Veriña G-7 strand at Gijon gave somewhat lower dust concentrations, but sufficiently similar so that design would not be affected. These results, together with values for SO_2 and NO_x are given in Table 2. Off-gas flow on this strand was about 65 m^3/s stp compared with about 95 m^3/s stp at Scunthorpe.

5. MESH TEST UNIT

At the start of the project, a major objective of the Iberian partners was to adapt a sinter box facility to test a variety of metal mesh filtration screens in order to establish optimum mesh characteristics, filtration velocities and pulse cleaning parameters, and to allow some evaluation of any corrosive attack on the screens. This work encountered many setbacks, and only limited information was generated. Because the main test filter operated successfully without undue sensitivity to dust characteristics and mesh parameters, achievement of the major objectives was not compromised. This section summarises the experimental work in Spain. A somewhat more comprehensive chronological description is given in Appendix 5. To avoid unnecessary duplication, in the following description references to figures are to those in Appendix 5.

An initial series of off-gas tests on the sinter pot facilities at CSI (Aviles) and CENIM (Madrid) gave indications that an appropriate range of dust concentrations might be generated, either by normal sinter box operation (for low concentrations) or with additional injection of ESP dust (for higher concentrations) for simulation of industrial conditions. It was realised that hot tests would have to be of limited duration.

A small test filter was therefore designed (Fig. A.5.1), with the aid of Parftec Ltd., housing 2 screen cylinders. This was subsequently constructed and incorporated into the sinter box facility as shown in Fig. A5.2. Sets of screens of 100, 130 and 170 mesh were provided. A Macawber injector was also incorporated to add ESP dust, and PCME tribological dust monitors were added to the instrumentation for continuous monitoring of dust concentration. Photographs of the equipment are shown in Fig. A5.3.

Initial cold tests with this equipment in the sinter box facility at Aceralia (Aviles), succeeded in establishing a cake on the screens after some difficulties. However, dust emissions from the stack were a problem, as was dust drop-out in the test unit and feed pipes. A series of equipment modifications was therefore undertaken, including improved access and viewing arrangements.

Because of Company restructuring, the Aceralia pilot sintering facility at Aviles was moved to Gijon. In order to allow tests to continue the mesh test unit and peripherals were transferred to the CENIM laboratory in Madrid. Here, electrical power failure led to damage to several items of equipment, including some of the required instrumentation. Subsequent to repairs, the experimental facility was modified in an attempt to allow long term tests at realistic industrial dust loadings by the addition of a flow splitter after the Macawber injector outlet, and a dust recycling filter (Fig. A5.4).

In the following tests, although it was possible to form a filter cake using precipitator dust injected by the Macawber feeder, attempts to operate the unit were obstructed by excessive dust deposition in the flow circuit, leading to the presentation of a variable dust concentration to the filter. At this stage Aceralia expressed an interest in a configuration in which a conventional precipitator is followed by a metallic mesh filter, which it was believed would give a very clean output gas. It was decided therefore to attempt to simulate this configuration. This required lower dust injection rates than those achievable by the Macawber injector. Accordingly, a low rate feeder was constructed (Fig. A5.5).

A number of tests subsequently failed to achieve a filter cake, even in tests of 4 h duration, and again, deposition of dust in the various parts of the gas circuit and filter housing was a problem. The failure to build a cake was ascribed to the unsteady nature of the dust feeding.

These deposition problems prompted the design of a cyclone pre-separator, and as the methodology is applicable at larger scale the calculations are reproduced in Appendix 9. However, since in this case elimination of the deposited dust would not help cake formation, the unit was not built.

A study was also made on the possibility of enhancing particle capture by creating an electric charge difference between the particles and the filter screens. It was concluded that considerable experimental work would be needed (with no guarantee of success). Also, the main pilot filter appeared to work adequately without this. As such enhancements remain a future option, the main findings of the study are summarised in Appendix 10.

As a result of the difficulties encountered during many attempts to produce consistent and reproducible operation, it had become apparent that the simulation of industrial off-gas conditions in a sinter pot facility is almost impossible, especially as the time required to cycle the filter screens was longer than a typical sintering test run. Also, the implementation of cold tests was problematic since the configuration of the flow circuit using the sinter pot equipment was far from ideal for the carriage of consistent dust concentrations. Application of the mesh test unit to an industrial sinter plant, where it might readily be tested both before and after the electrostatic precipitator, with consistent flows of real off-gas, appeared to offer the best possibility of meaningful results.

Accordingly, with agreement from Aceralia, the mesh test unit was transferred to the Gijon B sinter plant wind main at a late stage in the project. The unit was positioned about 1/3 of the length from the discharge end. Figures A5.6 and A5.7 illustrate the siting and arrangement. This position was chosen largely because access to the wind main was possible, but had the potential advantage of allowing tests at relatively high temperatures which might obviate problems of condensation due to the considerable heat losses expected from a small unit of large surface:volume ratio.

The filter was provided with instrumentation to measure temperature, gas flow and pressure drop, and the tribological dust monitors were fitted in the inlet and outlet.

A series of tests was carried out at a flow of approximately 16 m^3/min, corresponding to a velocity in the connecting pipework of about 15 m/s (presumably chosen to minimise dust drop-out). This is equivalent, for the filter sleeve area of 1.43 m^2, to a filtration velocity of 11 m/min, which is much higher than that employed on the pilot filter at Scunthorpe (2.3 m/min).

Although the filter siting was towards the hot end of the wind main, the heat loss from the ducting (which had to be 10 m long) was such that filter inlet temperatures were typically only 50 - 75°C. This led to considerable condensation problems, as did the water in the compressed air used for pulse cleaning which could not be eliminated by the dryer before the air receiver. However, some results of interest were obtained. Despite the high filtration velocity, the filter pressure drop traces, an example of which is given in Fig. A5.8, indicate cake formation. The build up to 25 mbar pressure drop, compared with 12-15 mbar on the filter at Scunthorpe, is again a consequence of the high filtration velocity. The concurrent dust monitor readings suggested about 95% filtration efficiency. Whilst this is not adequate for emission control, it is surprisingly good considering the high filtration velocity. There appeared to be no difference in the performance of the different screens.

It can be concluded, therefore, that cake building and filtration take place even at filtration velocities 5 times higher than might normally be used and with considerable free moisture in the gas stream. Conventional fabrics would almost certainly have become unusable in these circumstances.

6. CONSTRUCTION AND INITIAL TESTING OF THE PILOT FILTER

6.1 Construction

The filter construction was based on the 4 chamber design shown in Fig. 3 (note that the actual filter was a mirror image of this drawing). Each chamber houses eight filter tubes. Six of these are 1.8 m long, which has proved to be a length readily cleanable in other applications. The remaining two tubes are 50% longer. If these were to prove cleanable there would be important implications for any full scale designs since filter size and footprint

could be smaller. The design, based on the off-gas data and the constraints of the intended site, can be summarised as follows.

Overall size (W x D x H): 3.0 x 1.25 x 5.5 m

Main fan: paddle blade type; design duty 1.5 m^3/s, 3 kPa, at gas density of 0.507 kg/m^3

motor rating 15 kW

Recirculating fan: motor rating 4 kW

Filter elements: 0.19 m dia.; 8 per chamber, of which 6 x 1.83 m long and 2 x 2.74 m long (experimental length), each element supported by a heavier gauge mesh cylinder.

Mesh size: screen support 10 mesh (aperture size 1.6 mm), filtration screens 130 mesh (aperture size 0.112 mm, 34% open area)

Filtration area: 39.3 m^2 (4 compartments)
29.5 m^2 (3 compartments)

(Note that in practice it was not possible, without modifying the pulsing arrangements, to clean fully the lower third of the experimental longer elements. The operating filter area for three compartments has therefore been taken as 26.2 m^2 for calculation of filtration velocity).

Control: Hitachi EC-60HRP PLC with input signals from Photohelic differential pressure units measuring across the filter in total and across the recaking compartment. These inputs, and/or a timer in the PLC could be used to initiate compartment change over.

6.2 First Test Site

For the early tests it was decided to install the filter on an electric arc furnace (EAF) direct (fourth hole) extraction duct at the Aldwarke site of Corus Construction and Industrial (at the time of installation this was British Steel Engineering Steels' Rotherham Works, and subsequently Corus Engineering Steels). The rationale for this was:

(a) The required break-in to the sinter plant off-gas duct depended on a suitable time window when the plant was not operating. Delays were anticipated in that sufficient down time was not scheduled until several months later (the EAF site had weekly stoppages). In the meantime provisions for installation at the Scunthorpe sinter plant could be progressed.

(b) Commissioning and initial testing and familiarisation could be quicker and more efficient because of convenient location and higher and more varied dust loadings. Also the less severe negative pressure conditions compared with sinter plants would allow easier measurements to establish some of the characteristics of the device. The varied dust loadings would also provide useful data in the event of applications on other plants.

Following delivery the filter was connected to the off-gas ducting of 'T' EAF (one of 2 furnaces then operating in Aldwarke Melting Shop), and instrumentation and services (compressed air and electricity) installed. Figure 8 is a schematic of the siting, and the digital images in Figs. 9 and 10 illustrate some of the features.

6.3 Electric Arc Furnace Tests

6.3.1 Commissioning

The major effort in commissioning the unit involved changing parameters in the supervisory PLC governing the control cycle (pulsing, settling time, recirculating fan operation etc.) and in determining the compressed air pressure for pulse cleaning.

From the beginning, cake formation was quite rapid, taking typically around two minutes at high dust loadings. Indeed, the rapid cake formation and subsequent build-up of dust, giving high pressure drops (up to 3 kPa), meant that flow had to be limited to about 0.7 m^3/s, compared with a notional design level of about 1.5 m^3/s. The cleaning sequence had to be made as short as possible to maintain an acceptably low pressure drop, even at this flow. It should be remembered, however, that inlet dust concentrations were up to 20 g/m^3 on the EAF, an order of magnitude higher than on sinter plants. Also, EAF dust is finer than sinter plant off gas dust. A typical size distribution is shown in Fig. 11, where it can be seen that the peak is around 1 µm and almost all is less than 10 µm. This can be compared with data from sinter plants in Fig. 12 (compiled from the information in Appendices 3 and 4 and Figs. 6 and 7). Filtration of EAF dust might therefore be expected to be more difficult.

Typical operating traces after iteration to nominally acceptable performance are shown in Fig. 13, which illustrates the variation in filter flow, pressure drop and inlet temperature with time for part of an EAF cycle. The pressure drop across the filter exhibits the expected 'saw tooth' pattern, dropping sharply when a compartment is switched out for cleaning and is replaced by a newly conditioned compartment. In this example the amplitude of the swings was about 350 Pa. The flow can be seen to be quite steady as compartments were switched in and out, varying by only a few percent.

Although the EAF direct gases are considerably hotter than those from the sintering process, the heat losses from the long connecting ductwork on this installation were such that temperatures were quite similar to those expected on the Scunthorpe sinter plant. These levels were handled without problem. It was, however, decided that the inlet duct should be thermally insulated to enable testing at higher temperatures in case any future operators should require this, and also to lag the filter body in preparation for the sinter plant tests to help avoid condensation at the much higher water vapour levels expected.

Following lagging, a series of performance tests was undertaken as described below.

6.3.2 EAF Operating Tests

The measurement positions and techniques employed are summarised in Appendix 6. The measurements in the later tests at the Scunthorpe sinter plant were essentially similar.

The EAF tests totalled more than 200 operating h. The operational changes undertaken and their effects are described in Appendix 7, and summarised below.

The work involved modifications to the filter mesh cleaning and recaking cycle to establish a consistent operation at the lowest pressure drop, with acceptably low outlet dust

concentrations. This was achieved by investigating the effect of varying the flow level, and changing the pulse cleaning regime from sequential pulsing of the two filter tube banks in any compartment to simultaneous pulsing. Stable operation was experienced at an inlet flow of about 0.6 m^3/s, with a pressure drop of 16 to 22 mbar.

Details of the results are also given in Appendix 7. The achieved operating parameters are listed in Table 3.

Inlet gas temperatures of up to 270°C were handled without difficulty.

Filtration efficiency was approximately 99.9%. Inlet dust loadings of up to 12.4 g/m^3 stp gave short term outlet loadings in the range 2 to 40 mg/m^3 stp. Average outlet emissions for all the tests undertaken with the furnace operating (i.e. with power on and generally with oxygen injection taking place) were around 10 mg/m^3 stp. If allowance is made for air inleakage (see below), and the same amount of dust is assumed to be passed, this figure would increase to 14.4 mg/m^3 stp. These results were from samples of typically less than 20 min duration. A longer test over a complete furnace cycle produced a measured outlet loading of 3 mg/m^3 stp.

Continuous outlet dust measurements revealed peaks at compartment changeover and when pulse cleaning the screens, which contributed substantially to the overall average concentrations, because of the frequency of changeover needed at the high inlet dust loading (approximately every 4 min). Discussions with a large filter manufacturer have revealed that a similar pattern is encountered with conventional pulse jet filters.

Good filtration could be achieved at a flow of about 0.6 m^3/s (actual), with a corresponding pressure drop of 16 to 22 mbar. This flow equates to a filtration velocity, based on the filtration area of 3 on-line compartments, of 1.4 m/min. This was lower than that tentatively ascribed in the initial design, which was based on the expectation that the ability to clean metallic screens more thoroughly than fabric would allow filtration velocities higher than those for a fabric filter. It is widely held that the resistance to flow when filtering very fine dusts is largely due to the particulate cake, rather than the fabric substrate. It is perhaps not surprising, therefore, that filtration velocities similar to those of a conventional filter were experienced.

The variations in pressure drop caused by compartment changeover led to only small changes in flow, so that filter flow performance was very stable for a given setting.

Considerable inleakage was experienced as a result of the design feature whereby the sealing of the recirculation/changeover valves is accomplished by an air curtain (generated by the suction at the filter outlet). Simple tests to reduce this flow, without modifying slot dimensions or tolerances, reduced inleakage by around 50% whilst still allowing acceptable dust loadings. This design feature is experimental and changes can be envisaged for large scale operation.

The EAF tests, therefore, demonstrated that good filtration with a very fine dust was possible, and allowed useful experience to be gained quickly. For example, the importance of simultaneous cleaning of all the filter sleeves in a compartment was evident.

7. SCUNTHORPE SINTER PLANT TESTS

7.1 Installation

The filter was transferred to Scunthorpe sinter plant in mid-1998. Its position is shown schematically in Fig. 14, and Fig. 15 illustrates the actual site. Connection to the 4.6 m diameter section of the wind main was via 350 mm pipe, and isolation was provided by two 350 mm knife gate valves. The position was one wind box from the entry section of the ESP, and was chosen for ease of access and because hard standing was available. The wind main gas at this point was believed to be generally representative of the gas entering the ESP. The offtake nozzle in the wind main was set to face the oncoming gas stream, and sized to give nominally isokinetic conditions at the design flow. The inlet pipe to the filter was thermally insulated, and the insulation on the body of the filter was transferred from the EAF tests.

The instrumentation was essentially the same as for the EAF tests, described in Appendix 6.

Because of the difficulty of fully cleaning the fine mesh filter screens, a new set of filter tubes was installed. This avoided contamination of samples with EAF fume, and ensured that cake build up was not affected by the EAF dust residue. As sintering dust is coarser than EAF dust, the mesh size selected was somewhat larger. Two compartments (A and C) were fitted with 100 mesh (apertures 0.16 mm) and two (B and D) with 125 mesh (apertures 0.125 mm) for comparative tests. Both had the same free area (~34%) as the previous screens. Only one filter element per compartment was of the 2.74 m experimental length.

7.2 Commissioning and Initial Test Results

Before beginning commissioning, the open area of the hollow diverter valve spindles was reduced, since the suction in the filter outlet was much higher than in the EAF tests (-165 mbar compared with -20 mbar). Calculation suggested that an area reduction of about 2/3 should allow a similar air curtain flow to that which had proved adequate in the EAF tests, and this was simply accomplished by blocking the open end of the valve spindles, (the opposite side to the actuator coupling shown in Fig. 10).

The first series of tests was aimed at establishing a flow level at which a cake could be built reproducibly with the wind main dust. At 1.5 m^3/s, the design flow for the offtake nozzle, bleed through of dust occurred on 'A' chamber (the furthest from the inlet). At 1 m^3/s a cake could be built consistently in all chambers.

In order to determine the minimum overall pressure drop consistent with adequate filtration, a series of runs at this flow was undertaken. After vigorous pulsing of the screens, and with chamber changeover inhibited, dust was allowed to accumulate over periods of several hours whilst gravimetric dust concentration measurements were taken in the outlet and pressure drop was recorded. The results are shown in Fig. 16, where it can be seen that a pressure drop of about 15 mbar was associated with dust loadings below 10 mg/m^3 stp.

The inlet flow of about 1 m^3/s corresponds to a filtration velocity of 2.3 - 2.4 m/min, an increase of 70% over the EAF tests.

These results can be compared with information extracted from data made available from the filter suppliers from independent tests, at a variety of filtration velocities, using pulverised fuel ash (PFA) on a small test unit. The PFA was mainly spherical particles with a size range of 0 - 100 μm (50% > 20 μm). This is generally smaller than sintering dust, but

covers a substantial part of the range, and is much larger than EAF dust. The screen was 325 mesh. Figure 17 shows that the sinter plant results fit the broad pattern of the PFA results. As filtration velocity decreases, so does the outlet dust loading, but in all cases the outlet dust decreases to low levels at higher pressure drop (thicker cake). The implication is that it is possible to trade dust emissions for filtration velocity, and hence capital cost, although it is believed prudent to aim for low dust emissions at a reasonable filtration velocity.

Almost all subsequent tests were performed under normal cyclic operation with the filter set to change chambers when the pressure drop across the off-line chamber reached approximately 12.5 mbar, giving an average pressure drop of about 15 mbar across the filter as a whole. The cleaning cycle developed by experimentation is listed in Table 4. The pulse duration and pressure were both considerably less than required for the EAF dust.

Figure 18 illustrates typical flow and pressure traces. The time between chamber changeovers, at about 45 min, was much longer than with the higher dust burden from the EAF, and operation was more reproducible since the process is more consistent.

As on the EAF (and with fabric filters) peaks in dust emissions occurred at compartment changeover and on pulsing, as shown in Fig. 19, which gives a trace from the PCME tribological dust monitor on the outlet. However, these peaks should have a relatively small effect on mean dust loading because of their low frequency.

Table 5 shows the results of 10 gravimetric determinations of outlet dust concentration during periods when the filter pressure drop was greater than 12.5 mbar. The mean concentration was 9 mg/m^3 stp. The higher values in Table 5 were often associated with samples in which a compartment changeover took place. The effect of this on a 10 min sample would be expected to be significant.

The initial performance is summarised in Table 6. The effectiveness of filtration and the increased filtration velocity compared with the EAF performance were encouraging. If the filtration velocity proved typical, working filter area for a given duty could be considerably smaller than for an equivalent fabric filter.

7.3 Filter Problems/Refurbishment

At the commencement of the next test campaign problems were experienced with the movement of the experimental diverter valves. One of the valves was sticking badly and not completing its travel in either direction of movement, and another was intermittently failing to reach the 'chamber on-line' position. It proved impossible to free the valves in situ, and it was necessary to remove the two valve cassettes for remedial work in the workshop facility. One such cassette is shown in Fig. 20. The problem was found to be one of accreted dust which inhibited free movement of the valve blade. The accretions may be associated with intermittent operation, allowing moisture to cement the dust on the metal surfaces of the valve assembly. The internal surfaces were shot blasted and painted, and in order to reduce the likelihood of subsequent repetition of the problem, the edges of the blades were ground back to increase the clearance by about 1 mm all round. These valves were reinstalled, but in view of the findings, the remaining two valves were inspected, and it was judged that they should be removed and similarly refurbished.

As part of the above work, the filter compartment lids were removed to allow cleaning of the area above the filter tubes, so that any dust accumulated as a result of poor valve performance would not prejudice the results of future tests. The silicone sponge seals

around the lids were found to have been compressed with a consequent danger of inleakage. These were replaced by harder, more resilient neoprene rubber strips, which subsequently proved to give good performance.

7.4 Performance After Valve Refurbishment

Because of the increased valve clearances created during the refurbishment, it was believed important to establish whether the outlet dust concentration had been increased by leakage of dust from the recycling manifold to the outlet manifold, via the clearance gaps. The filter was operated, as before, with the open end of the valve spindles blocked, and the actuator linkage end open. Operating parameters (pressure drop, flow and filtration velocity) were similar to those established prior to the remedial work. A series of tests gave the outlet levels shown in Table 7. It can be seen that dust loadings were low, averaging 4.75 mg/m^3 stp, indicating that no deterioration in performance had been caused. Indeed, the results were better than those measured before the refurbishment, where mean outlet loadings of about 9 mg/m^3 stp were found.

Measurements were also made of the dust loading in the inlet duct to the filter. The results are shown in Table 8. The mean inlet concentration of about 1 g/m^3 stp is somewhat higher than that measured earlier in the inlet to the electrostatic precipitator. This might be expected as there are drop out valves in the wind main between the pilot filter and the precipitator, and also some dust settles out in the inlet to the precipitator. The measurements confirm that the gas and dust at the filter inlet are reasonably representative of conditions in the wind main.

The improved filtration performance indicated that the indrawn air forming the diverter valve seals was adequate, or possibly more than required. Since this indrawn air has to be handled by the main fan, it is important that the level is minimised. Attempts were therefore made to assess the effect of varying the sealing air flow (see next Section). A base level was determined in readiness for this by simultaneous measurement of inlet and outlet flows. Typical results can be seen in Fig. 21, together with other operational parameters. These traces also serve as an example of the filter operating parameters during this test campaign. It can be seen that the indrawn air represents about 45% of the inlet flow. If the outlet dust loading is modified to account for this dilution the effect is not great, the level of 4.75 mg/m^3 stp increasing to 6.6 mg/m^3 stp.

Note: As part of a series of carbon powder injection tests (for control of trace organic emissions - see Section 7.9) some months later, outlet dust concentration and inleakage were measured again. The inleakage was found to have reduced to around 15% of the inlet flow, probably because of some dust build up around the diverter valve blades. The outlet dust loadings for the base case were, however, very similar at 4.9 mg/m^3 stp (uncorrected for inleakage) to those given above.

7.5 Effect of Changing the Valve Sealing Air Flow

Following calibration of the tribological dust monitor in the outlet duct against gravimetric samples, the effect on emissions of varying the sealing air flow was investigated.

Starting from a period of normal operation with the open end of each valve spindle blocked as usual, the actuator coupling ends were progressively sealed. Figure 22 illustrates the effect on flow and Fig. 23 shows the corresponding inlet and outlet dust monitor traces. Initially, with the indrawn air at about 0.25 m^3/s stp (similar to the base case in Fig. 21), the outlet dust loading was generally at a level of <2 mg/m^3 stp. Sealing half of the open area

for air inspiration (Point A in Fig. 22) caused the indrawn air to reduce to about 0.15 m^3/s stp and the dust emission to increase to around 5 mg/m^3 stp. Further sealing of half the remaining area (Point B) caused another increase to 6.5 mg/m^3 stp, and full obscuration of the aperture (Point C) resulted in a level of 8 mg/m^3 stp. Also, the number of transient excursions in addition to those routinely associated with compartment changeovers increased markedly when the indrawn air was restricted.

Inlet dust loading was sensibly constant over the period of the test. The modest increase in inlet flow evident in Fig. 22 was a consequence of the increased suction available at the filter inlet as sealing was progressively increased.

It can be concluded from this test that the level of air flow is important for this type of valve, and that careful design and manufacture would be required if such a design were to be adopted for a full scale unit. It should be remembered, however, that at increased scale the air flow would be proportionally reduced because the valve blade periphery and the valve area do not increase at the same rate. For example, a doubling of valve cross section would require an increase in sealing flow of 40%.

Previous and subsequent operation of the filter was with the aperture at the blade coupling end fully open, as at the left of Fig. 22, since the lowest dust emissions are desirable.

7.6 Recirculation Control

A strategy suggested for control of filter cake build up in the off-line compartment and subsequent compartment changeover involved the use of a continuous dust monitor in the recirculation circuit.

A PCME continuous dust monitor was therefore fitted to the recirculation duct, between the recirculation fan and the junction with the filter inlet manifold, with the aim of assessing the potential for using the signal from this device to control compartment changeover and/or the recirculation fan.

Normally, the pressure differential across the off-line compartment is monitored and when this reaches a preset level (typically about 12 mbar) the cake is deemed to be established and compartment changeover is triggered. It was considered possible that a measure of outlet dust burden from the off-line compartment might be a better indicator of cake integrity. This could allow the recirculation fan to be switched off as soon as a cake is established, and the overall filter pressure drop would then be used to trigger changeover. Shortly before changeover the recirculation fan would be started, and the recirculation dust monitor interrogated again to ensure cake integrity has not deteriorated. The recirculation fan should also be running down during changeover to minimise cross leakage of dust during the travel of the diverter valve blade. This strategy would optimise energy use for recirculation, and should give a better guarantee of readiness for filtration than off-line compartment pressure drop. Alternatively, overall filter pressure drop (and hence operating cost) might be reduced by initiating compartment changeover as soon as the dust monitor indicates that a cake has been established.

Figure 24 shows both the recirculating compartment pressure drop and dust monitor signal, together with the filter outlet dust monitor signal. The dust monitor signal appears to drop well before the trigger level of 12 mbar pressure drop is reached, suggesting that the above strategy may be viable. However, two factors throw doubt on this conclusion. Previous experience showed that triggering changeover at lower levels of off-line compartment pressure drop, and hence lower overall filter pressure drop, adversely affected outlet dust

loading. Figure 16 illustrates this. Also, other observations have shown evidence that switching off the recirculation fan increases the outlet dust loading. This is attributable to the increase in pressure difference between the outlet manifold and recirculation duct when the fan is off, which can cause leakage across the air curtain seal of the diverter valves.

It can be concluded therefore that, at least with the present diverter valves, the use of a pressure difference signal is preferable. The recirculation duct dust monitor can be viewed as useful primarily as an indicator of physical problems with the screens (e.g. uneven coating or minor damage to the mesh).

7.7 Cold Start Test

Concern has been expressed regarding the ability of any filter which generates a cake to operate successfully when the sinter strand is started from cold after a prolonged stoppage. The condensation on cold surfaces of water vapour from the strand might be expected to cause severe problems from wet dust either blocking the filter or hindering proper cake formation. It was hoped that the use of metallic screens would reduce the potential for such problems compared with fabric filters, because of the ease of cleaning and lack of wettable fabric.

The many start up operations in which the cold filter was switched on and began taking off-gas (containing approximately 11% H_2O v/v) from the wind main without problem were encouraging. However, in order to investigate this condition more fully, at the end of the stop period in August 1999 when No. 2 Strand had been off for 10 days, the filter was started at the same time as the main fan serving the wind main.

Figure 25 shows the flow and pressure drop for a period of about 5 h after start up, and Fig. 26 the filter inlet gas temperature (mirroring that in the wind main). Figure 26 also shows the filter inlet and outlet dust monitor traces. Unfortunately these were not available from the start as a power interruption had caused the internal settings to be lost and reprogramming was necessary.

The flow trace is unsteady because the filter flow was periodically adjusted as wind main suction changed when the main fan damper was opened in stages. Pressure drop built up steadily after about an hour until it reached its set level, at much the same time as the wind main gas temperature reached its usual value. Subsequent operation was normal.

The outlet dust monitor trace was noisier than usual because compartment changeover had been set to trigger at a lower pressure drop than ideal. This was to ensure that enough changeovers occurred during the test period to allow evaluation of the pattern of operation. A lower setpoint has the effect of allowing occasional peaks in the outlet loading, since filtration performance is affected by pressure drop (see Fig. 16). There is no reason to suppose that a higher set point would not have given a perfectly normal trace.

Later inspection during a scheduled short stoppage revealed some water in the hoppers, notably below D compartment, nearest the filter inlet. However, the screens appeared unaffected, with no evidence of 'sludging'.

Clearly, fully effective filtration performance was not achieved until about an hour after switch-on, but ESP performance is also poor when temperatures are low during cold start up. Injection of fume or some other material (e.g. lime) prior to the strand starting could perhaps have allowed effective filtration from the start of operation. The important outcome

was that the filter suffered no problems during these cold start conditions, although it should be noted that the test was performed in summer.

7.8 Dust Properties

Dust properties vary considerably from plant to plant, and are determined by, for example, the particular recycling practice employed. The following results from the pilot filter should therefore be considered in the context of the Scunthorpe operation, outlined below.

Typically, the ESP dust from the first two fields was recycled, and that from the third and final field discarded. The type of reverts used were blast furnace flue dust, clean (non-oily) mill scale, various clean metallurgical fines and low zinc fractions of blast furnace slurry. Amounts of individual reverts varied according to availability, but typically the total revert burden would be up to 5%. Chlorine inputs, although not routinely measured, would typically be in the range 75-200 mg/kg sinter mix, which is believed to be typical of many European plants. Limestone and olivine were used as fluxes (no burnt lime). The injection of carbon only occurred in the experimental unit, and not in the wind main.

7.8.1 Collected Dust

7.8.1.1 Pilot Filter

When the dust hoppers were opened for dust removal it was always found that the quantity collected in the 4 compartments was far from uniform. When the hopper beneath 'A' compartment (the farthest from the inlet duct entry) was almost full, 'B' hopper was about 40% full, 'C' was about 20% full, and 'D' (nearest the inlet) was perhaps 10% full or less. The nature of the dust also varied substantially, in that the dust from 'A' compartment was coarser and free flowing.

Samples of the dust from the 4 hoppers, plus a sample scraped from the filter screen in 'A' compartment were analysed for comparison. Table 9 gives the results for significant components. Clearly chlorine, sodium and potassium, and hence alkali chlorides increase in proportion towards the inlet. From these data and the relative proportions collected it would appear that the heavier dust particles, more typical of bed material, tend to progress further down the inlet duct, resisting the change of direction needed for entry into the filter chambers. Once in the chambers, they tend to drop out before filtration, whereas the smaller particles, richer in alkali chlorides, are perhaps more evenly distributed and collect on the screens before they are shed during pulse cleaning of the mesh. Indeed, the visual appearance of the dust in the hoppers showed a stratification consistent with this hypothesis. In the earlier EAF tests, where the dust was predominantly sub-micron, distribution was even.

These observations suggest that inlet manifold design will require careful consideration in any large scale unit to ensure that loads on hoppers, valves and conveyors are reasonably uniform. A further possibility suggested by Table 9 is that a combination of a cyclone or settling chamber followed by the filter might be the best configuration. This would allow the larger particles to be collected by the cyclone and sent for recycling, whilst the dust from the filter screens, higher in unwanted components, could be treated separately.

Further samples were collected during the summer shutdown (when access was possible) for more rigorous analysis by CENIM. The distribution was similar to that found earlier with a diminishing quantity of dust in the bins nearer the inlet to the filter. The results of the analysis are outlined in Appendix 8. This information confirms the previous impressions of

segregation. The material collected from the screens was predominantly small particles, and was relatively rich in K, Na, Cl, Pb, Zn, and S. Also Se, Br, and Tl were at detectable levels in the smaller fractions.

7.8.1.2 Mesh Test Filter

It was also found in tests with the small unit at CENIM that considerable dust drop-out occurred on various surfaces in the filter housing (see Section 5 and Appendix 5). Although this might have been expected, CENIM personnel regarded it as a problem. Indeed it was a problem in operating this installation since it prevented proper conveying by the gas stream of particles to the filter surface, thus hampering attempts to establish a cake for mesh testing. This experience, together with the preceding observations on the pilot filter that inertial pre-separation of dust might be beneficial, prompted an outline design exercise for a cyclone in the filter circuit at CENIM. Although not constructed, the principles are applicable to a large-scale unit, and the observations and calculations are summarised in Appendix 9, as they may prove useful in the future. Also included is some original work on the determination of transport velocity.

7.8.2 Outlet Dust

7.8.2.1 General Properties

To help assess the nature of the dust passed by the filter, the deposit on the glass fibre filter used in one of the gravimetric measurements of outlet dust loading was examined using an ISI 100A scanning electron microscope (SEM) and associated energy-dispersive X-ray analysis (EDA) equipment.

Figure 27 shows a SEM image of an area of the filter disc x 1000 (1 mm on the photograph is ~1 µm), and Fig. 28 a similar area x 2000. The particles observed were 98% <10 µm, and generally under ~ 3 µm. The larger particles appeared to be agglomerations of the smaller ones. The long straight objects are fibres from the filter pad.

It was only possible to provide EDA spectra for particles (or clusters) of 4 µm or greater. Figures 29 to 31 show typical spectra for particles of 4, 12 and 20 µm respectively. The counts per second for all 8 of the spectra obtained are summarised in Table 10. The only differences apparent with change of particle size are a tendency towards increased potassium levels in the larger particles and increased calcium in the smaller. Generally the spectra indicate that alkali and alkaline earth metals are major components, probably associated with the chlorine and sulphur. Notably, lead and zinc were not detected, although both were prevalent in the dust collected on the screens (Section 7.8.1).

This information confirms the capability of filtering down to particles of very small size, and that the emitted species are predominantly alkali and alkaline earth chlorides.

7.8.2.2 Heavy Metals

Heavy metals associated with emitted dust from sinter plants are an environmental issue, and efficient filtration would be expected to reduce atmospheric emissions of these pollutants. To evaluate the filter's performance in this respect, samples were taken of the outlet dust from the filter, with simultaneous sampling of the ESP inlet dust and the dust in the gas at the base of the main stack (representative of stack emissions for comparison). These samples were submitted for analysis for Pb, Zn, Cd, Cu, Mn, Se, Fe, Na, K, and SO_4.

The results are summarised in Table 11. As expected, because of the enhanced removal of the particulate material in the filter, all the analysed components were reduced. Indeed, Table 12 shows that in general the concentration of the species after the ESP and fan was approximately 4 times higher than after the filter. This is consistent with the ratio of dust concentrations at the two sampling positions. It should also be noted that the dust concentration after the ESP recorded at the time was uncharacteristically low, at 23 mg/m^3 stp. This is lower than is achieved at most sinter plants fitted with ESPs, and the improvements using the filter would consequently be greater in general. The performance of ESPs is dependant on the characteristics of the dust, whereas the filter has no such dependency.

7.8.2.3 Radioactive Species

The concentration of naturally-occurring radioactive species present in the materials, in particular of Pb-210 and Po-210, into the outlet dust means that consent from the licensing authorities is required in the UK and the Netherlands for these emissions. It is understood that radioactive emissions are also of interest in other EC member states.

As these species are associated with dust particles, it would be expected that the levels in the filter outlet should show reductions. In order to quantify performance in this respect, glass fibre filter pads obtained during gravimetric dust sampling from the filter outlet and during sampling from after the ESP for comparison were submitted to the National Radiological Protection Board (NRPB) for analysis. The results have been used, in conjunction with the sampling volumes, to evaluate the concentrations shown in Table 13.

It is clear that emissions of Pb-210 and Po-210 are reduced compared with the ESP outlet, and that the reduction is in the same proportion as the reduction of emitted dust, in this case by 95%.

7.9 Carbon Injection Tests For The Control Of Organic Micropollutants

It is known that activated carbon injection into bag filters can reduce emissions of trace organic micropollutants, such as the dioxin and furan family of compounds (PCDD/Fs), from a number of processes (e.g. waste incinerators). It was therefore believed that this should also be the case for the KN Filter. In order to give some idea of potential performance under sinter plant conditions in this respect, a quantity of steam activated carbon was obtained, and a trial conducted. This is described in Section 7.9.1 following. The results were promising.

During the term of this project, the injection of lignite coke powder into sinter plant ESPs was reported (Reference (3) gives an example). Lignite coke may be well-suited for the adsorption of compounds such as PCDD/Fs. Most sorbents are specified according to their active surface areas, but it does not necessarily follow that the ideal material for a given application is the one with the highest specific surface. Materials that are effective sorbents usually have a highly porous structure and for efficient adsorption it is important for the pore radii distribution to be matched according to the dimensions of the molecules to be adsorbed. Pore radii are classified as micropores, mesopores and macropores and these have radii of <1, 1-50 and >50 nm respectively, and materials with very high specific surface areas (>2000 m^2/g) generally have large numbers of micropores. According to information published by Rheinbraun Brennstoff GmbH, the molecular dimensions of the PCDD/Fs are such that materials with high concentrations of micro- and submicropores, such as activated carbons, are less suitable for the separation of these compounds than materials that have

large concentrations of macro- and mesopores such as lignite coke. With ESPs adsorption is believed to be principally a time-of-flight phenomenon. It is possible that the combination of in-flight adsorption and that which might occur during the passage of gas through a filter cake can give similar or better performance with reduced consumption of carbon. A further series of tests using both lignite coke powder and activated carbon as injectants was therefore carried out, as described in Section 7.9.2 below.

7.9.1 Preliminary Tests (Activated Carbon)

Details and full results are given in Appendix 11 and summarised below.

A relatively crude batch injection technique was employed. The carbon used was Mesocarb FGT Plus, a proprietary coal-based steam-activated carbon powder, 85% < 75 µm, at an injection rate of 400 g/h, equivalent to approximately 180 mg/m^3 stp. This rate was higher than the supplier thought necessary because, for reasons outlined in Appendix 11, injection had to be into the inlet manifold and the likely degree of drop-out before the powder reached the filter screens was not known.

Samples from the filter outlet gas stream were collected during 2 days of normal operation and 2 days with injection of the carbon. These were analysed for dioxin and furan (PCDD/F), polycyclic aromatic hydrocarbons (PAH) and polychlorinated biphenyls (PCB). Dust samples were also collected from the bins at the base of the hoppers, (representative of normal operation and carbon injection), and from the screens themselves after carbon injection. These were analysed for carbon and PCDD/F. The injection and sampling points are shown in Fig. 32.

A summary of the results is shown in Table 14. The use of this carbon reduced PCDD/F emissions by 1/2 to 2/3. The dust from the screens showed a marked increase in the concentration of these compounds, indicative of capture by the filter cake, which contained about 13% carbon. PAH emissions were reduced by 2/3, and PCBs by almost a half.

The reduction in PCDD/F was very similar to that achieved during trials of lignite coke injection before a sinter plant ESP at a Corus plant. These tests, therefore, gave encouraging results, especially in view of the simple techniques employed.

7.9.2 Lignite Coke and Activated Carbon Tests

These tests are summarised below and described in greater detail in Appendix 12.

Fifty kilogram samples of two grades of pulverised lignite coke were obtained from Rheinbraun Brennstoff GmbH. These were the 'normal' grade of 63 µm median grain size, and a 'reactivity enhanced' grade of 28 µm median grain size. A quantity of the steam activated carbon had also been retained from the previous trial.

Injection was again into a single point in the filter inlet duct, but for these tests a screw feeder fed the powders continuously into a valved pipe with a nozzle facing the oncoming gas stream. Three feed rates were employed, approximately equivalent to 50, 150 and 250 mg carbon powder per m^3 stp of gas. PCDD/F and PAH samples of 80 to 120 min duration were taken for each material and feed rate, together with base case samples before and after the feeding tests. Dust samples were taken from the filter collecting bins and screens.

The emission results are summarised in Table 15, both as measured and corrected for inleakage. Inleakage was only 15% in these tests, probably because of accreted dust on the diverter valve surfaces.

Corrected results for PCDD/F were in the range 0.14 to 0.39 ng I-TEQ/m^3 stp during injection of the 3 materials, which represents a major reduction when compared with the normal stack emission of around 1 ng I-TEQ/m^3 stp at this plant. There was, however, no consistent pattern of removal with increasing injection rate or with the different carbonaceous injectants, and the base cases also gave low results. This was attributed to two factors. First, as can be seen in Table 15, the carbon in the dust from the screens did not vary systematically, almost certainly because pulse cleaning removed only a proportion of the powder, so that each test had some injectant from one or more previous tests on the screens (including the base cases, the first of which was preceded by trial injections). Secondly, the continuous outlet dust monitor showed substantial variations during the sampling periods, as did the spot gravimetric determinations, and it would be expected that this would affect PCDD/F measurement. Indeed, outlet dust loadings were approximately doubled during injection, and were highest for the smaller grade of lignite coke.

The dust samples from the filter screens contained PCDD/F at around 2000 ng I-TEQ/m^3 stp, confirming the effectiveness of capture.

PAH removal was more closely related to injection rate, perhaps suggesting that PAH adsorption occurred during particle flight. Typically 60 to 80% removal was achieved.

Gaseous pollutants (CO, SO_2 and NO_x) were, as expected, not affected by injection.

It was concluded that, although no dosage rate correlation could be established for PCDD/F, emission levels of 0.1 to 0.2 ng I-TEQ/m^3 stp are achievable, and that PAHs can also be substantially reduced. The normal grade of lignite coke appeared superior to the reactivity enhanced grade, probably because some of the smaller particles of the latter material passed through the filter cake to a greater degree. Outlet dust loadings, although higher during injection, were still low at about 14 mg/m^3 stp, and might be reduced further by reducing the filtration velocity.

7.10 Corrosion Coupons

The filter screens on the pilot filter were manufactured from 316 grade stainless steel mesh. The long term use of this type of filter would be prejudiced if corrosion and/or erosion of the meshes were to take place. Erosion is unlikely to be a severe problem since particle velocity should generally be low at the screen surface. The corrosion resistance of stainless steel in this environment is, however, unknown. Accordingly, corrosion coupons (Fig. 33) of candidate mesh materials were assembled, comprising 3 samples each of 304, 316, and 430 grade stainless mesh, 3 samples of 304 and 316 strip and 3 pairs of wires of a duplex 2205 grade selected for corrosion resistance. These were inserted into the wind main at the precipitator inlet, for subsequent periodic removal for inspection by corrosion experts. In this position the coupons would be continuously subject to the wind main gas, albeit at gas velocities of about 10 m/s, rather than the 2 m/min prevalent at the filter screens.

The first samples were removed for inspection after 6 months exposure. They were examined as-removed and after cleaning in 15% nitric acid for 5 min, followed by 15% nitric acid + 2% HF for 2-3 min, all at room temperature. Samples were examined at up to x 200 magnification. Whilst some slight dulling from abrasion was evident, no corrosion could be seen in any sample. The abrasion might be expected at the velocities prevailing in

the ESP inlet. Figures 34 and 35 show photographs of the 304 and 316 stainless steel coupons after cleaning.

Before replacement of the coupon holders, specimens of ETFE (ethylene tetrafluoroethylene) plastic mesh were added to the holders, since it was possible that plastic mesh could prove to be a suitable, less expensive, alternative to stainless steel. This material was selected for its temperature stability and resistance to chemical attack.

The second set of coupons was removed after one year's exposure. The frames holding the 304 grade mesh samples had broken away and been lost (vibration in the gas stream was quite intense in this location). The 316 and 430 grade stainless steel mesh coupons showed no significant signs of corrosion. The 304 and 316 grade strip samples showed slight pitting, and the 2205 grade duplex material showed no evidence of corrosion. Although there had been some weight loss on most of the samples, equivalent to a thickness loss of around 0.01 mm/year, it is believed that this was caused by abrasion from hard particles travelling at the velocities prevailing in the ESP inlet, rather than by corrosion. It was believed by the corrosion expert that a life of at least 10 years could be expected.

The ETFE plastic mesh was removed after 6 months exposure. Although it showed no visible sign of damage, the mesh was impossible to clean fully, with particles adhering to the filaments, and had become relatively easy to tear with only modest force. This material was therefore considered unsuitable for this application since continual pulse cleaning would be expected to cause eventual damage.

After 18 months exposure the remaining coupons were found to have been lost from the support frames, presumably because of the vibration caused by the high gas velocities.

These tests, therefore, apparently showed encouraging resistance to corrosion in the wind main environment. However, it should be stressed that the conditions at the ESP inlet were very different from those that would be encountered in the filter itself, and the impact of high velocity particles on the coupons could have removed some evidence of corrosion.

8. FULL SCALE PLANT

In view of the success of the pilot scale filter in terms of dust removal and its potential for abatement of other pollutants, it was considered that an estimate of the cost, size and arrangement of a full scale installation would be of interest.

A UK company, Boustead International Heaters Ltd., had performed a design and costing exercise for a full scale plant based on the KN Filter technology, and a summary of the outcome was made available for this project.

The basis of the design is a large twin strand application with a gas flow of 2 - 2.5 x 10^6 actual m^3/h at 130°C.

Figures 36 and 37 are an elevation and plan view. A clearer impression might be gained from the illustrations in Figs. 38, 39 and 40.

It is assumed that the filter will sit between existing fan sets and a stack (not included), so that the filter ID fans have only to overcome the resistance of the filter.

The plant would be of modular construction, comprising 8 streams, each of 8 filter modules (i.e. 64 identical filter modules), each stream having its own ID fan and recirculation fan.

The 8 ducts from the ID fans connect to a single main outlet duct. Each pair of filter modules rests on a structure and shares a dust hopper divided by an internal plate. The stainless steel mesh filter elements are supported on cell plates and held by quick release clamping frames. These are accessed by doors on top the modules (from suitable railed walkways), such that it would take one man about 5 min to change a filter element.

There are 150 individual filter screens per chamber (i.e. 9600 in total), each 2 m long by 190 mm diameter.

Each pair of modules shares a reverse jet pulse manifold, and each module has its own differential pressure and temperature gauges. All compressed air is supplied by a main compressor.

Each of the 8 streams has a main control panel, including a motor starter for the recirculation fan, and a PLC. Each of the 64 modules has a small control panel with a PLC for control of the diverter valve and cleaning operations.

Eight carbon injector packages are envisaged, each with a hopper designed for 1 m^3 bags to be fork-lifted into filling position. The injector systems may operate at material flows of 2-10 kg/min. Each injector has a local control panel and is powered by a varispeed inverter drive. The injection points are at the entry of each of the 8 streams.

All ductwork is of 6 mm thick plate. Total steelwork is approximately 2000 t.

In order to minimise condensation and corrosion the filter system is externally clad with mineral wool slab covered by aluminium sheeting.

The required plot area is about 100 x 50 m, and height is 15 m.

Approximate cost for the system including carbon injection packages, conveyors and controls would be £6.5 million delivered UK site. Foundation and civil works are excluded. The unusually large scale of the plant (2 x 10^6 m^3/h) should be noted when considering this cost, which would be approximately proportional to flow capability since the design is modular.

Recent considerations indicate that 4 streams, with larger filter units may be preferred, which would give a worthwhile cost reduction.

This level of cost is towards the lower end of the range given in Reference 1 for bag filters (when scaled to equivalent flow capacity) and is similar to that quoted for ESPs. It is considerably lower than the cost of modern scrubber systems, and the problem of cross-media transfer of pollutants is avoided.

Utility and consumable requirements are estimated as follows.

Main ID fans	8 x 225 kW
Recirculation fans	8 x 60 kW
Carbon injection	25 kW
Compressor	27 kW
	2332 kW
Activated carbon	~ 35 kg/h

The required maintenance comprises simple inspection of the compressor package and greasing of the fan bearings as per normal planned maintenance of rotating equipment. The filters themselves would require only periodic inspection of the compressed air valves, dust discharge valves and diverter valves.

9. CONCLUSIONS

Construction and testing at pilot scale (~1 m^3/s), and at much smaller sinter pot scale, of a novel filtration device, the KN Filter, has been carried out. This device employs metal mesh screens and relies on the building of a filter cake which then acts as the filtration medium. Otherwise operation is similar to that of a pulse jet bag filter.

Initial testing of the pilot filter on the direct (or 4th hole) extraction of an electric arc furnace demonstrated good filtration with predominantly sub-micron dust at temperatures up to 270°C. Operation at higher temperatures is possible. An average outlet dust loading of 10 mg/m^3 stp was achieved in active periods of furnace operation (during power input and oxygen injection) for an inlet dust concentration of 8 g/m^3 stp. Outlet dust concentrations as low as 3 mg/m^3 stp were achieved over a complete furnace operating cycle. Filter pressure drop was 16-22 mbar and filtration velocity was 1.4 m/min. These parameters are similar to those commonly encountered with fabric filters on EAF plants.

Installation on a side stream of the wind main of an operating sinter plant allowed extensive testing. Filtration performance was good with outlet dust loadings of 5 - 6 mg/m^3 stp for inlet loadings of 0.5 - 1 g/m^3 stp. Pressure drop was 15 mbar (1.5 kPa) which again is similar to fabric filter operation. Filtration velocity was 2.3 m/min, which is higher than would normally be chosen for a conventional fabric filter.

There was no apparent difference in performance with screen meshes of 0.125 and 0.16 mm aperture.

The filter operated without problem during a cold start of the sinter strand despite considerable condensation of water vapour. This would have been expected to cause severe difficulties with fabric bags.

Concurrent work with the smaller test filter on a sinter pot facility met with many problems, largely due to an inability to simulate industrial conditions for a sufficient period with the equipment. Subsequent tests with the same filter on a side stream from the wind main of a Spanish sinter plant were hampered by condensation and other operational difficulties, but demonstrated promising performance under adverse conditions.

The composition of the collected dust in the pilot filter indicated that the smaller particles, relatively rich in alkali chlorides, lead, zinc and sulphur, predominate on the filter screens, whereas the larger particles (more typical of sinter bed materials) tend to settle out of the gas stream before the screens. A combination of a cyclone or settling chamber and a KN Filter may therefore provide an effective configuration, allowing segregation of less desirable components for separate treatment.

Capture of heavy metals was improved in proportion to dust filtration performance when compared with the electrostatic precipitator. Typically outlet concentrations were ¼ of those in the main stack after the ESP.

Radioactive species in the outlet dust were reduced by 95% compared with the main stack.

As has been shown with ESPs, the injection of carbon based sorbents, such as steam activated carbon and lignite coke, can be used to reduce emissions of trace organic micropollutants. The injection of steam activated carbon and lignite coke powders effectively reduced emissions of trace organic micropollutants. Although the effect of dosing rate was not fully established, levels of 0.1 - 0.2 ng I-TEQ/m^3 stp of PCDD/F were achieved, compared with a typical level of 1 ng I-TEQ/m^3 stp in the main stack. PAH compounds were reduced by around 75%, and PCB compounds by a half.

Samples of candidate mesh materials continuously exposed to wind main conditions for a year showed little evidence of corrosive attack, but the abrasive conditions might have masked some evidence of corrosion. Further verification is needed.

An outline design of a full scale filter with associated costs has been prepared. Costs are similar to those expected for a fabric filter, but operating costs should be less.

In summary, the testing of a KN Filter on sinter plant wind main gas has shown considerable promise in abating emissions to atmosphere of dust, associated heavy metals and radioactive species, and trace organic compounds. The device has the potential to give bag filter performance without the drawbacks of fabrics in this application. Some design modifications, notably to the outlet diverter valves, may be beneficial. An application has been made for an ECSC Pilot/Demonstration Project to allow longer term testing at larger scale.

Although good performance has been demonstrated with raw wind main gas there are still questions regarding a possible configuration in which the filter would follow an electrostatic precipitator, as might be the case in a retrofit application. The characteristics of the dust presented to the filter would be quite different in this case and it would be necessary to test whether acceptable pressure drop at reasonable filtration velocity can be achieved.

REFERENCES

1. Integrated Pollution Prevention and Control (IPPC); Best Available Technologies Reference Document on the Production of Iron and Steel, European Commission, http://eippcb.jrc.es.

2. Integrated Pollution Prevention and Control (IPPC); Guidance for the Coke, Iron and Steel Sector; Sector Guidance Note IPP S2.01 (Draft); Environment Agency.

3. K. Kersting, J. Wirling, W. Esser-Schmittmann and U. Lenz: 'Removal of Dioxins and Furans from Waste Gases of a Sintering Plant by Using Lignite Coke', Stahl und Eisen, 1997, Vol. 117, pp49-55.

TABLE 1
SCUNTHORPE ESP ENTRY CONDITIONS

Parameter	Value	Units
Gas Temperature	158	°C
Pressure	-121	mm Hg
Mean Velocity	8.2	m/s (at duct conditions)
Flow	206	m^3/s (at duct conditions)
Flow	98	m^3/s stp(dry)
O_2	15	%,dry
CO_2	6	%,dry
$CO + N_2$	79	%,dry
Moisture	11	%
Dust Concentration (Strand 1)	481	mg/m^3 stp (mean of 3 samples)
Dust Concentration (Strand 2)	998	mg/m^3 stp (mean of 3 samples)

TABLE 2
DATA FROM CSI PLANOS (G-7 LINE BEFORE PRECIPITATOR)

Sample	Particles (mg/m^3 stp)		SO_2 (mg/m^3 stp)		NO_x (mg/m^3 stp)	
	Measured	Corrected for 8% O_2	Measured	Corrected for 8% O_2	Measured	Corrected for 8% O_2
1	-	-	392	1018	-	-
2	391	1015	310	806	256	666
3	493	1282	477	1241	243	632

TABLE 3
SUMMARY OF FILTER PERFORMANCE ON EAF

Flow	0.6 m^3/s (actual)
Pressure Drop (Initial Tests)	24 - 28 mbar
Pressure Drop (Final Tests)	16 - 22 mbar
Inlet Temperature	Up to 270°C
Filter Area (3 compartments)	26.2 m^2
Filtration Velocity	1.4 m/min
Average Inlet Dust Loading	8 g/m^3 stp
Average Outlet Dust Loading	10 mg/m^3 stp

TABLE 4
CLEANING CYCLE DEVELOPED FOR SINTER PLANT

1	Compartment changeover
2	20 s delay
3	Pulse both tube banks in off-line compartment. Pulse duration 200 ms. Pulse pressure approx. 1 bar gauge
4	5 s delay
5	Start recirculation fan for cake building
6	Stop recirculation fan when pressure drop across off-line compartment reaches setpoint (12.5 mbar)
7	Bring newly conditioned compartment on-line and take next compartment off-line

TABLE 5
INITIAL OUTLET DUST LOADINGS – SINTER PLANT

Sample Duration (min)	Dust Concentration mg/m^3 stp
20	6.0
10	11.0
20	2.0
20	11.1
10	8.7
10	23.8*
10	10.9*
10	3.8
20	4.9*
12	10.2*

* Test includes compartment changeover

TABLE 6
SUMMARY OF EARLY PERFORMANCE ON SINTER PLANT

Flow	1 m^3/s (actual)
Pressure drop	12.5 - 17.5 mbar
Inlet temperature	approx. 130°C
Filter area (3 chambers)	26.2 m^2
Filtration velocity	2.3 -2.4 m/min
Outlet dust loading	9 mg/m^3 stp

TABLE 7
OUTLET DUST LOADINGS AFTER VALVE REFURBISHMENT

Sample No.	Duration (min)	Dust Loading (mg/m^3 stp)	Filter Pressure Drop (mbar)
329	20	5.9	14.7
330	10	1.6	16.4
331	9	3.0	16
333	14	1.5	13.4
334	16	5.3	16.2
335	16	7.0	15.7
336	20	3.4	18.6
337	16	9.8	15.7
338	20	5.3	16.7
Mean		4.8	

TABLE 8
INLET DUST LOADINGS

Sample No.	Duration (min)	Dust Loading (g/m^3 stp)
94	20	0.94
50	20	1.32
43	20	1.01
30	20	0.83
Mean		1.03

TABLE 9
COMPOSITION OF DUST FROM BINS AND 'A' SCREEN

Source	SiO_2	CaO	MgO	MnO	Al_2O_3	Fe_2O_3	K	Na	Cl	Pb	Zn	C	S	LOI
Bin A	7.4	6.3	3.1	0.4	1.7	74.0	0.05	0.03	0.19	0.29	0.17	2.3	0.32	4.79
Bin B	7.0	6.7	3.0	0.4	1.6	72.6	0.14	0.06	0.34	0.26	0.17	2.5	0.40	6.21
Bin C	7.5	7.2	3.1	0.6	1.6	69.1	0.15	0.07	0.52	0.24	0.24	3.6	0.38	8.75
Bin D	6.2	8.2	2.4	0.8	1.5	65.4	0.68	0.30	1.38	0.33	0.99	2.8	1.00	10.00
Screen A	4.8	13.1	1.3	0.3	1.7	48.6	1.84	0.58	2.83	0.61	0.22	5.2	1.80	22.60

TABLE 10
SUMMARY OF EDA COUNTS PER SECOND FOR ALL PARTICLES EXAMINED

	Na	Mg	Al	Si	P	S	Cl	K	Ca	Mn	Fe
4 µm	0.2	0.2	2.0	6.5	1.0	2.2	10.0	3.0	12+	0.2	6.0
5 µm	0.4	0.5	1.0	3.0	0.5	1.0	3.0	1.5	13+	0.2	0.5
8 µm	-	0.5	1.0	2.5	-	1.0	2.5	1.5	17+	-	1.0
8 µm	0.5	1.0	2.5	6.0	-	2.5	21+	3.0	12.5+	-	2.0
12 µm	0.1	<0.1	0.2	0.6	-	0.2	0.9	0.4	4+	-	3.0
20 µm	0.5	0.5	1.5	4.0	0.7	2.2	4+	2.8	0.5	-	0.7
20 µm	0.2	0.3	1.9	8.8	0.4	4.2	8.2	9+	4.8	-	1.0
20 µm	0.7	-	1.8	6.0	-	3.2	7+	7.0	5.4	-	2.5

TABLE 11
DUST COMPOSITION FROM METALS SAMPLING TESTS

Component	ESP Inlet[1] ($\mu g/m^3$ stp (dry))	ESP Outlet[1] ($\mu g/m^3$ stp (dry))	Pilot Filter Outlet ($\mu g/m^3$ stp (dry))
Pb	3076	850	199
Zn	1019	44	14
Cd	23	6	1.5
Cu	493	79	21
Mn	923	30	8
Se	152	36	8
Fe	57797	2588	598
Na	3394	901	86
K	13509	2990	744
SO_4	36299	<1000	207
Dust (mg/m^3 stp)	437	23.4	6.2

Note: 1 – mean of 3 samples

TABLE 12
METALS REMOVAL EFFICIENCY

Component	ESP % Removal	Pilot Filter % Removal	Outlet Concentration Ratio ESP:filter
Pb	72.4	93.5	4.27
Zn	95.7	98.6	3.17
Cd	73.9	93.5	4.19
Cu	84	95.7	3.74
Mn	96.7	99.1	3.77
Se	76.3	94.7	4.49
Fe	95.6	99	4.28
Na	73.5	97.5	10.48
K	77.9	94.3	4.02
SO_4	97.2	99.4	-
Dust	94.6	98.6	3.77

TABLE 13
RESULTS FROM SAMPLING FOR RADIOACTIVE SPECIES

	Particulate Concentration (mg/m^3 stp (dry))	Po-210 Concentration (Bq/m^3 stp (dry))	Pb-210 Concentration (Bq/m^3 stp (dry))
ESP outlet (sample 1)	55.5	3.19	0.65
ESP outlet (sample 2)	34.7	6.3	1.17
ESP mean	45.1	4.75	0.91
Pilot filter outlet	2.23	0.25	0.04
Reduction	95%	95%	96%

TABLE 14
SUMMARY OF RESULTS FROM FIRST CARBON INJECTION TESTS

Emission Samples – PCDD/F

Carbon Injection	PCDD/F (ng I-TEQ/m^3 stp)
No	0.96
No	0.94
Yes	0.49
Yes	0.3

Dust Samples – PCDD/F

Source	PCDD/F (ng I-TEQ/kg)
Before Injection	69
After Injection	254
Screens	2731

Emission Samples – PAHs
Main species naphthalene (44%) and phenanthrene (23%)

Carbon Injection	PAH (US EPA 16) (µg/m^3 stp)
No	73.5
No	85.7
Yes	26.7
Yes	25.5

Emission Samples – PCBs
Sum of tri- to hepta- chloro substituted biphenyls.
Dominated by tri- and tetra-chlorinated homologues

Carbon Injection	Total PCB (ng/m^3 stp)
No	1342
Yes	756

TABLE 15
SUMMARY OF RESULTS FROM CARBON AND LIGNITE COKE INJECTION TESTS

Case	Mean % C in Dust from Screens	Measured			Adjusted for Inleakage Across Filter		
		Outlet Dust Loading (mg/m^3 stp)	PCDD/F ($ng\ I\text{-}TEQ/m^3$ stp)	PAH EPA 16 Targeted ($\mu g/m^3$ stp)	Outlet Dust Loading (mg/m^3 stp)	PCDD/F ($ng\ I\text{-}TEQ/m^3$ stp)	PAH EPA-16 Targeted ($\mu g/m^3$ stp)
Base (no injection)	-	3.2 3.5 5.4 7.5	-	-	3.7 4.0 6.2 8.6	-	-
Base (no injection)	5.2	-	0.22	51.1	-	0.25	58.8
Lignite coke (63 µm) 2 g/min	7.9	6.8 14.5	0.31	25.2	7.8 16.7	0.36	29.0
Lignite coke (63 µm) 6 g/min	16.3	6.4 11.5	0.12	16.1	7.4 13.2	0.14	18.5
Lignite coke (63 µm) 10 g/min	22	12.6	0.16	16.4	14.5	0.18	18.9
Lignite coke (28 µm) 2 g/min	17.2	13.4 17.5	0.20	106	15.4 20.1	0.23	121.9
Lignite coke (28 µm) 6 g/min	21.8	8.5 17.4	0.34	43.8	9.8 20.0	0.39	50.4
Lignite coke (28 µm) 10 g/min	23.1	38.2*	0.23	28.7	43.9*	0.26	33.0
Steam activated carbon 2 g/min	18.7	-	0.18	69.8	-	0.21	80.3
Steam activated carbon 6 g/min	18.2	10.1 16.4	0.16	41.5	11.6 18.9	0.18	47.7
Base (no injection)	14.8	8.8	0.20	94.9	10.1	0.23	109.1
Inlet	-	-	0.65	109	-	-	-

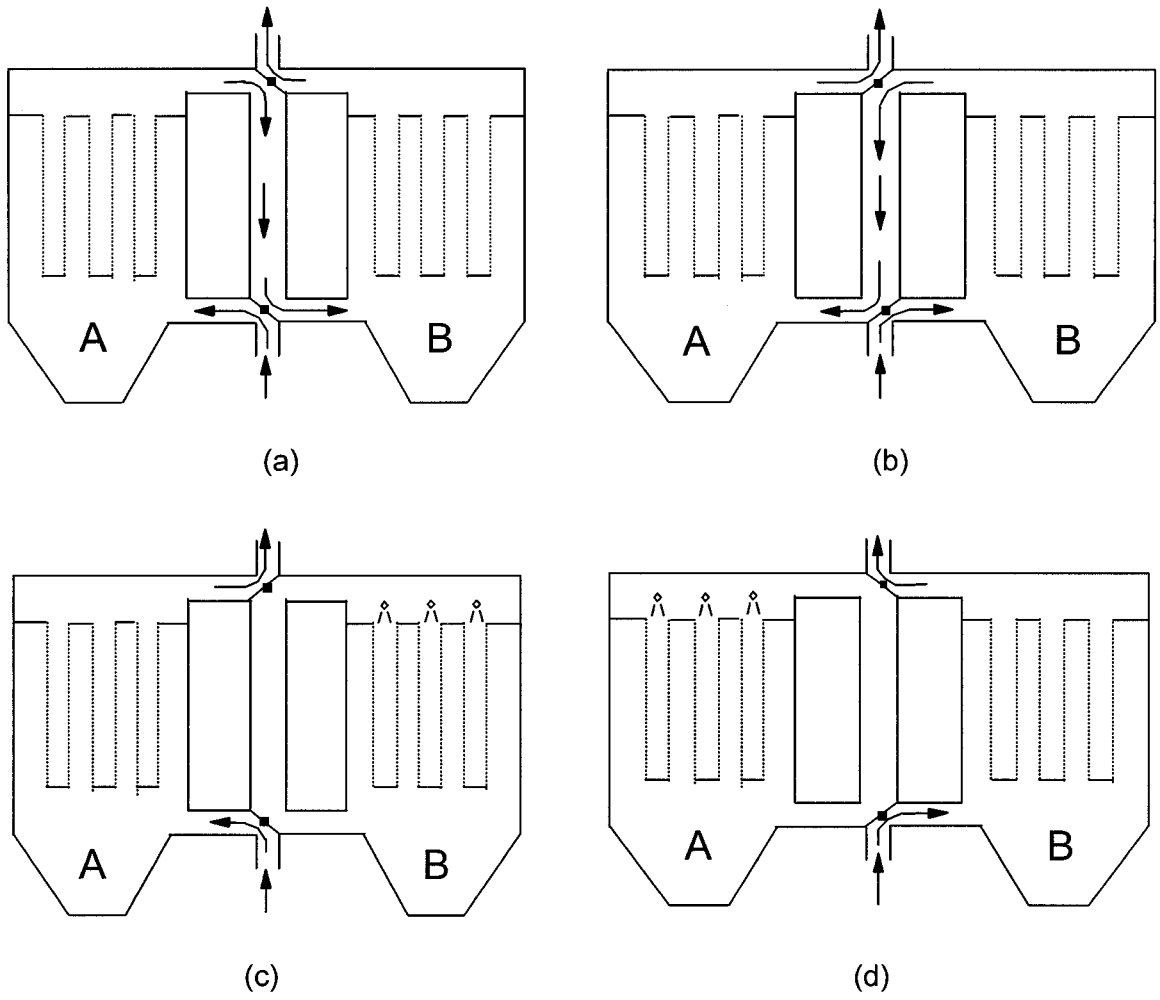

FIG. 1(a-d) **OPERATING PRINCIPLES OF THE KN FILTER** **(D0231J07)**

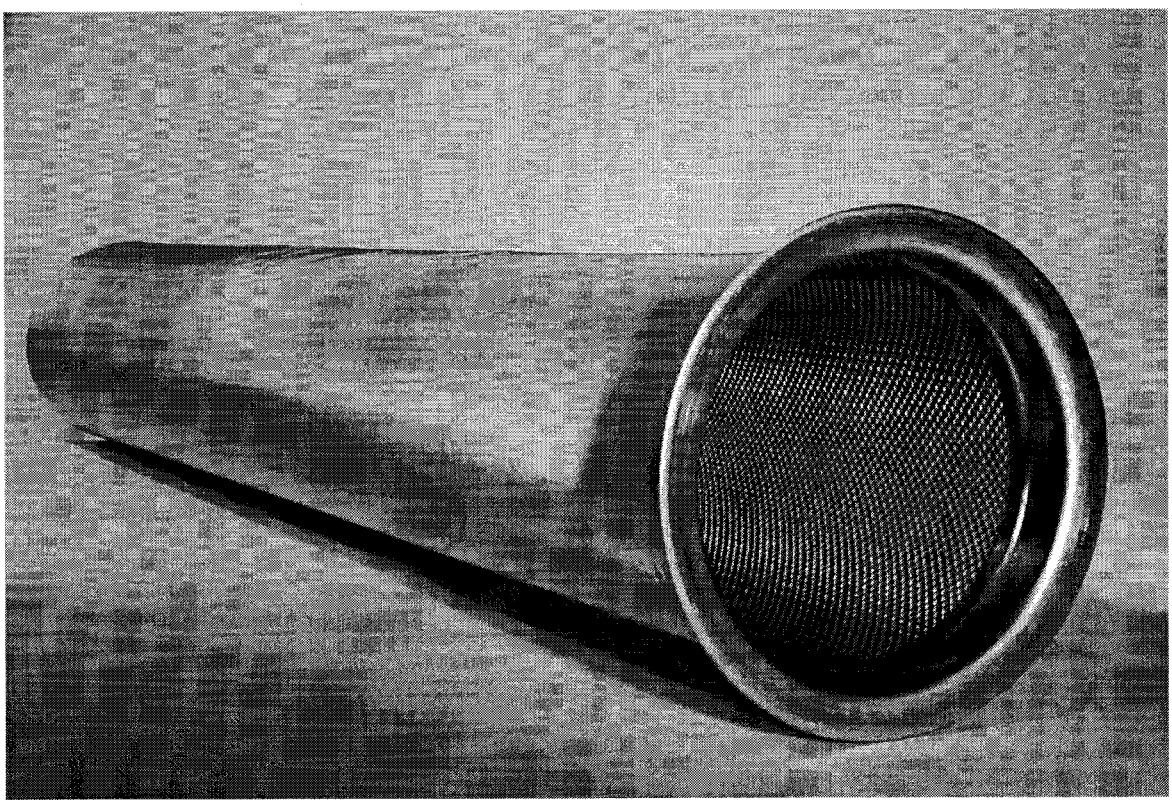

FIG. 2 **TYPICAL FILTER SCREEN SHOWING INTERNAL SUPPORT MESH** **(D0231J07)**

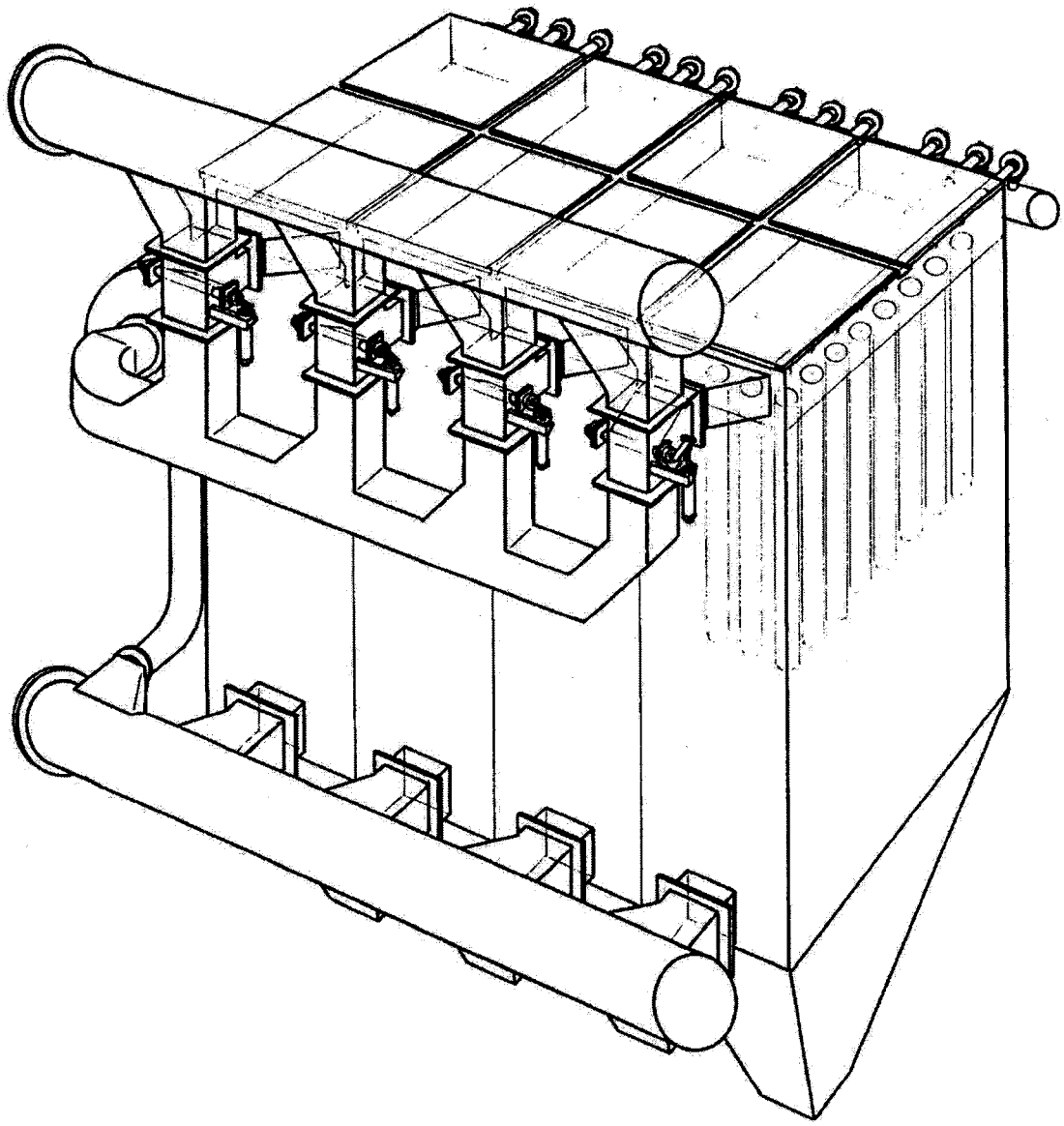

FIG. 3 **NEW FILTER DESIGN**

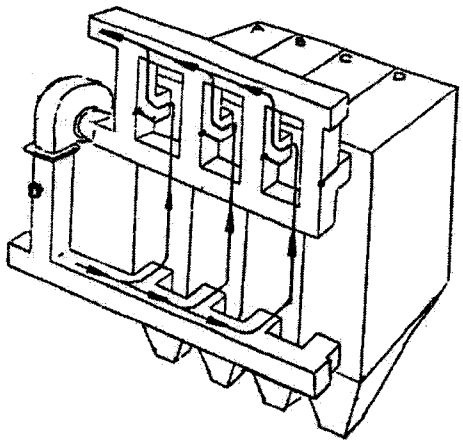

LEFT - Normal operation with 3 **run** on line, in this case A,B & C. The filter will continue in this mode until a cleaning cycle is signalled. Chamber D has been cleaned and is **standing by**.

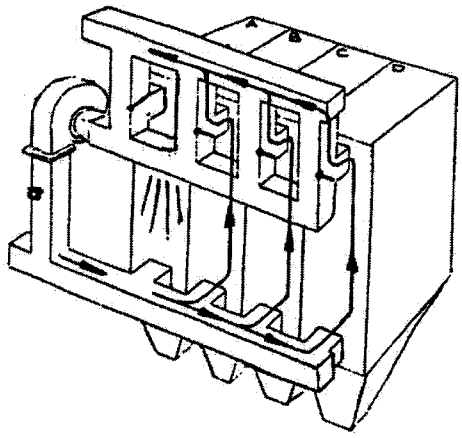

RIGHT - Cleaning cycle signalled. Chamber A taken off line and isolated for cleaning. Now 3 **run** on line B,C,D. A delay period after pulse cleaning allows removed dust to settle.

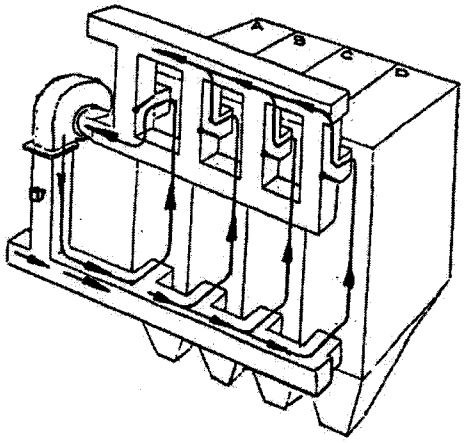

LEFT - Fan ON, circulating dust laden air to the cleaned filter screens in order to re-establish the full filter cake. This process uses the **run** chambers as second stage in the KN-FILTER 2 stage patented process.
When recaking is achieved the chamber is **standing by** for the next cleaning cycle.

PULSE CLEANING CYCLE WITH CIRCULATING FAN FOR CAKE REBUILDING

FIG. 4 **FILTER OPERATION**

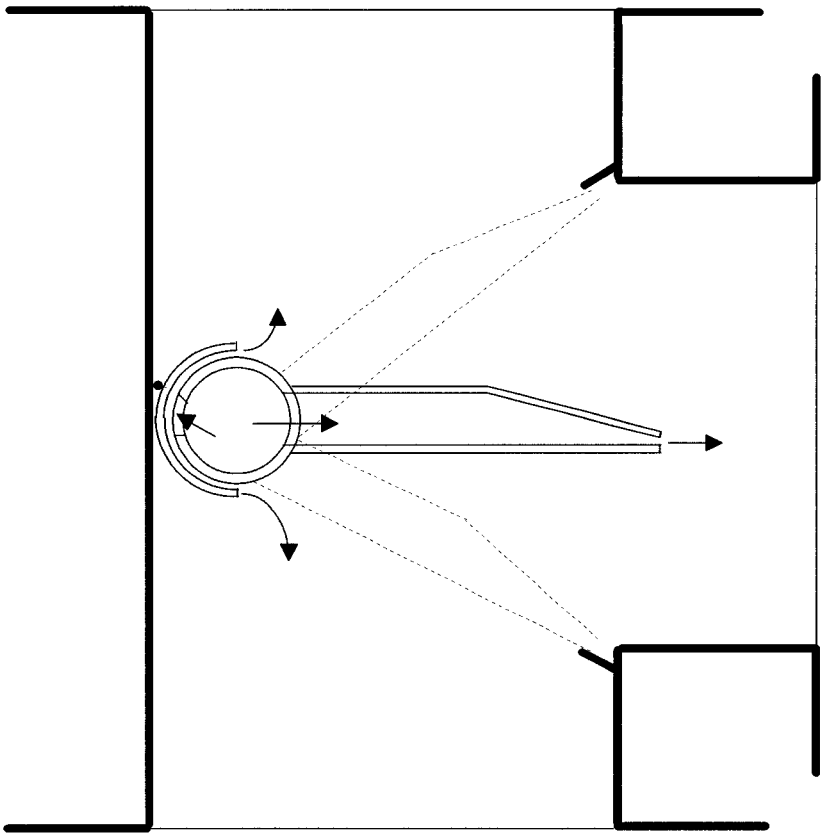

FIG. 5 SECTION THROUGH OUTLET DIVERTER VALVE (D0231J07)

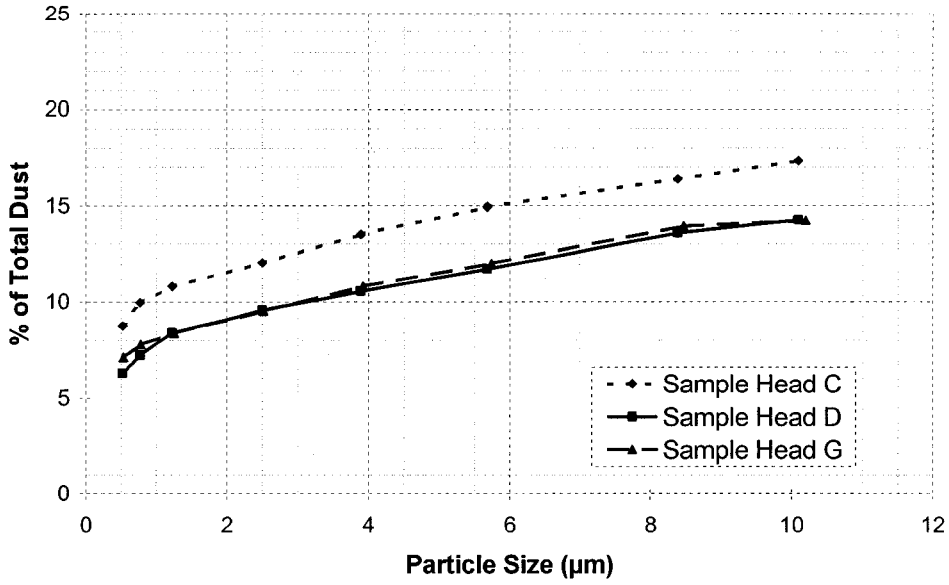

FIG. 6 CUMULATIVE PARTICLE SIZE DISTRIBUTION (D0231J07)
No. 1 ESP INLET

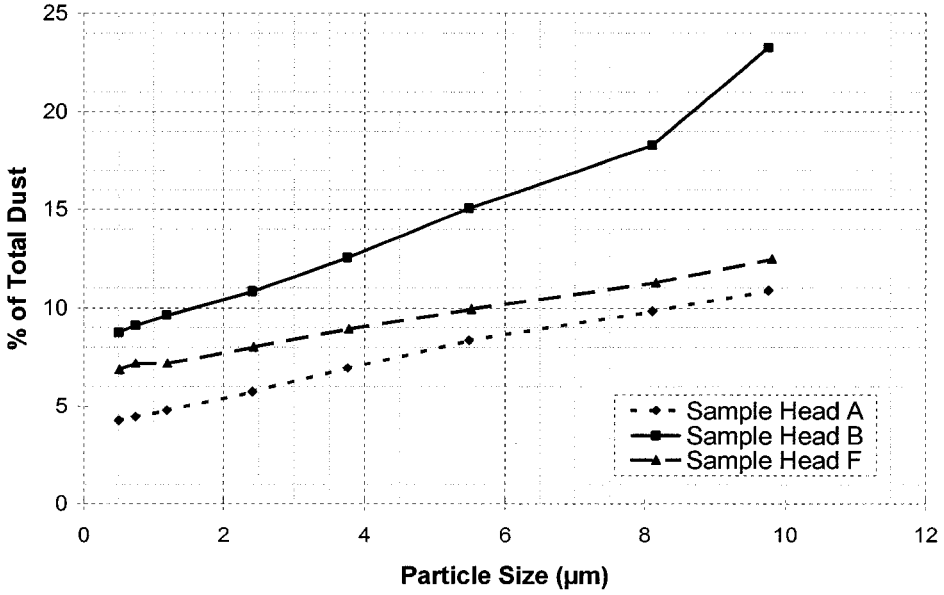

FIG. 7 CULMULATIVE PARTICLE SIZE DISTRIBUTION (D0231J07)
No. 2 ESP INLET

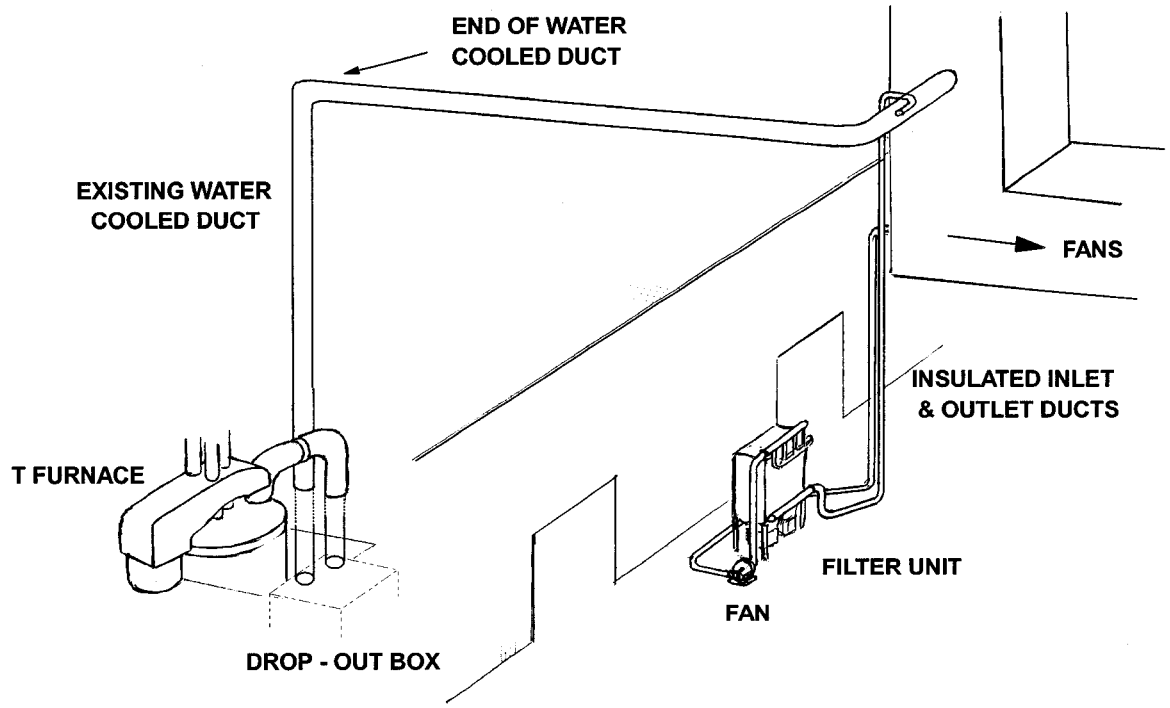

FIG. 8 SKETCH OF FILTER INSTALLATION ON EAF PLANT (D0231J07)

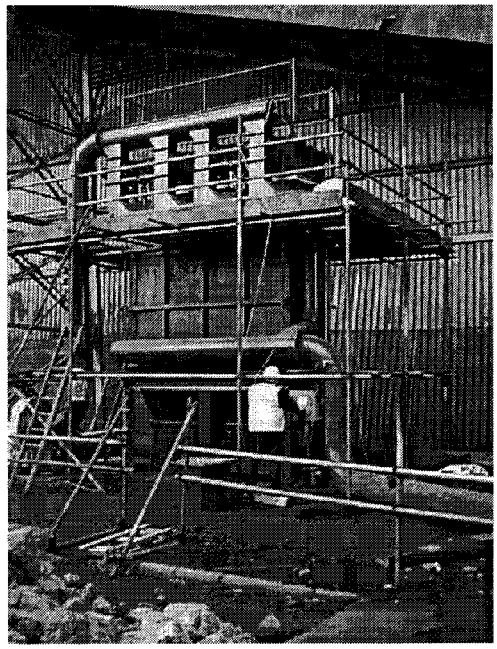

General View

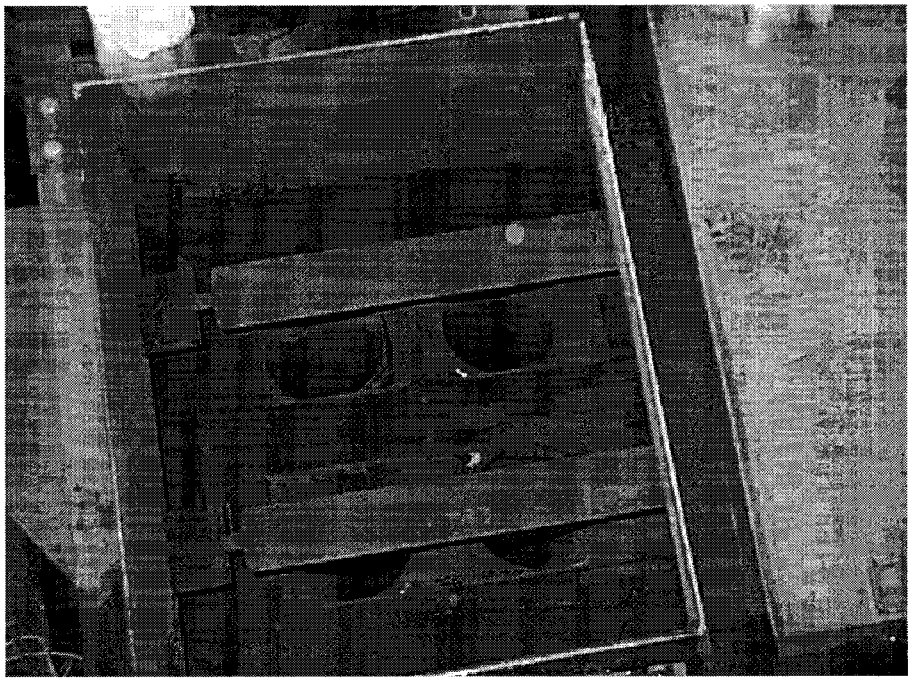

Pulse Air Supplies Over Filter Tubes (Lid Removed)

FIG. 9 **DIGITAL IMAGES OF FILTER (1)** **(D0231J07)**

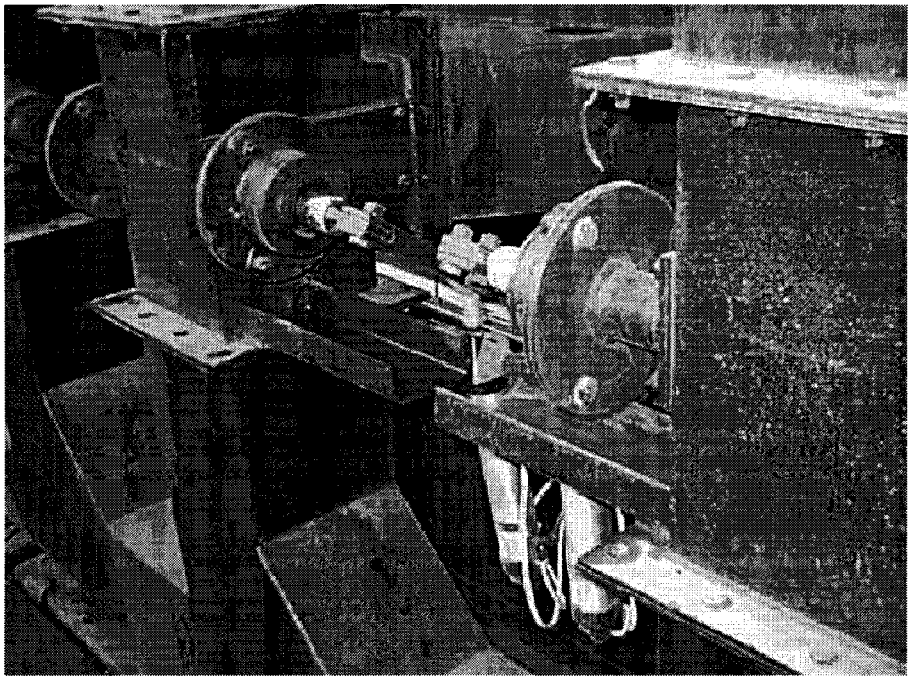

Outlet/Recirculation Valves

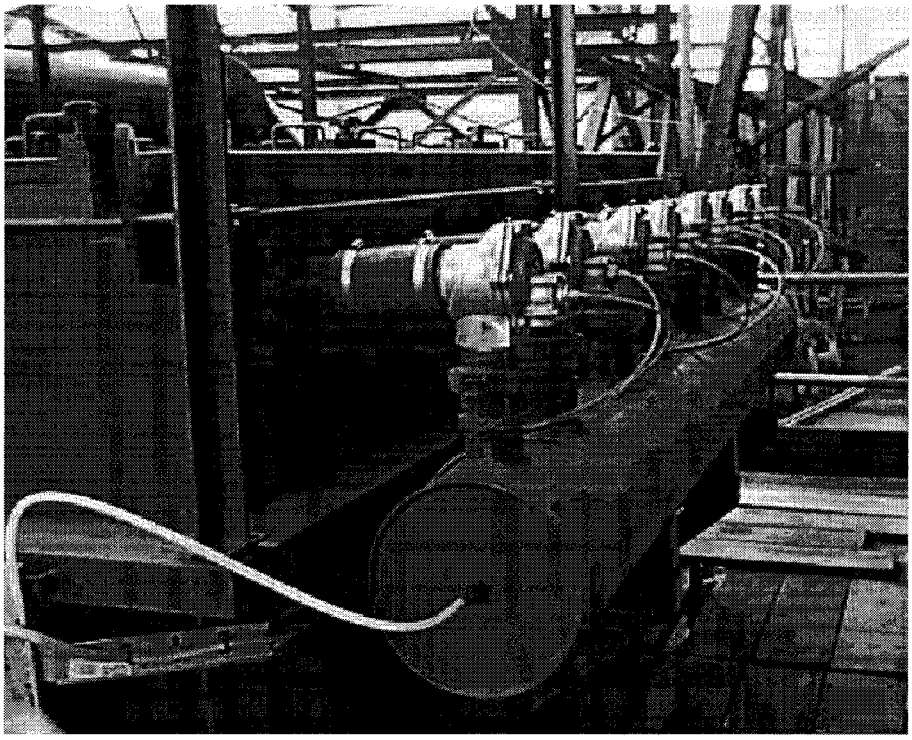

Pulse Air Manifold

FIG. 10 **DIGITAL IMAGES OF FILTER (2)** **(D0231J07)**

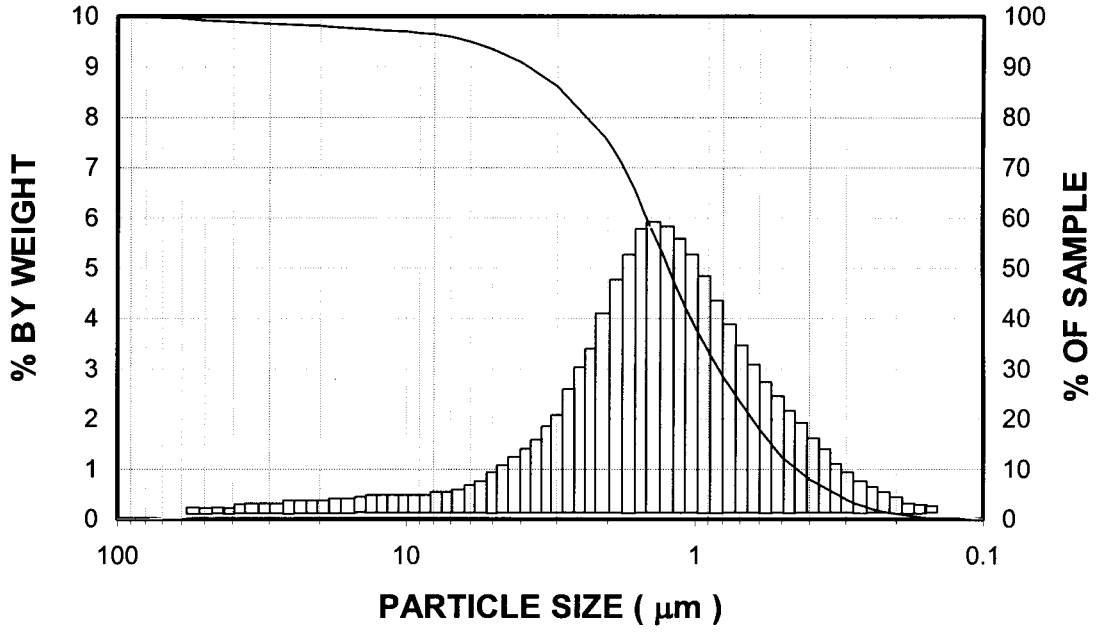

FIG. 11 TYPICAL EAF FUME PARTICLE SIZE DISTRIBUTION (D0231J07)

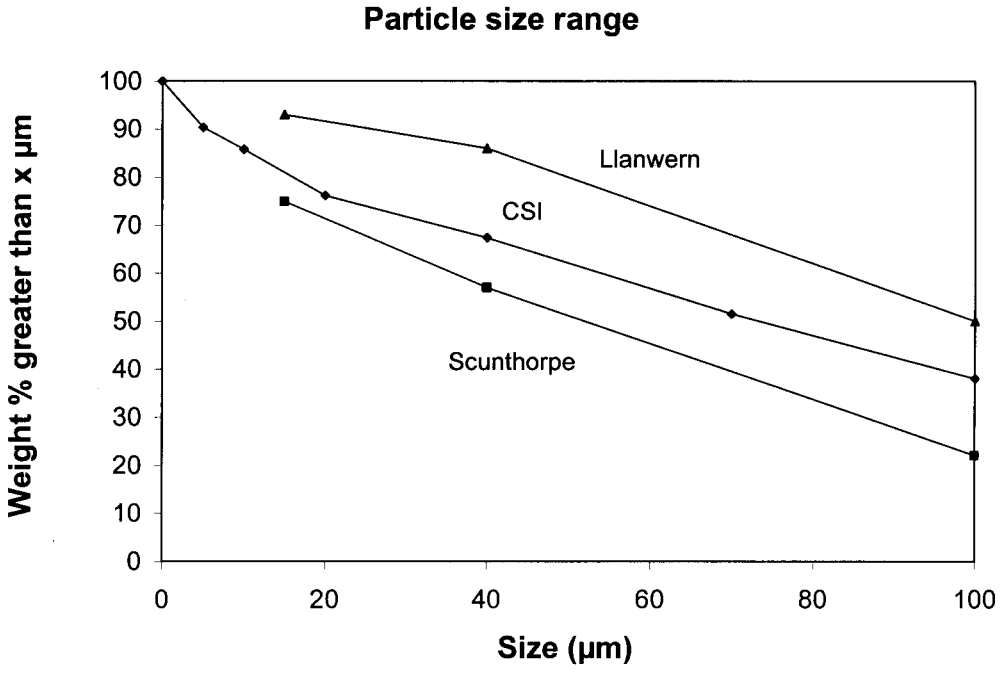

FIG. 12 SINTERING ESP DUST SIZE (D0231J07)

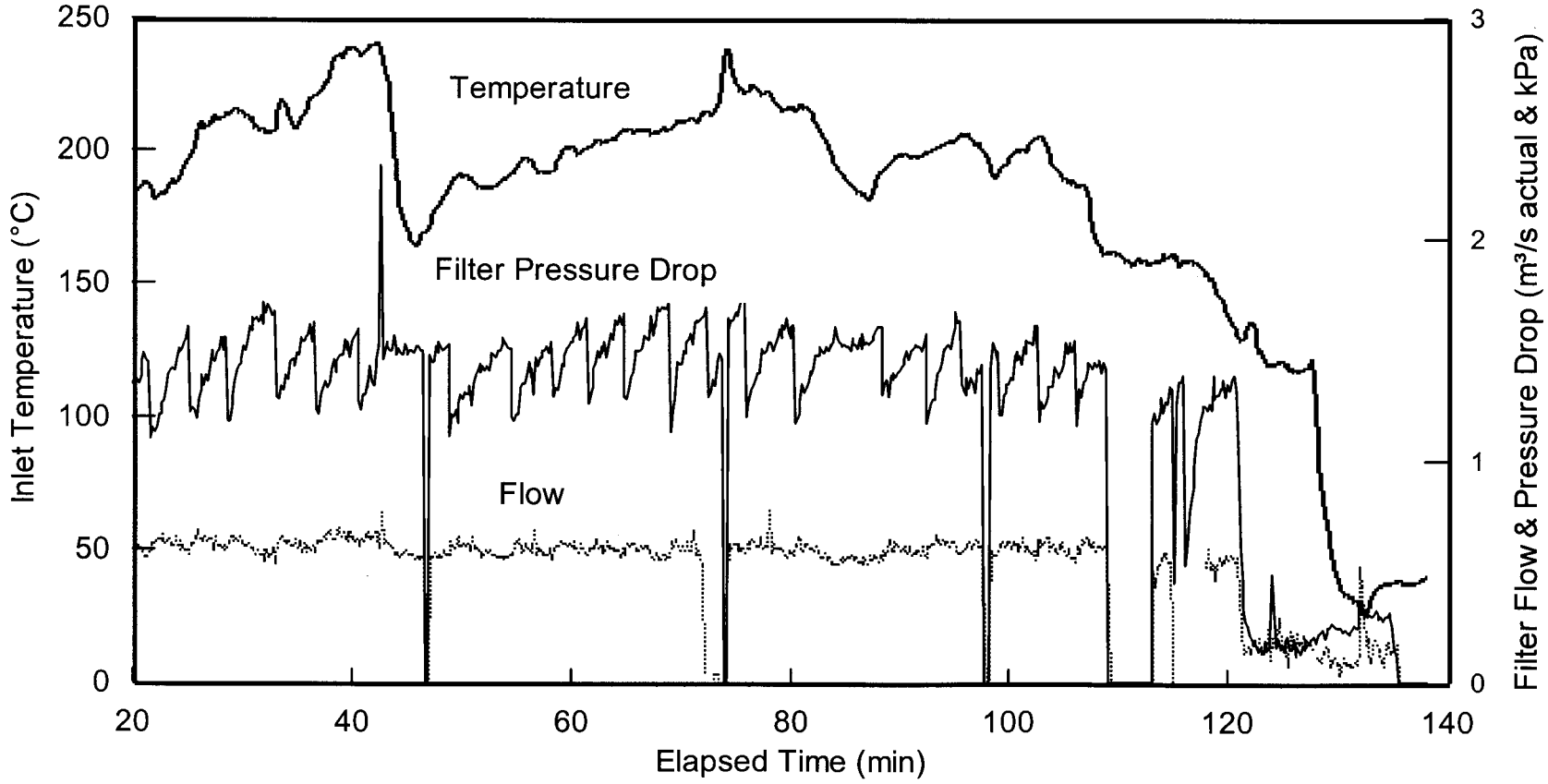

FIG. 13 **FILTER OPERATING PARAMETERS AFTER COMMISSIONING** **(D0231J08)**

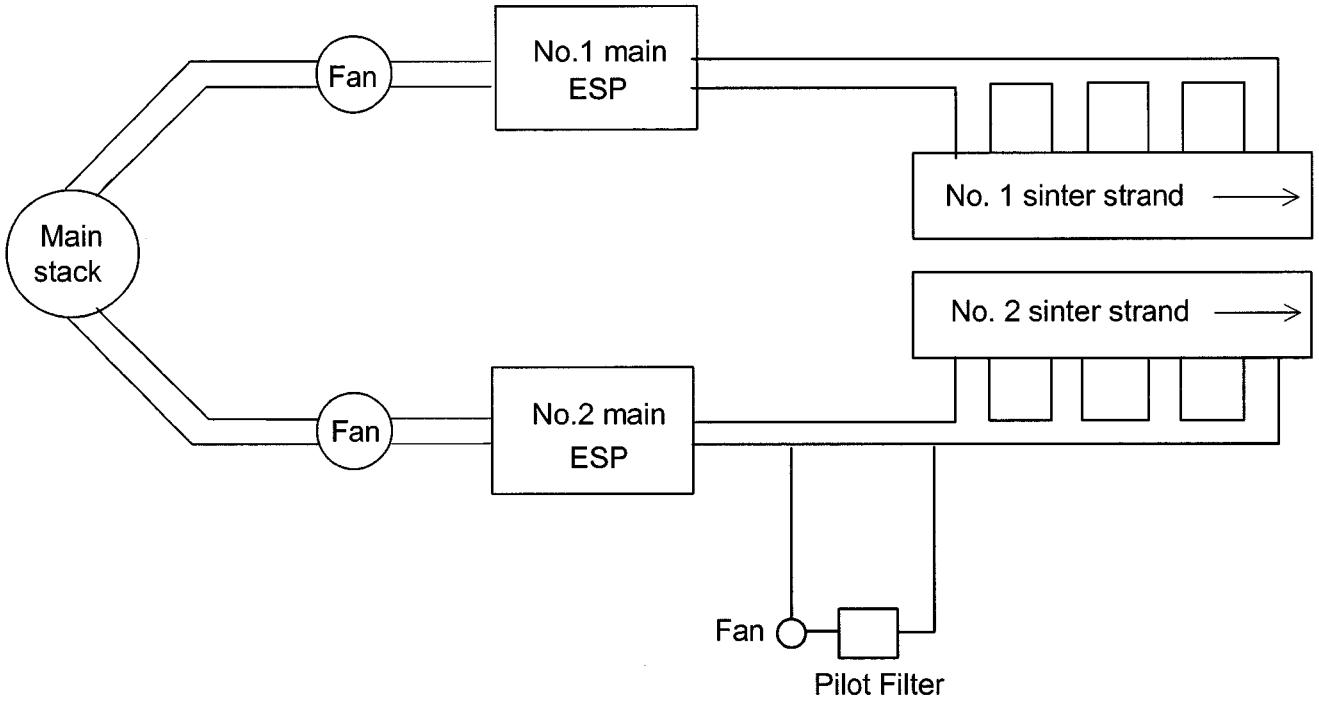

FIG. 14 **FILTER SITE FOR SINTER PLANT TESTS** **(D0231J08)**

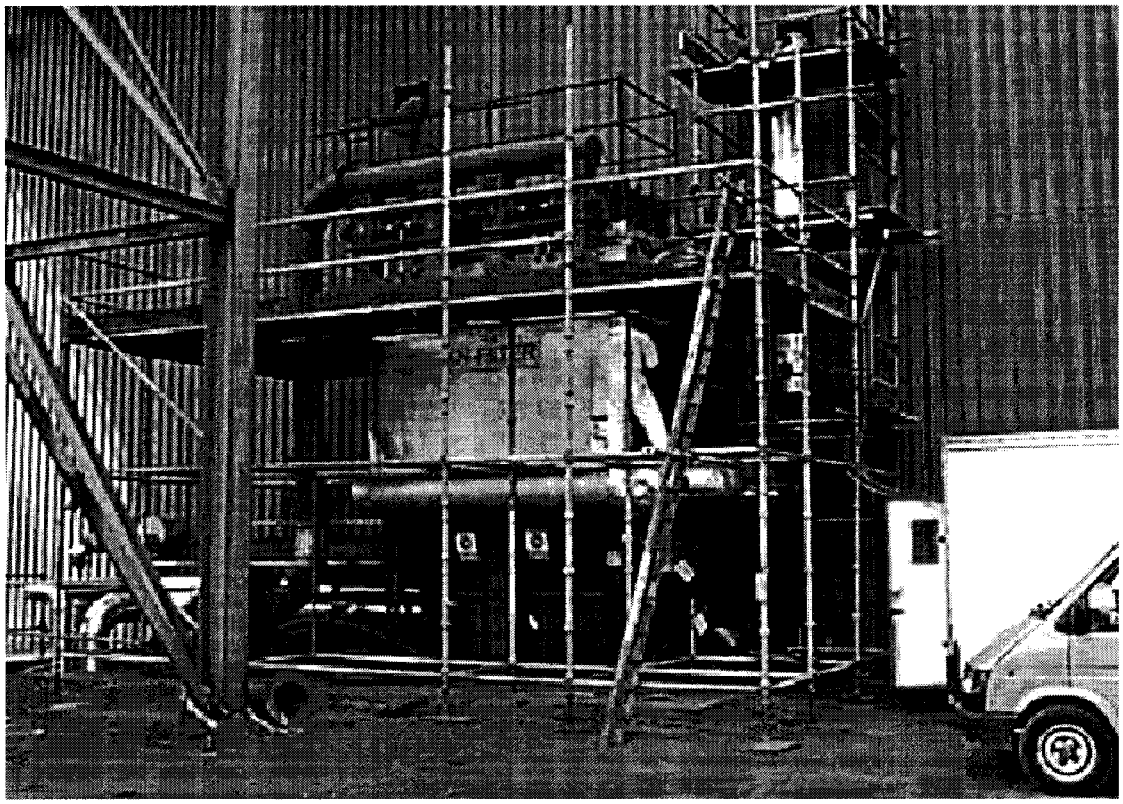

FIG. 15 GENERAL VIEW OF PILOT FILTER AT SCUNTHORPE SINTER PLANT (D0231J09)

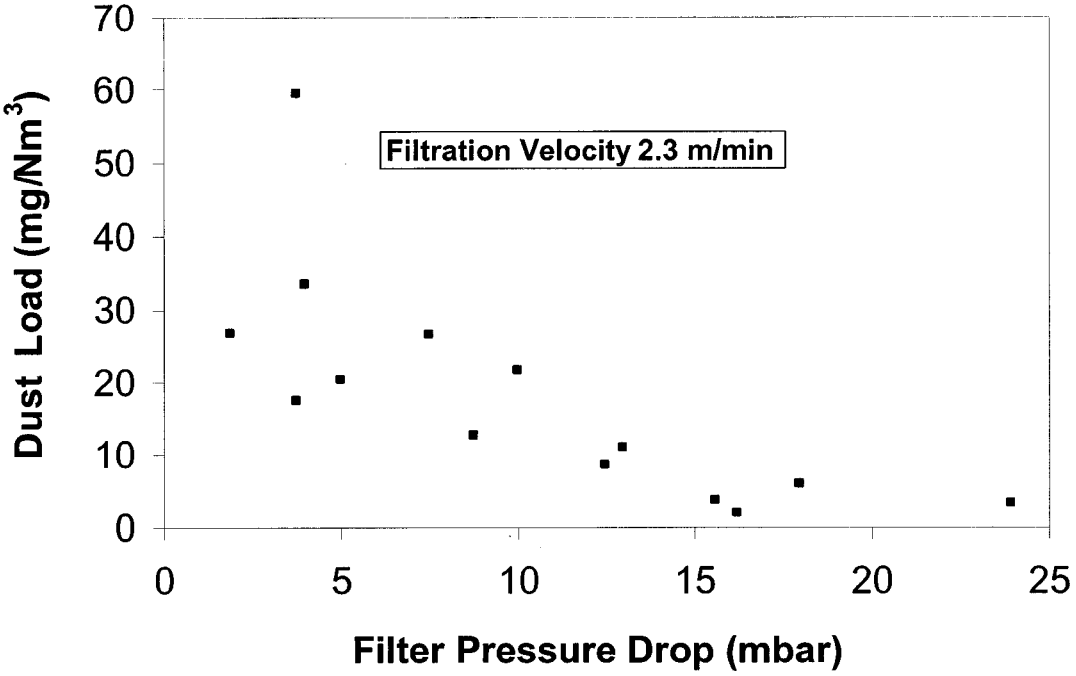

FIG. 16 OUTLET DUST v PRESSURE DROP TESTS (D0231J09)

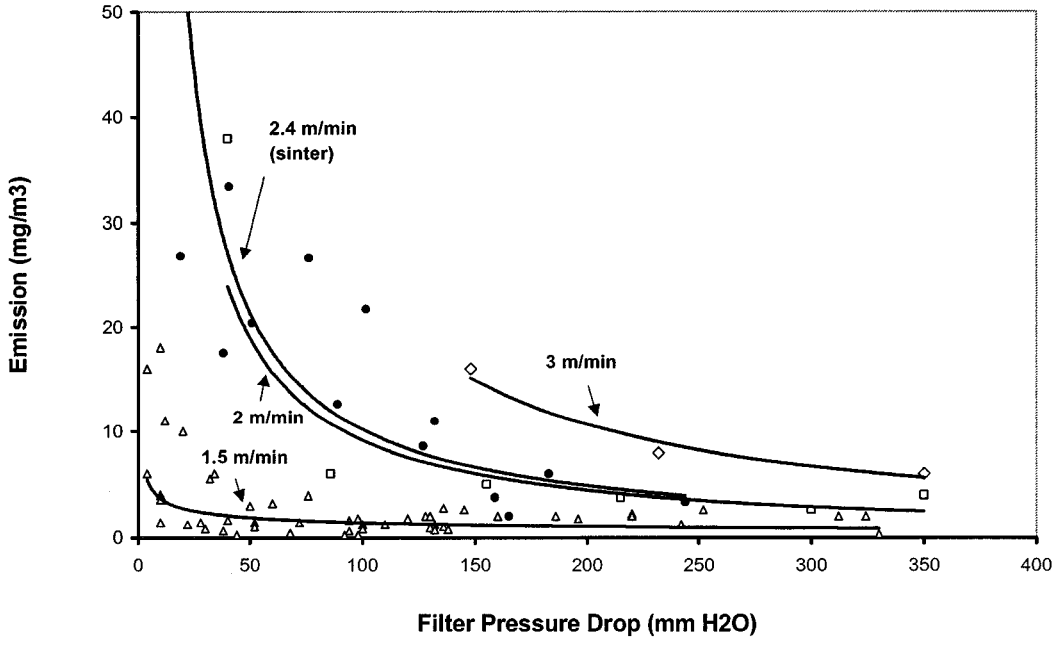

FIG. 17 COMPARISON WITH PFA TEST DATA AT DIFFERENT FILTRATION VELOCITIES (D0231J09)

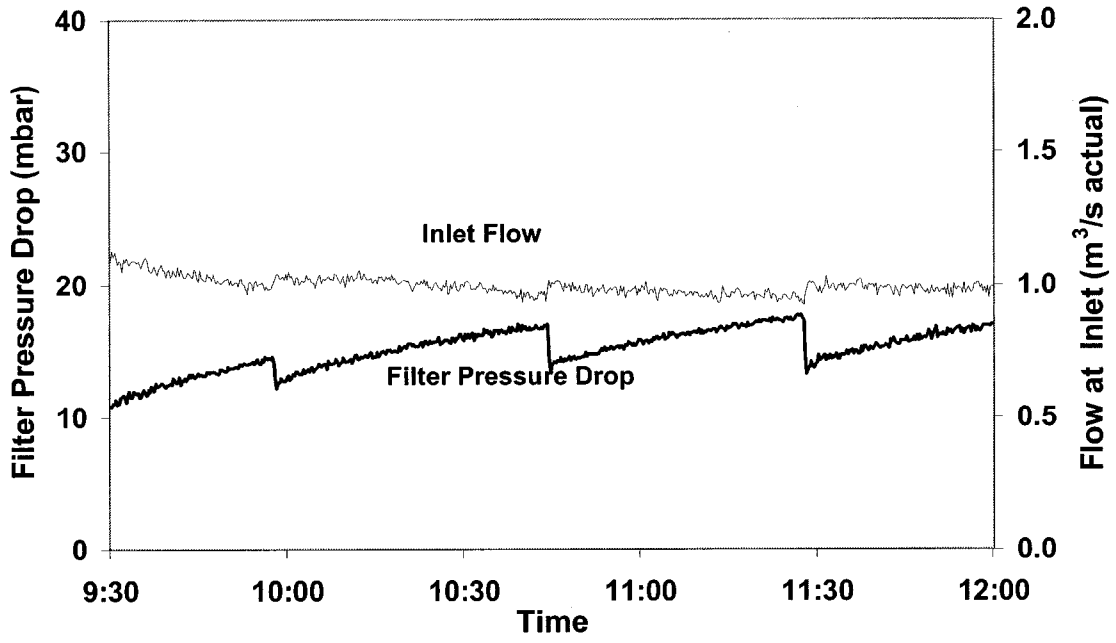

FIG. 18 EARLY OPERATING DATA – SINTER PLANT (D0231J09)

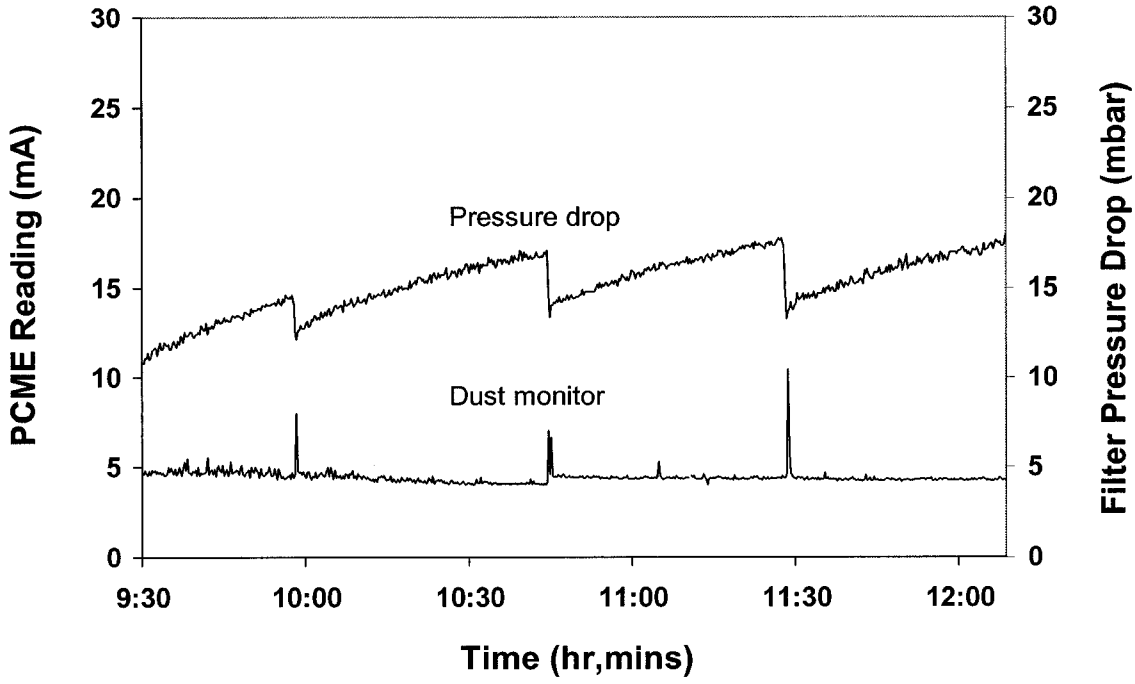

FIG. 19 CONTINUOUS DUST MONITOR TRACE - SINTER PLANT (D0231J09)

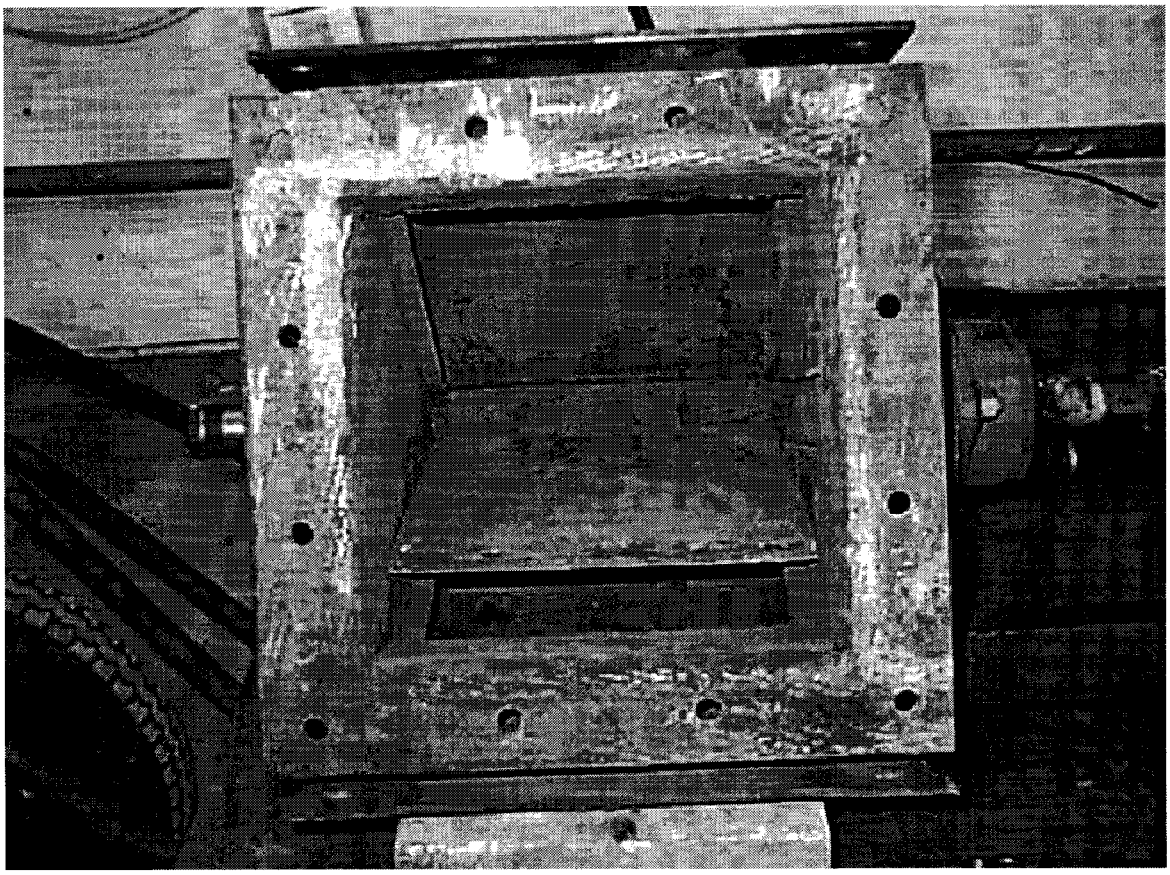

FIG. 20 VALVE CASSETTE AFTER REMOVAL FROM FILTER (D0231J09)

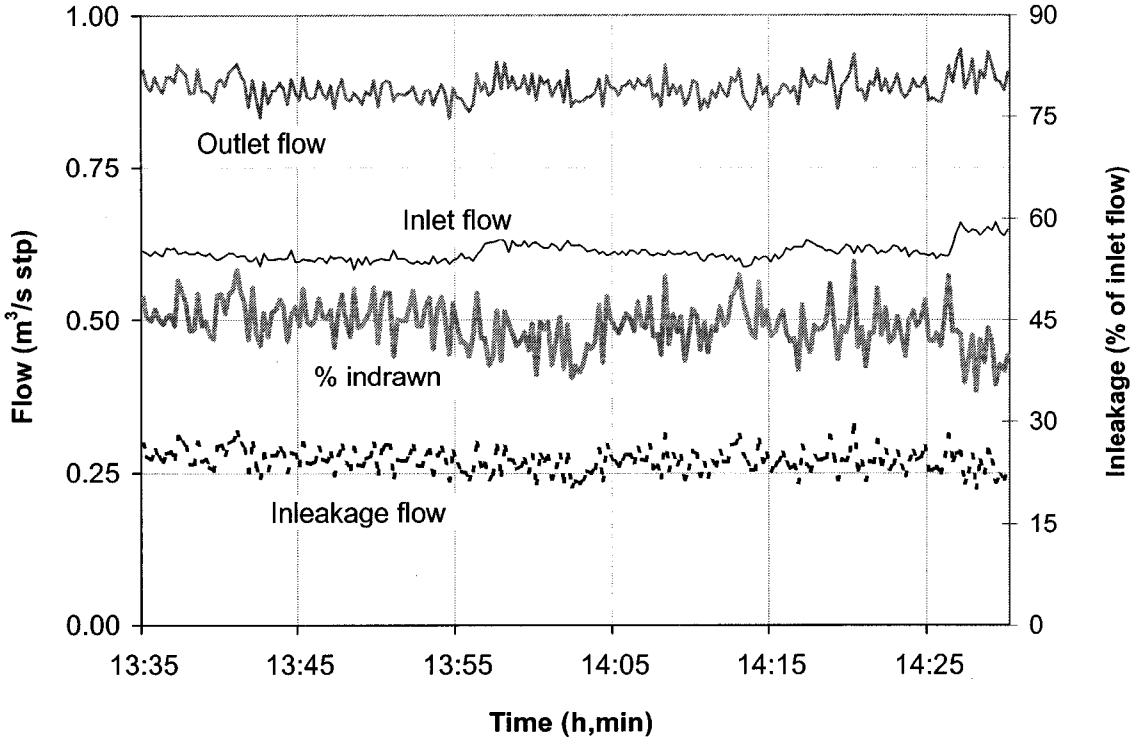

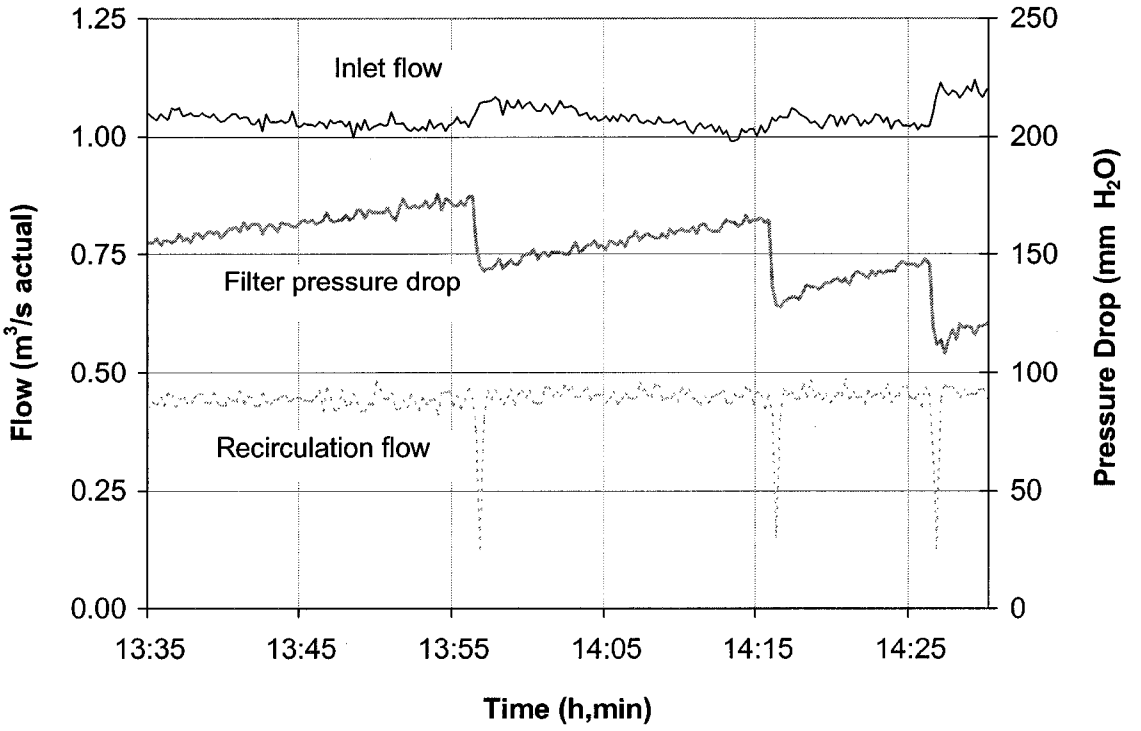

FIG. 21 EXAMPLE OF OPERATION DURING INLEAKAGE TESTS (D0231J09)

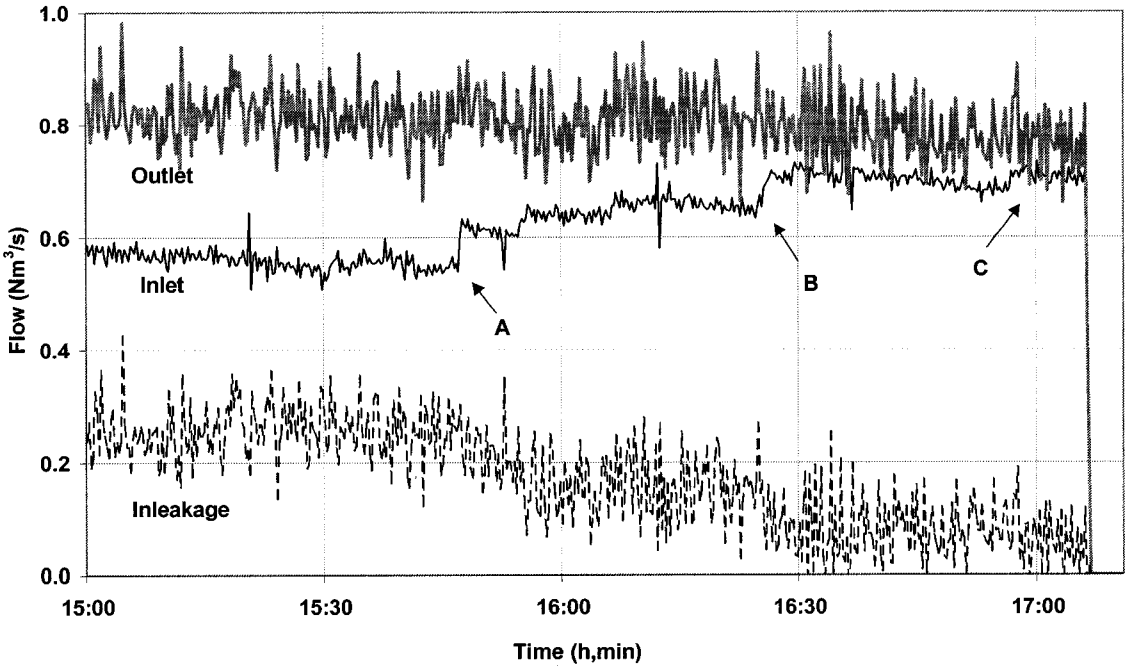

FIG. 22 FLOW TRACES DURING SEALING AIR TESTS (D0231J09)

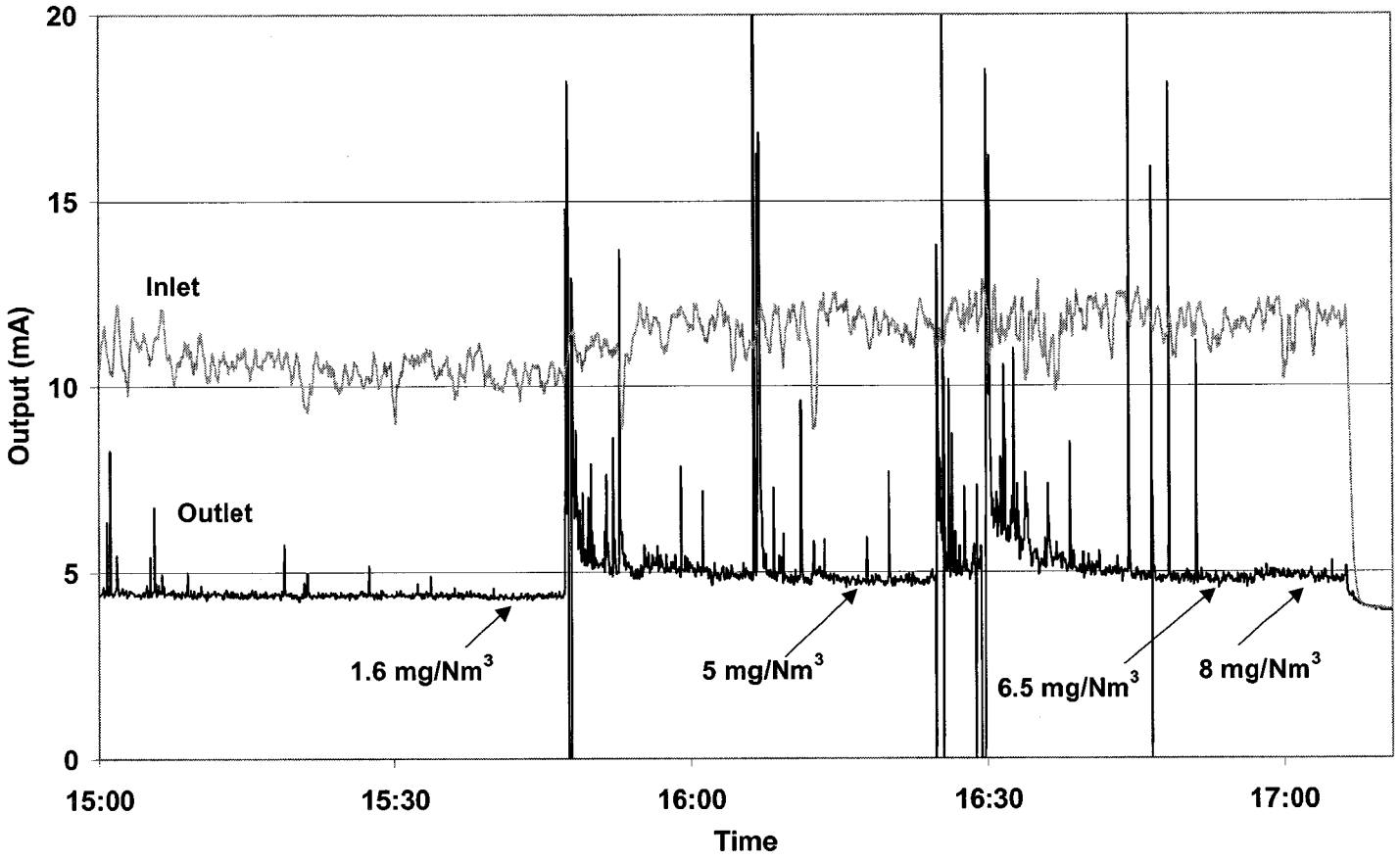

FIG. 23 DUST MONITOR TRACES DURING SEALING AIR TESTS (D0231J08)

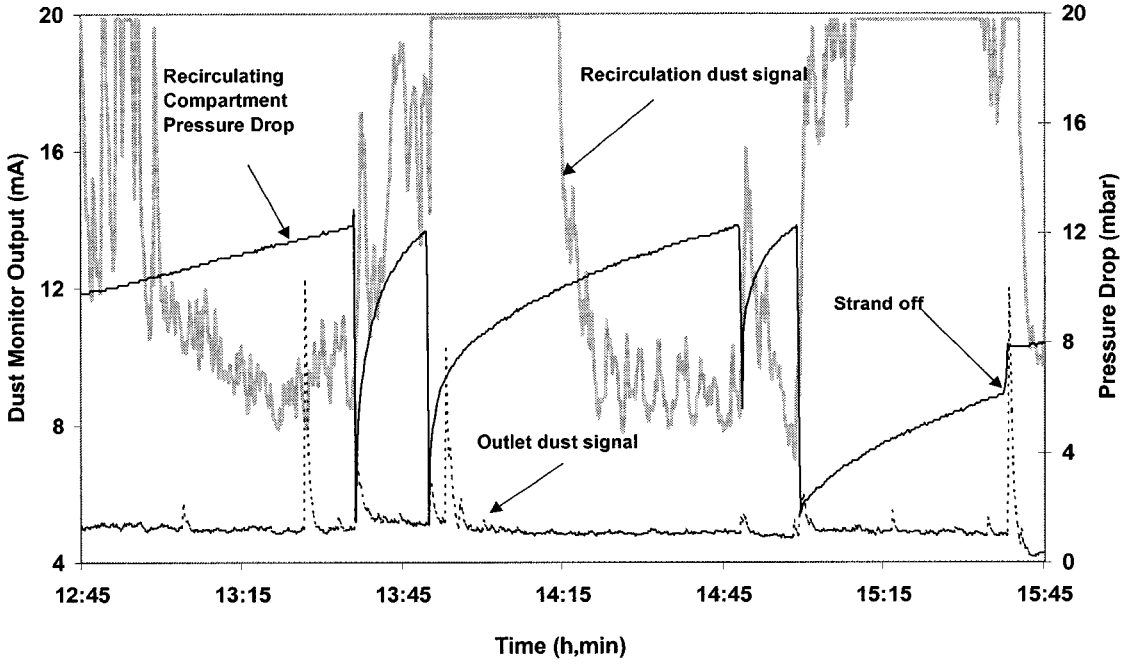

FIG. 24 DATA FROM DUST MONITOR CONTROL TESTS (D0231J09)

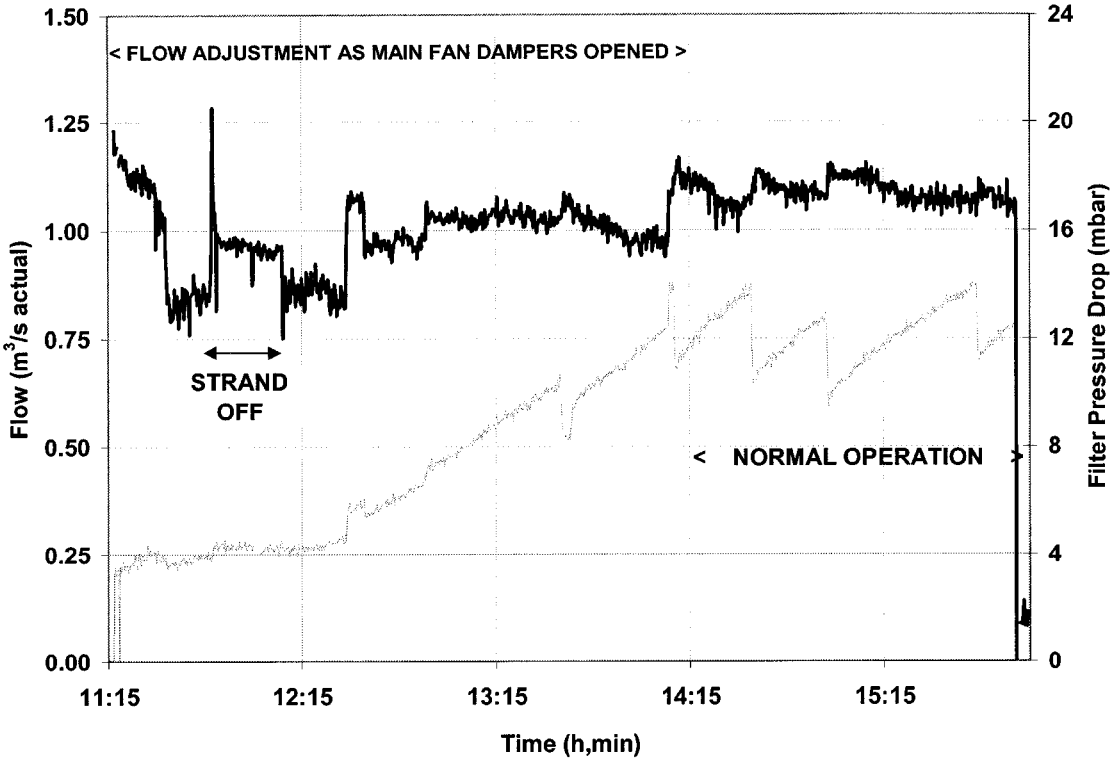

FIG. 25 FLOW AND PRESSURE DROP DURING COLD START-UP (D0231J09)

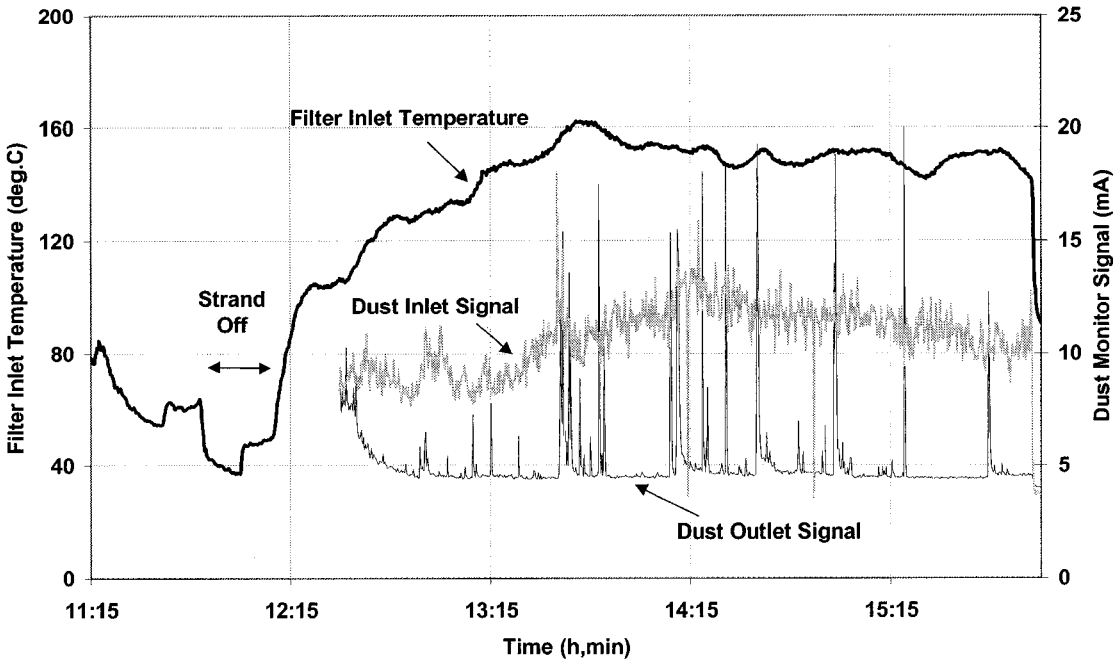

FIG. 26 TEMPERATURE AND DUST MONITOR DATA DURING COLD START-UP (D0231J09)

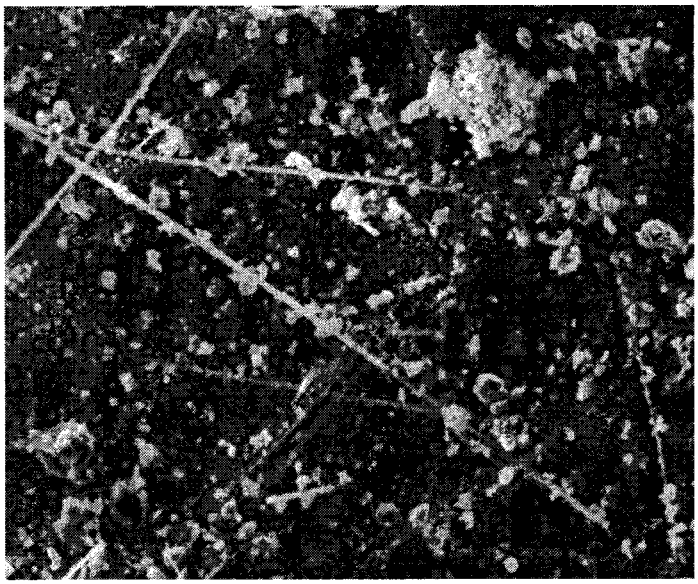

x 1000

FIG. 27 **SEM IMAGE OF OUTLET DUST** **(D0231J09)**

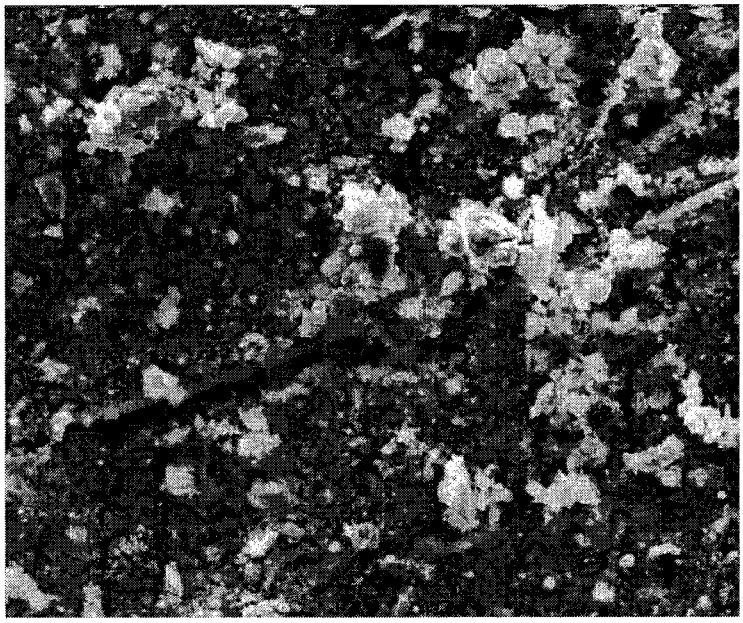

x 2000

FIG. 28 **SEM IMAGE OF OUTLET DUST** **(D0231J09)**

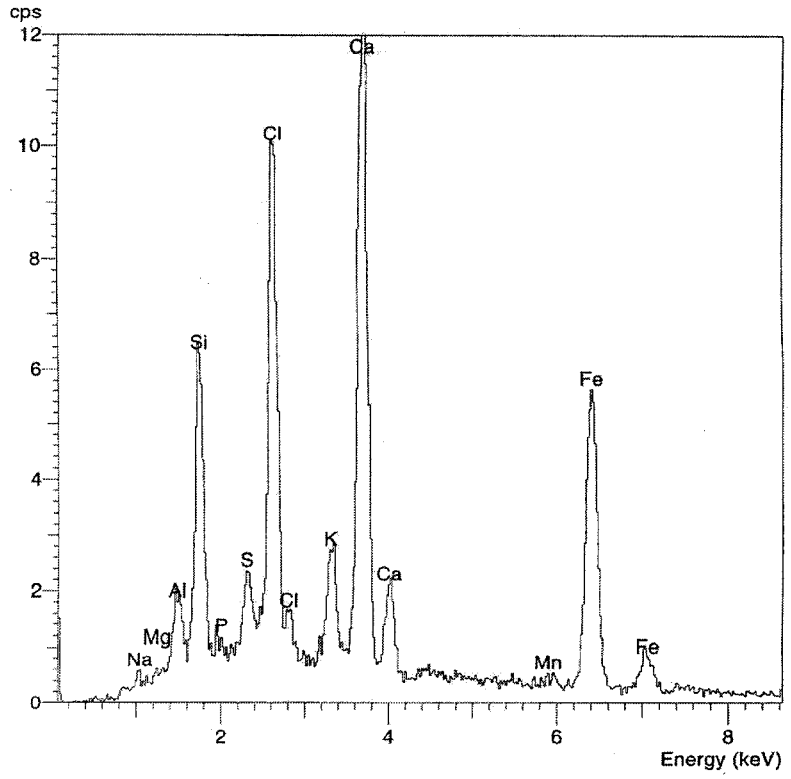

FIG. 29 EDA SPECTRUM OF 4 µm PARTICLE (D0231J09)

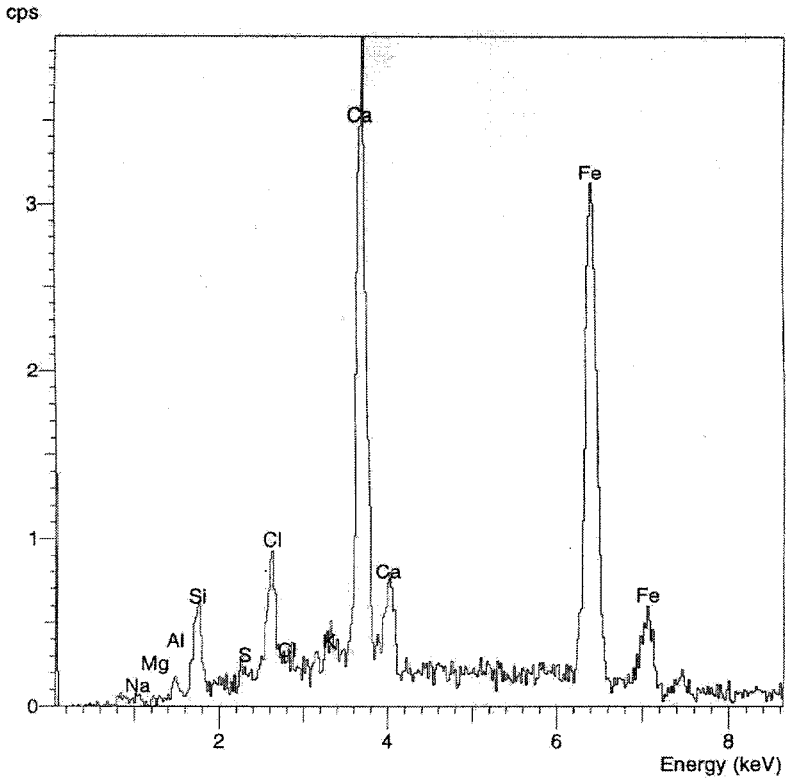

FIG. 30 EDA SPECTRUM OF 12 µm PARTICLE (D0231J09)

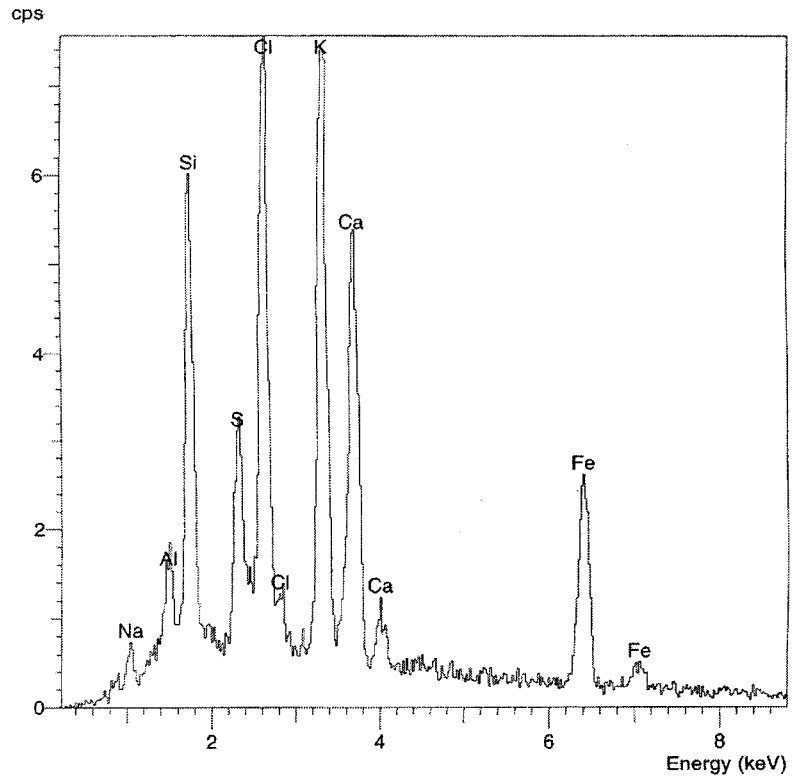

FIG. 31 EDA SPECTRUM OF 20 µm PARTICLE (D0231J09)

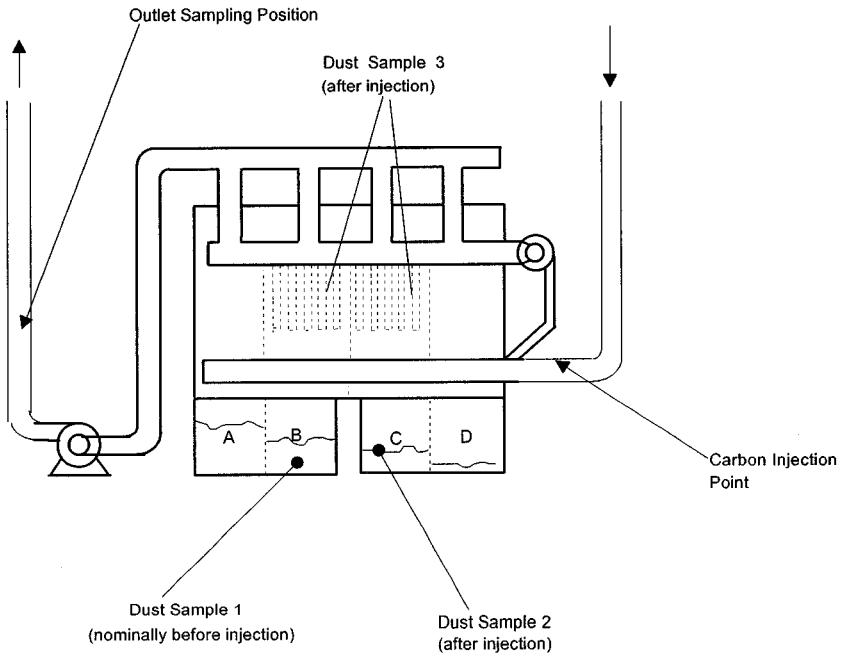

FIG. 32 DUST SAMPLING POSITIONS AND CARBON INJECTION POINT (D0231J09)

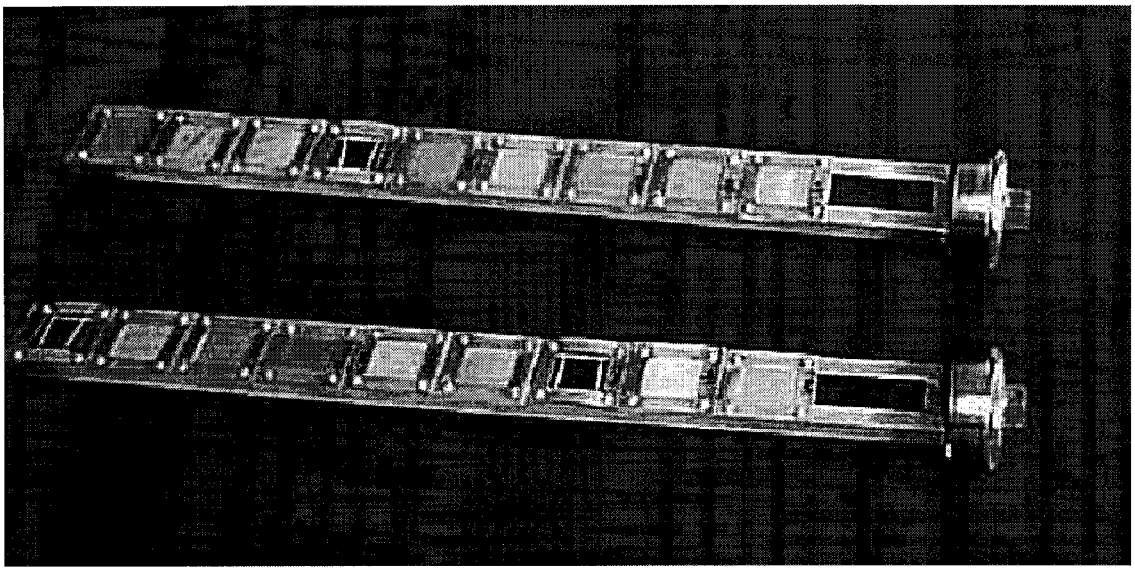

FIG. 33 CORROSION TEST COUPONS (D0231J09)

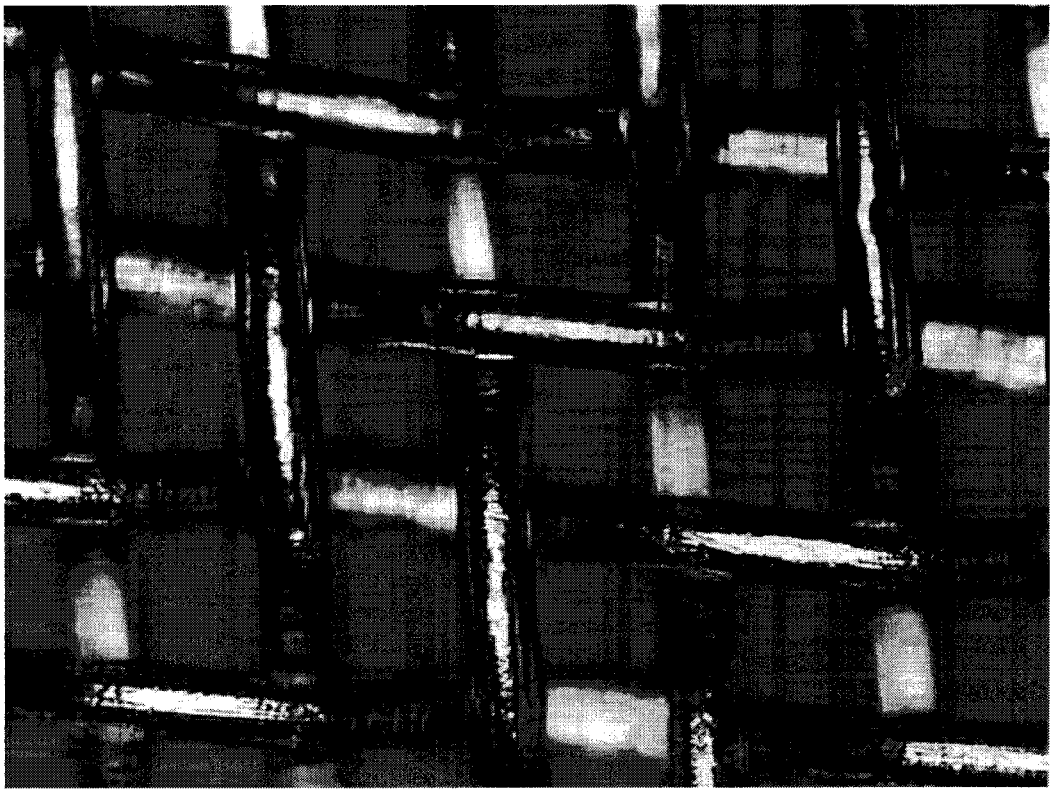

FIG. 34 304 STAINLESS STEEL MESH COUPON AFTER 6 MONTHS EXPOSURE (D0231J09)

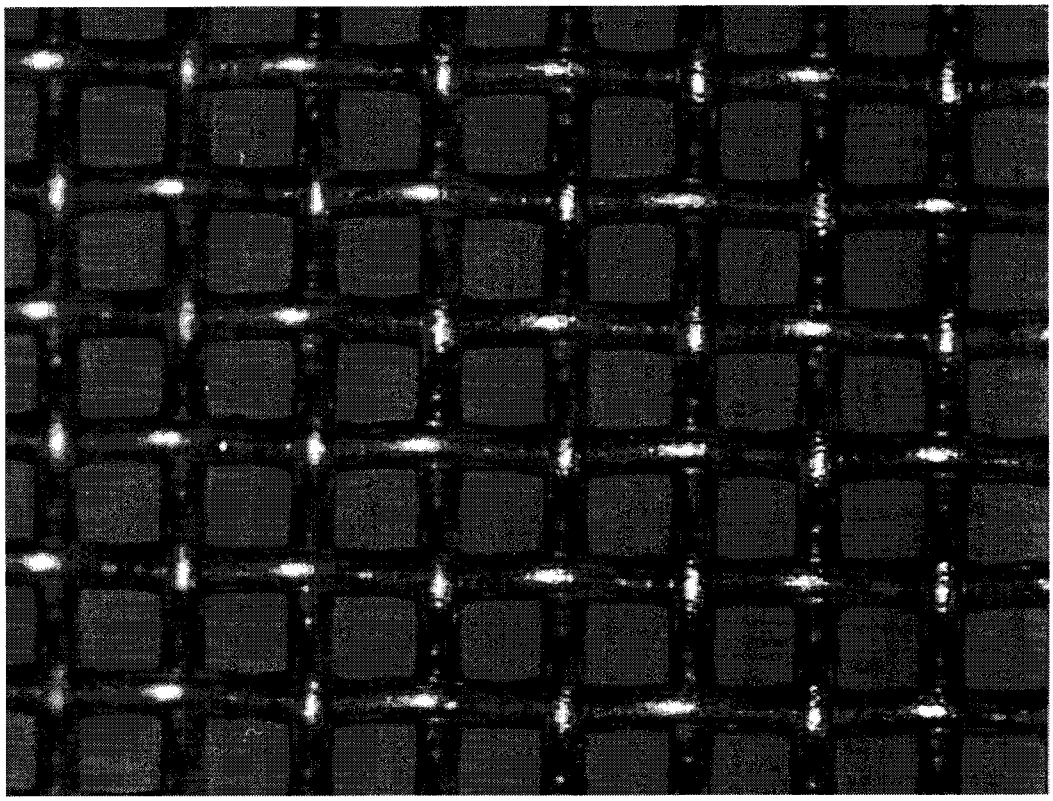

FIG. 35 316 STAINLESS STEEL MESH COUPON AFTER 6 MONTHS EXPOSURE (D0231J09)

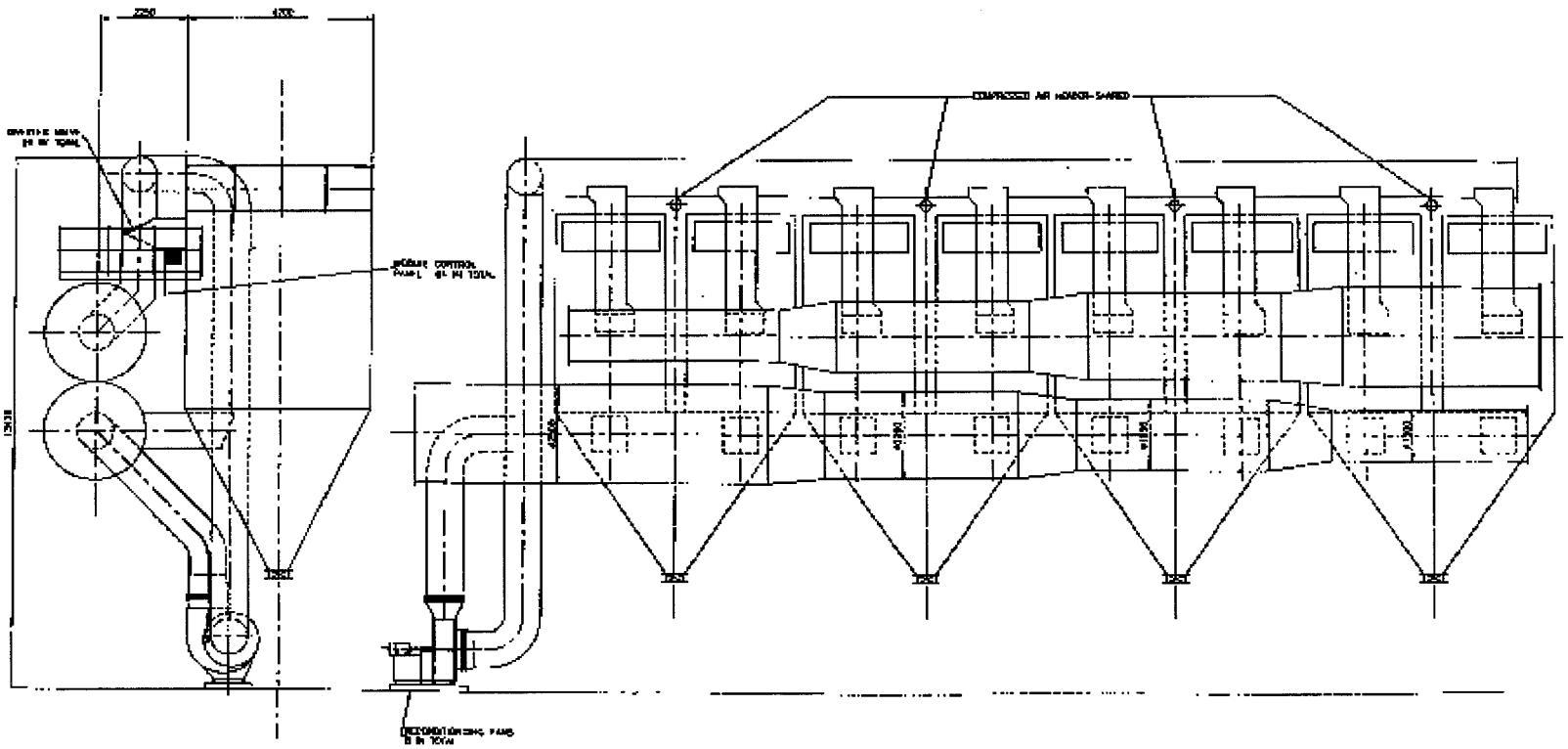

FIG. 36 SIDE ELEVATIONS OF LARGE SCALE PLANT (D0231J08)

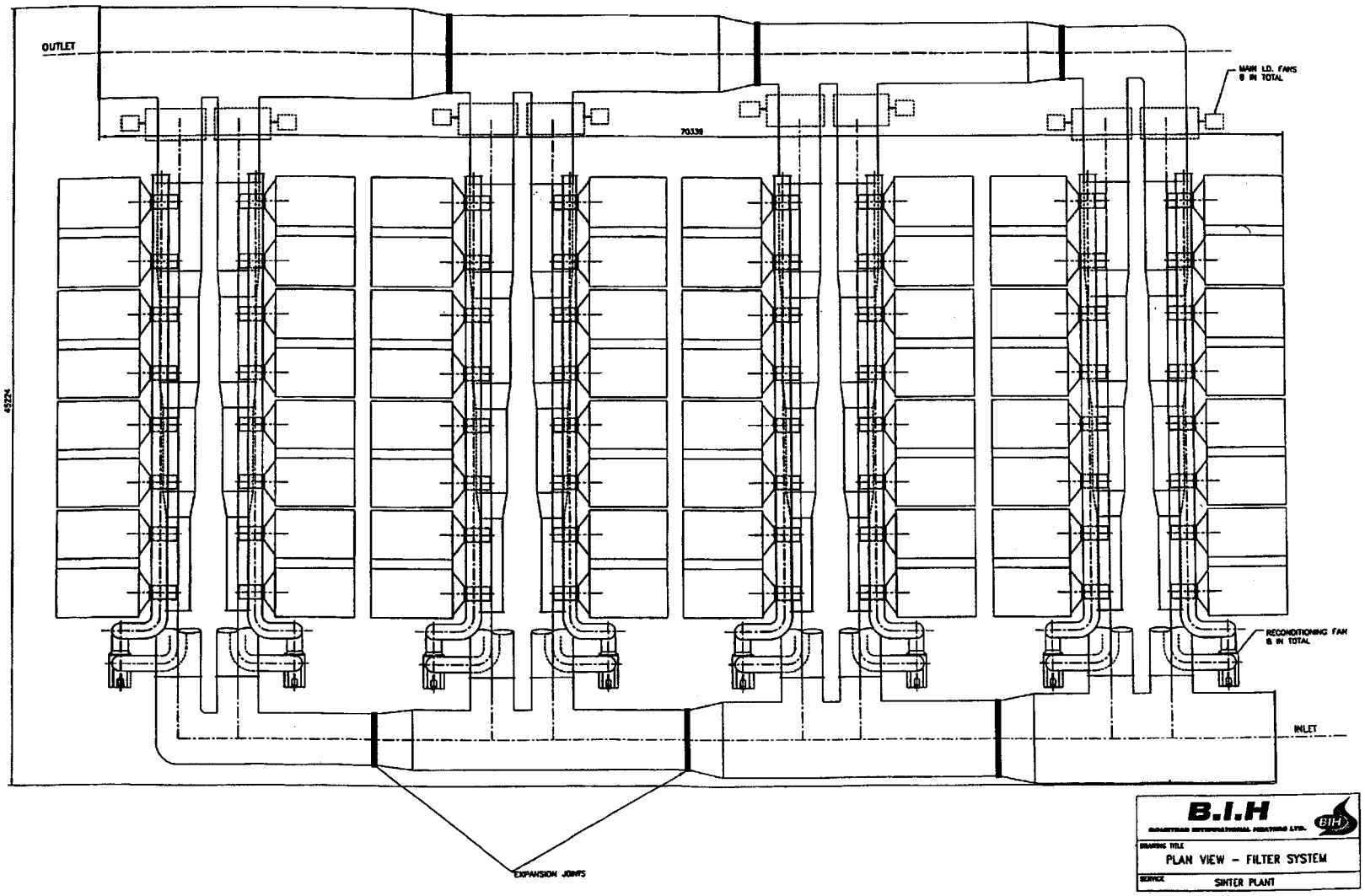

FIG. 37 PLAN OF LARGE SCALE PLANT (D0231J10)

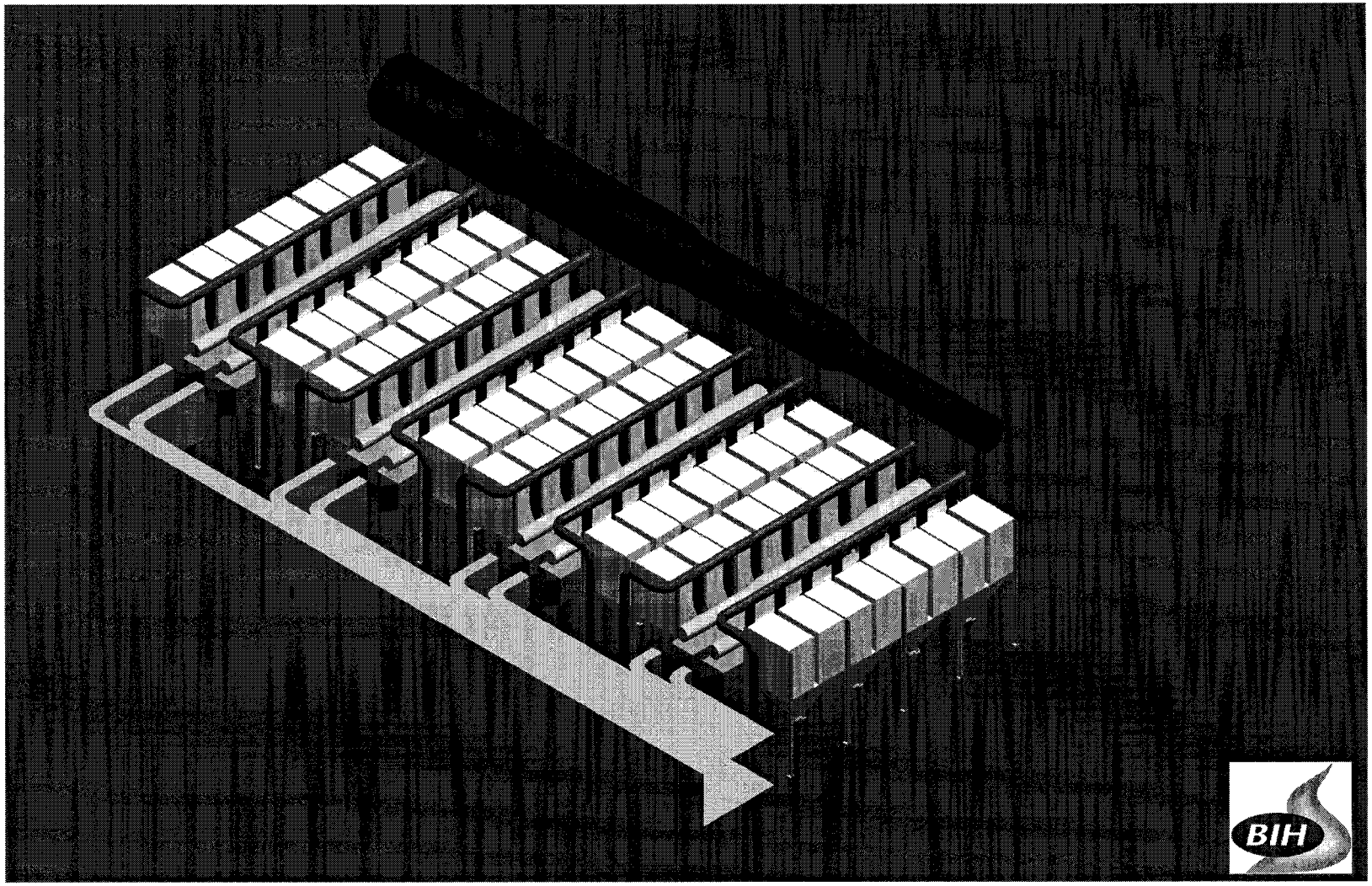

FIG. 38 ISOMETRIC IMPRESSION OF LARGE SCALE PLANT (D0231J10)

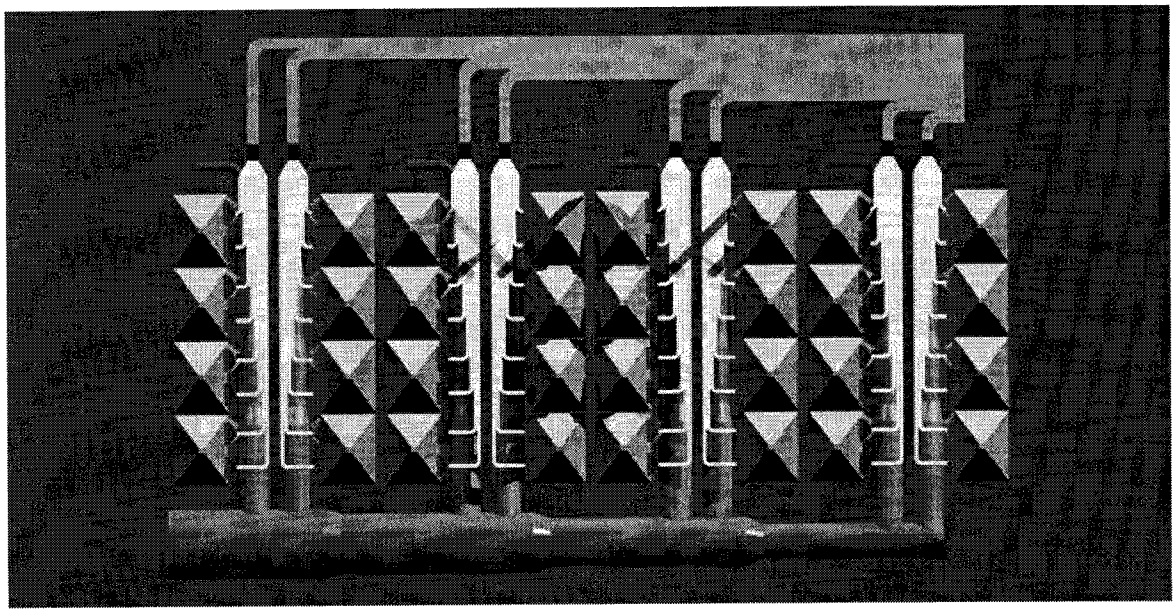

FIG. 39 UNDERSIDE VIEW OF LARGE SCALE PLANT (D0231J09)

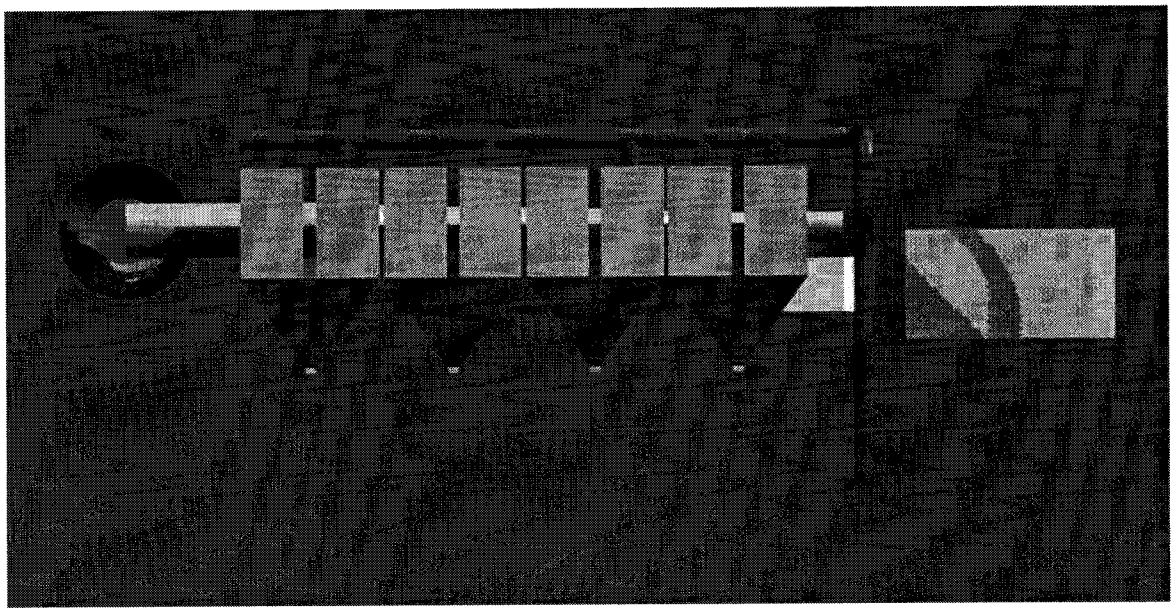

FIG. 40 END VIEW OF LARGE SCALE PLANT (D0231J09)

APPENDIX 1

BACKGROUND TO THE PROJECT (1996)

The Council of the European Communities adopted a Directive (84/360/EEC) on 28 June 1984 aimed at preventing or reducing air pollution from industrial sources. The Directive provides that a wide range of industrial processes shall be subject to a prior authorisation by competent authorities in each member state.

A key element of this Directive is that the required authorisation may not be granted unless the competent authority is satisfied that all appropriate measures have been taken to prevent air pollution, including the use of the best available technology, providing that the application of these measures does not entail excessive costs.

The Directive set the basis for changes in national legislation and more recently the Commission, DG XI/A/3, has produced a framework Directive on integrated pollution prevention and control (IPPC). This was adopted in October 1996 and published as Council Directive 96/61 EC.

The purpose of this Directive is to provide for measures and procedures to adopt an integrated approach so as to achieve as high an overall level of protection as possible for the environment as a whole, and for human health in particular, by preventing or minimising emissions arising from industrial installations.

The Directive refers to "best available techniques" (BAT) which signifies the latest stage of development (state of the art) of activities, processes and their methods of operation which indicate the practical suitability of a particular technique for preventing, or where that is not practicable, minimising emissions to the environment as a whole.

Within this context DG X1/A/3 have produced technical notes on the best available technologies (referred to as BAT notes) to reduce emissions from sinter plants and similar guidance notes have been introduced at national level to meet national regulations, such as the UK Environmental Protection Act 1990, Integrated Pollution Control.

Within the guidance notes the concept of achievable release levels (ARL) has been introduced which should be applied to *new* plants where the best combination of process design and abatement technology can be readily applied. It is intended that ARL be applied to *existing* plants by requiring the upgrading of these plants within defined timescales.

Typical Existing Emission Range for Sinter Plant Main Stacks Against Achievable Release Levels (ARL)

	Existing*	ARL
Air Flow (dry m^3/h)	350000-1600000	-
Dust (mg/m^3 stp)	50-200	50
SO_2 (mg/m^3 stp)	400-750	250
NO_x (mg/m^3 stp)	400-600	-
Dioxins (ng/m^3 stp TEQ)	2-47	1
CO (ppm)	6300-12000	-

* Source: Working Group Members from Germany, Italy and Belgium, 1992 DG X1/A/3.

The list above shows a comparison of typical emission ranges in Europe against ARL for sinter plant main stacks as proposed in the BAT Notes. Legislation in the EU will aim to achieve these levels, potentially with a new more stringent dioxin emission limit of 0.1 ng/m^3 stp (TEQ) and particulate emission limits of 50 mg/m^3 and lower. In addition some nations have introduced emission limits on NO_x (e.g. TALuft (Germany) propose 400 mg/m^3 stp) and other substances.

Typically, sinter plant main stacks account for up to 30% of the total mass of airborne pollutants from an integrated steelworks, mainly because emissions are continuous and associated with high volume gas flows. Any substantial improvement in pollution control at the main stack would therefore be regarded as a major contributor in reducing environmental impacts of steelwork's processes generally.

Throughout Europe, main stack sinter plant emissions are controlled mainly by electrostatic precipitators (EP). Precipitators rarely clean particulates effectively below 100 mg/m^3 as their efficiency is variable owing to their dependence upon factors such as dust resistivity, dew point, gas temperature, plant maintenance, plate corrosion and rapping procedures, thus making the achievement of consistent performance difficult to control. In addition, emissions are highly dependent upon sinter feedstock composition and the composition of recycled material.

Recent work in Italy has focused on attempting to reduce emissions by the treatment of the sinter strand[A1.1] both by suppressing the formation of pollutants and by introducing treatments which enhanced precipitator performance. The work concluded that emissions could be reduced but that the treatments introduced operating costs which were economically unfavourable. Other work in France has focused on end of pipe technology[A1.2, A1.3] in particular the use of bag filter plants for both the control of particulate emissions and to introduce reagents, such as hydrated lime, into the gas stream for desulphurisation purposes. The work demonstrated that particulate emissions could be reduced by this technology in the range 10-25 mg/m^3 but that problems could arise from the moisture content of the gases, the abrasive nature of the dust and potentially from high gas temperatures which can be damaging to fabric filters. Further problems can arise from particulate adhesion to the filter surface owing to 'stickiness' caused by the alkali and hydrocarbon content of the flue gases.

Other technologies are being developed or are being used to solve the emissions problems of sinter plants such as the Japanese-developed technique of on-line cleaning of precipitator plate deposits using Moving Electrode Electrostatic Precipitators (MEEP) and Emissions Optimised Sintering[A1.4] developed by Lurgi at Hoogovens, Netherlands in which the gas stream is partially recirculated through the sinter strand. Voest Alpine (Austria) have developed the Airfine process which uses advanced wet scrubbing technology to reduce gaseous emissions but introduces more complex secondary treatment plants. Whilst these measures have achieved positive results in terms of reduced emissions there is still a need to consider alternative technologies which may be universally applicable to the sinter plant application and which will provide a viable technology to reduce particulate emissions to less than 50 mg/m^3.

Where plants use high-sulphur raw materials, formation of sulphur dioxide can prove a problem requiring control measures. Typically untreated emissions of SO_2 are in the range 400 to 750 mg/m^3. Depending upon local and national regulations, control of SO_2 releases may be necessary, through an appropriate flue gas desulphurisation technology. These technologies, principally wet scrubbing, can achieve over 90% removal efficiency for the gas treated but require capital intensive plant with significant operational costs.

Other gaseous pollutants, such as nitrogen oxides (NO_x) and hydrogen fluoride (HF) do not cause significant problems at most sinter plants, although once again this is dependent on emission limits stipulated in national regulations. Typically, untreated emissions of these pollutants are in the range of 400-600 mg/m^3 and less than 10 mg/m^3 HF.

Alternative technologies must be sought if the steel industry is to approach the achievable release levels for new plants of 50 mg/m^3 for particulate emissions. The high temperature metallic filter is a technology offering promise in this respect. In addition, the two stage filtering process requires that gases pass through a filter cake to achieve effective filtration efficiency, thus by dosing the gas streams with suitable absorbents there is potential to reduce SO_x, dioxin and possibly NO_x emissions.

REFERENCES

A1.1 ECSC Contract 7261/01/502/04 'Reduction of CO, NO_x and SO_2 from Sintering Plants by Action on Charging and Process'. L. Corsi, CSM, Italy.

A1.2 ECSC Contract 7261-01/432/03 'Study of Fabric Filters to Reduce Particulate Pollution from Sinter Plants'. Report LECES, France RE 75.

A1.3 ECSC Contract 7261-01/455/03 'Study of Fabric Filters to Reduce Particulate and Gaseous Emissions from Sinter Plants'. Report LECES, France RE/L 85.

A1.4 ECSC Pilot Plant and Demonstration Contract 7215.AA/602, Demonstration Plant for Sintering with Reduced Volume of Flue Gases, HOOGOVENS, Holland.

APPENDIX 2

EXTRACT FROM BEST AVAILABLE TECHNIQUES REFERENCE DOCUMENT ON THE PRODUCTION OF IRON AND STEEL, MARCH 2000

For sinter plants, the following techniques or combination of techniques are considered as BAT. The order of priority and the selection of the techniques will differ according to local circumstances. Any other technique or combination of techniques achieving the same or better performance or efficiency can also be considered; such techniques may be under development, an emerging technique or a technique which is already available but not mentioned or described in this document.

1. Waste gas de-dusting by application of:

   - Advanced electrostatic precipitation (ESP) (moving electrode ESP, ESP pulse system, high voltage operation of ESP ...) *or*
   - electrostatic precipitation plus fabric filter *or*
   - pre-dusting (e.g. ESP or cyclone) plus high pressure wet scrubbing system.

   Using these techniques dust emission concentrations < 50 mg/Nm^3 are achieved in normal operation. In case of application of a fabric filter, emissions of 10-20 mg/Nm^3 are achieved.

2. Waste gas recirculation, if sinter quality and productivity are not significantly affected, by applying:

   - recirculation of part of the waste gas from the entire surface of the sinter strand, *or*
   - sectional waste gas recirculation

3. Minimising of PCDD/F emission, by means of:

   - Application of waste gas recirculation;
   - Treatment of waste gas from sinter strand;
   - use of fine wet scrubbing systems, values < 0.4 ng I-TEQ/Nm^3 have been achieved.
   - Fabric filtration with addition of lignite coke powder also achieves low PCDD/F emissions (> 98% reduction, 0.1 - 0.5 ng I-TEQ/Nm^3 - this range is based on 6 hours random sample and steady state conditions).

4. Minimisation of heavy metal emissions

- Use of fine wet scrubbing systems in order to remove water-soluble heavy metal chlorides, especially lead chloride(s) with an efficiency of > 90% or a bag filter with lime addition;

- Exclusion of dust from last ESP field from recycling to the sinter strand, dumping it on a secure landfill (watertight sealing, collection and treatment of leachate), possibly after water extraction with subsequent precipitation of heavy metals in order to minimise the quantity to dump.

8. Minimisation of SO_2 emissions by, for example:

- Lowering the sulphur input (use of coke breeze with low sulphur content and minimisation of coke breeze consumption, use of iron ore with low sulphur content); with these measures emission concentrations < 500 mg SO_2/Nm^3 can be achieved.

- With wet waste gas desulphurisation, reduction of SO_2 emissions > 98% and SO_2 emission concentrations < 100 mg SO_2/Nm^3 are achievable.

  Due to the high cost wet waste gas desulphurisation should only be required in circumstances where environmental quality standards are not likely to be met.

9. Minimisation of NO_x emissions by, for example:

- waste gas recirculation
- waste gas denitrification, applying
- regenerative activated carbon process
- selective catalytic reduction

Due to the high cost waste gas denitrification is not applied except in circumstances where environmental quality standards are not likely to be met.

APPENDIX 3

ANALYSIS OF ELECTROSTATIC PRECIPITATOR DUST FROM CSI PLANOS

1. INTRODUCTION

ESP dust was collected from the sinter strands at Aviles for characterization as an aid to the design of the new filter.

2. CHARACTERIZATION OF ESP DUST

2.1 Chemical Analysis

The first chemical analysis in Table 1(a) below was performed by CENIM.

Fe_2O_3	SiO_2	P_2O_5	CaO	MgO	Al_2O_3	Na_2O	K_2O	MnO
49.3	4.3	0.11	12.5	1.0	2.0	0.4	7.15	0.44

C	S	PxC
3.5	2.5	19.4

Table 1(a). Chemical analysis of ESP dust

The dust was also sent for the chemical analysis to the company EMGRISA, the results of which are shown in Table 1(b).

Fe_2O_3	SiO_2	P_2O_5	CaO	MgO	Al_2O_3	Na_2O	K_2O	MnO
56.35	5.07	0.09	10.77	0.79	2.00	0.48	6.20	0.50

C	S	Cu*	Pb*	Zn*	Sr*	Cr*	TiO_2	Cl	PxC
3.97	1.95	670	4.70	205	43	6.1	0.10	7.64	10.37

* = ppm

Table 1(b). More complete chemical analysis of the ESP dust

2.2 X-Ray Fluorescence Analysis

A complete scan of the sample was carried out to detect all the elements which could be present in the ESP dust. The following elements were detected:

Fe, Ca, K, Cl, S, P, Si, Al, Mn, Mg, Na, Ti, Zn, Cu, Pb, Cr, Sr, C

This is a qualitative analysis which makes it possible to obtain rapid information about the elements which are present in a sample.

Table 2 presents a semi-quantitative analysis of all the elements detected.

2.3 Microstructural Analysis (SEM)

Analyses were performed by scanning electron microscopy (SEM) using a Jeol Model JXA-840 instrument, which has a scanning electron microscope and a microanalyzer which allows energy-dispersive and wavelength-dispersive XRF analyses.

Microstructurally, it was observed that the ESP dust is constituted by different particles differentiated by their morphologies. Particle sizes varied between 5 and 100 μm, though with a predominance of particles larger than 15 μm.

In photo 1 both compact and porous particles are observed. Fe (Fe_2O_3), SiO_2 and Ca (in the form of $CaCO_3$) are compact particles while the very porous particles with irregular forms consist of complex formations of several elements which generally include Cl – S – K and probably Na (not detectable with this analytical technique).

Compound particles:

Fe > Al – Si > P – Cl – Ca
Ca > Fe >> K – Cl – S – Si – Al
Fe > Si – Al – Cl – K – Ca
Si – Ca > Mg – Al > K – Cr - Mn

Formations of calcium ferrites were also detected with the composition Fe – Ca > Si > Al > Mn in a phase segregated from Ca > Si > Fe >> K – Ti. These ferrites are present only in small quantities.

The presence of carbon was also observed.

In photo 2 it is possible to observe in greater detain the Fe particles (in the form of Fe_2O_3) which are presented in the energy dispersive spectrum in a light grey tone, it also being possible to see other porous particles of Fe > Si-Al in a medium grey tone and Si particles (SiO_2) in a dark grey tone.

CENTRO NACIONAL DE INVESTIGACIONES METALURGICAS - CENIM (C.S.I.C.)
Avda Gregorio del Amo

J08.001
PW1404 Rh 80kV LiF220 Ge111 TlAP
Ident.Muestra = FINOS SINTER

Calcula como : Oxidos Datos impurezas Espec. : 909.TEFLON
Medio rayos-X = Vacuum Tipo de Film = No hay film soporte
Num. de Caso = 2 %Resto desconocido
Diam. Efect. = 23.70 mm Superf.Efect. = 440.9 mm2
Conc.conocida = 0 %
Resto = ? % CO2
Dil./Muestra = 0
MasaAnalizada = 985.924 mg
AlturaMuestra = 3 mm

< Indica que la concentración est < 100 mg/kg
<2e = %peso < 2 StdErr. + indica que se ha usado en la Suma=100%

Z	wt%	StdErr	Z	wt%	StdErr	Z	wt%	StdErr
SumBe..F	0.92	0.19	29+CuO	<2e	0.07	51 Sb2O3	<	
11+Na2O	1.23	0.42	30+ZnO	0.035	0.002	52 TeO2	<	
12+MgO	0.71	0.04	31 Ga2O3	<		53+I	<	
13+Al2O3	2.86	0.09	32 GeO2	<		55+Cs2O	0.021	0.002
14+SiO2	4.84	0.17	33 As2O3	<		56+BaO	0.027	0.003
15+P2O5	0.10	0.01	34+SeO2	0.039	0.003	SumLa..Lu	0.07	0.09
16 S			35+Br	0.11	0.01	72 HfO2	<	
16+SO3	6.33	0.25	37+Rb2O	0.079	0.006	73 Ta2O5	<	
17+Cl	8.22	1.14	38+SrO	0.020	0.002	74 WO3	<	
18 Ar	<		39+Y2O3	<		75 Re2O7	<	
19+K2O	10.27	0.50	40+ZrO2	<		76 OsO4	<	
20+CaO	14.24	0.10	41 Nb2O5	<		77+IrO2	<	
21 Sc2O3	<		42 MoO3	<		78 PtO2	<	
22+TiO2	0.12	0.01	44 RuO4	<		79 Au	<	
23 V2O5	<		45 Rh2O3	<		80 HgO	<	
24+Cr2O3	0.014	0.004	46 PdO	<		81+Tl2O3	<	
25+MnO	0.48	0.03	47+Ag2O	<		82+PbO	0.60	0.03
26+Fe2O3	48.54	0.59	48 CdO	<		83 Bi2O3	<	
27+Co3O4	0.025	0.003	49 In2O3	<		90 ThO2	<	
28+NiO	<		50 SnO2	<		92 U3O8	<	
=== Elementos Ligeros ===			==== Elementos Nobles ===			===== Lantanidos ======		
4 BeO			44 RuO4	<		57 La2O3	<	
5 B2O3			45 Rh2O3	<		58 CeO2	<	
6 CO2			46 PdO	<		59 Pr6O11	<	
7 N			47+Ag2O	<		60 Nd2O3	<	
8 O			75 Re2O7	<		62+Sm2O3	<2e	0.02
9+F	0.92	0.19	76 OsO4	<		63 Eu2O3	<	
			77+IrO2	<		64 Gd2O3	<	
			78 PtO2	<		65+Tb4O7	<2e	0.02
			79 Au	<		66 Dy2O3	<	
						67 Ho2O3	<	
						68+Er2O3	0.044	0.010
						69 Tm2O3	<	
						70 Yb2O3	<	
						71 Lu2O3	<	

TABLE 2

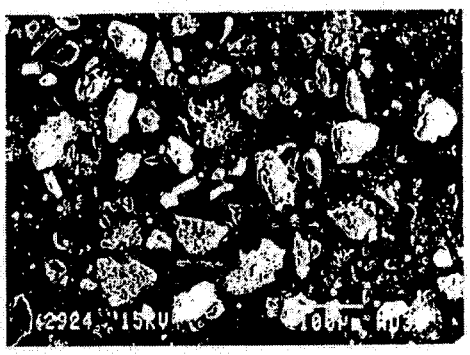

Photo 1: General appearance of the particles which make up the electrofilter dust.

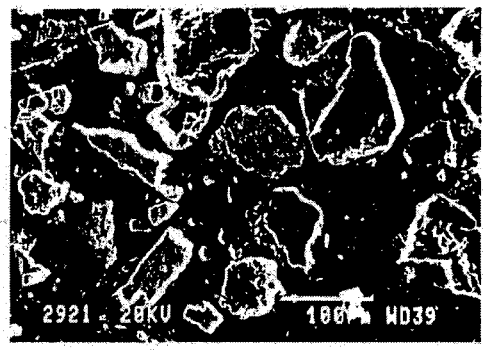

Photo 2: Detail of some particles of Fe_2O_3, SiO_2 and silicates.

2.4. X-Ray Diffraction Analysis:

XRD Analysis indicates the presence of crystalline phases which are detailed in Table 3. In the XRD spectrum given in figure 2 it is possible to see the distribution of peaks with different intensities for each crystalline phase.

Compound	Formula
Haematites	Fe_2O_3
Potassium chloride (Sylvite)	KCl
Calcium silicate	$CaSi_5O_5$
Calcium carbonate	$CaCO_3$
Magnesium and Aluminium silicate	$MgO.\ Al_2O_3.\ SiO_2$
Potassium chlorate	$KClO_4$
Carbon	C

Table 3. Compounds identified by X-Ray Diffraction.

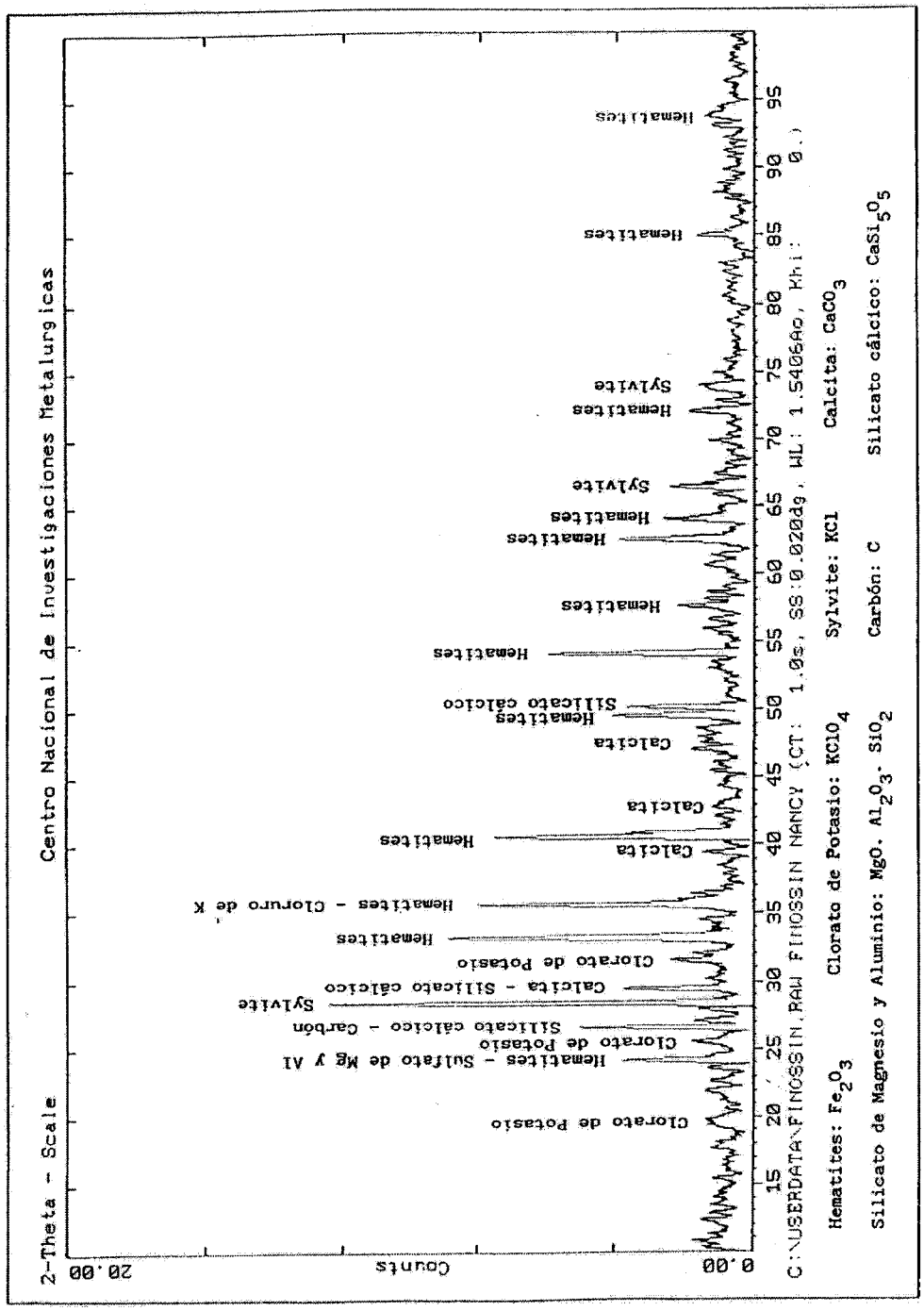

Figure 2: X-Ray Diffraction Spectrum

3. PARTICLE SIZE FRACTIONATION CUT AT 15 µm

Particle size analysis was performed in a liquid medium and with 50 g of sample. The fraction >015 µm had a brown tone and the particles tend to agglomerate. The fraction <15 µm had a darker colour (dark brown). The losses were high, indicating that part of the sample dissolved in the water.

The chemical analyses of the fractions >15 µm and <15 µm are given in Table 4.

The weight distributions of the particle size fractionation were as follows:

Fraction	Weight (g)	% Weight (with losses)	% Weight (without losses)
>15 µm	23.78	47.56	59.1
<15 µm	16.46	32.92	40.9
Losses	9.76	19.52	100

	As-Received	>15 µm	<15 µm
Fe	34.4	47.0	40.8
SiO_2	4.3	7.2	6.60
P	0.050	0.060	0.065
CaO	12.5	9.0	16.5
MgO	1.0	1.30	1.0
Al_2O_3	2.0	1.90	2.60
Na_2O	0.40	<0.05	<0.05
K_2O	7.15	0.10	0.12
Mn	0.34	0.32	0.50
C	3.5	5.0	5.0
S	2.5	0.66	0.64
PxC	19.4		

Table 4. Chemical analysis of the fractions >15 µm and <15 µm

4. WASHING OF THE ESP DUST

The ESP dust was washed in distilled water which had previously been stirred for 1 hour. The purpose of this was to determine what part of the ESP dust's constituents were soluble in water.

The results of chemical analysis of the washed sample and of the wash water are shown in Table 5.

Initial weight	30 g	100%
Final weight of washed sample	25.15 g	83.8%
Losses	4.85 g	16.2%
Vol. distilled water used	403 ml	
Vol. wash water for analysis	390 ml	

	As-Received	Washed Sample	Wash Water
Fe	34.45	42.4	<0.005
SiO_2	4.30	5.10	"
P	0.050	0.055	"
CaO	12.5	14.0	0.80
MgO	1.0	1.13	<0.005
Al_2O_3	2.0	2.17	"
Na_2O	0.40	0.08	0.55
K_2O	7.15	0.19	8.7
Mn	0.34	0.40	<0.005
C	3.5	4.80	"
S	2.5	0.60	"
PxC	19.4		

Table 5. Chemical analysis of the washed sample and the wash water

5. HEAT TREATMENT

A sample of ESP dust was calcined in a muffle at different temperatures for 1 hour. Calcining losses were subsequently determined by comparison with the initial weight of each sample.

Table 6 shows the results obtained from the heat treatment. The % of equivalent magnetite was also determined. The values of equivalent magnetite were low, indicating that all of the Fe is present as Fe_2O_3 and not as Fe_3O_4.

All heat treatment tests of the samples were carried out using the as-received material.

At 400°C there was a slight weight loss of the sample owing to the elimination of moisture. No visible changes took place.

At 600°C calcining losses (PxC) increased due to the elimination of C in the form of CO_2.

At 800°C the PxC were lower, in comparison with the previous temperature of 600°C, due probably to the oxidation of some element, after reduction takes place. At this temperature S starts to volatize in the form of SO_3 and the same is true for the chlorides.

At 1000°C the PxC of the sample increased again, without the ESP dust reaching the point of sintering. Volatilization of S in the form of SO_3 of chlorides, Na and K takes place at this temperature.

At 1200°C the PxC increased considerably, due to the total volatilization of S. At this temperature the calcined sample presented a sintering effect.

Initial Weight (g)	Temperature (°C)	PxC	Equivalent Magnetite
As-received		19.4	3.99
10.86	400	4.33	2.02
10.23	600	12.71	4.37
10.75	800	10.83	2.88
10.70	1000	14.77	1.34
10.23	1200	20.82	1.94

Table 6. Experimental data for the series of heat treatments

5.1 Chemical Analysis of the Heat Treated Products

Table 7 displays the results of chemical analysis of the series of heat treatments carried out on the ESP dust.

	As-Received	600°C	800°C	1000°C	1200°C
Fe	34.45	36.8	38.8	43.5	48.0
SiO_2	4.30	5.5	5.7	6.75	7.2
P	0.05	0.052	0.060	0.060	0.058
CaO	12.5	14.5	14.5	14.8	15.0
MgO	1.0	1.0	1.2	1.20	1.25
Al_2O_3	2.0	2.1	2.3	2.55	2.70
Na_2O	0.40	0.45	0.31	0.17	<0.05
K_2O	7.15	7.0	4.55	1.90	<0.05
Mn	0.34	0.36	0.40	0.41	0.44
C	3.5	0.22	0.060	0.020	0.11
S	2.5	2.22	1.95	2.20	0.014
PxC*	19.4	12.70	13.99	13.34	18.63

* Calcining losses were determined from the C and S analyzed, considering that all of the C is present in the form of CO_2 and the S in the form of SO_3.

Table 7. Chemical analysis of the different heat treated samples

6. MAGNETIC SEPARATION OF THE ELECTROFILTER DUST

Magnetic separation was carried out in order to concentrate the Fe in the magnetic product and to obtain possible segregations of other elements. Magnetic separations were carried out in a Davis Tube and in a Rapid.

Magnetic separation in the Davis Tube was performed at a low intensity (SMBIH), while magnetic separation in the Rapid was performed at a high intensity. Both were performed in a liquid medium.

The results of the magnetic separation in the Davis Tube are:

Initial Weight 100 g	Magnetic	Non-Magnetic	Losses
Final Weight (g)	7.48	71.78	20.74

The results of the magnetic separation in the Rapid are:

Initial Weight 100 g	Magnetic	Non-Magnetic	Losses
Final Weight (g)	51.27	19.15	29.58

In both tests significant losses were seen in the sample, due to the fact that part of it dissolves in the water.

	As-Received	Magnetic Separation Davis Tube		Magnetic Separation Rapid	
		Magnetic Wt. 9.4%	Non-Magnetic Wt. 90.6%	Magnetic Wt. 72.8%	Non-Magnetic Wt. 27.2%
Fe	34.45	52.6	40.55	47.7	27.5
SiO_2	4.30	4.2	5.75	4.5	7.2
P	0.050	0.050	0.065	0.066	0.068
CaO	12.5	9.1	14.5	12.5	20.6
MgO	1.0	2.1	1.13	1.13	1.13
Al_2O_3	2.0	1.42	2.46	2.27	3.0
Na_2O	0.40	0.02	0.04	0.02	0.09
K_2O	7.15	0.06	0.40	0.11	0.46
Mn	0.34	0.50	0.40	0.42	0.40
C	3.5	-	5.40	2.50	11.75
S	2.5	-	0.32	0.24	1.0

Table 8. Chemical analysis of the magnetic and non-magnetic products of the magnetic separations

Good results were not achieved with the magnetic separation in the Davis Tube. However, with the magnetic separation in the Rapid, the results are seen to improve considerably with regard to the yield and recovery of Fe. It is only possible to segregate CaO, C and some SiO_2 in the non-magnetic product.

APPENDIX 4

CHARACTERISATION OF SAMPLES FROM THE UK AND SPAIN

1. Introduction.

Three Scunthorpe samples are referred to as A, B and C. All are of fine grain size (less than 200 μm) and have been collected from the electrostatic precipitators (ESPs) which are fed by two lines, (see the diagram in figure 1).

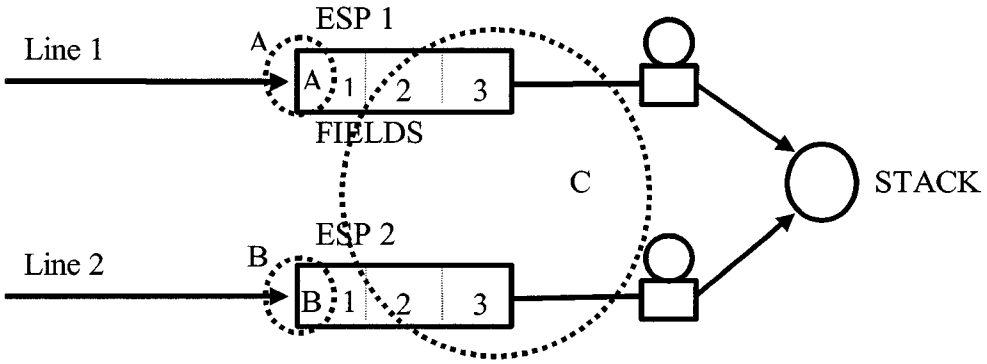

Figure 1. Source of samples A, B and C.

Another sample of ESP dust from South Wales was also studied, referred to in this study as sample D. This was nominally a mixture from all the four fields of the precipitator.

2. Objectives

The objective of the microstructural and physical-chemical characterisation of the ESP dust is to compare the UK dusts with those provided by CSI Planos, considering the constituent elements of each sample, majority components, morphology and particle size.

3. Microstructural and Physical-Chemical Characterisation

The samples were washed in order to determine the water solubility of some elements present in the ESP dust. The equivalent magnetite of each sample was determined and size separations were made at 15 μm in order to detect possible segregations in the final fractions. A global particle size analysis was also carried out. The analytical techniques used for the microstructural and physical-chemical characterisation were electron microscopy and X-ray fluorescence.

3.1. Washing of Samples

The 4 samples, A, B, C and D, were washed with water, with prior stirring for one hour. Subsequently the washed samples were filtered and dried in an oven. The initial weight of the samples was 50 g, and the weight of each sample after washing is displayed in Table 1.

Sample	Initial weight (g)	Final weight (g)	Losses (g)	Weight (%)
A	50 g	48.97	1.03	98
B	50 g	49.35	0.65	99
C	50 g	47.97	2.03	96
D	50 g	46.50	3.5	93

Table 1. Washing of samples A, B, C and D.

The losses which occurred during washing were minimal in the case of samples A and B. However, the losses in samples C and D were greater, due to the presence of a finer grain size in sample C and the dissolution of alkaline metal salts in sample D. Table 4 (a, b, c and d) presents the results of these washed samples.

3.2. Particle Size Analysis

The particle size analyses were carried out with the dry samples. The samples were screened for fractions less than 0.104 mm to -0.043 mm, and the fraction greater than 0.104 was reserved. The results of these particulate shares can be seen in Table 2 (a, b, c and d).

SAMPLE A			
Fraction (mm)	Weight (g)	Weight (%)	Accum. (%)
Ungraded	50		
0.104	13.05	26.1	26.1
0.104 - 0.053	13.36	26.7	52.8
0.053 - 0.043	4.51	9.00	61.8
- 0.043	19.08	38.2	100

Table 2 (a)

SAMPLE B			
Fraction (mm)	Weight	Weight (%)	Accum. (%)
Ungraded	50		
0.104	9.22	18.4	18.4
0.104 - 0.053	13.58	27.2	45.6
0.053 - 0.043	5.40	10.8	56.4
- 0.043	21.80	43.6	100

Table 2 (b)

SAMPLE C			
Fraction (mm)	Weight	Weight (%)	Accum. (%)
Ungraded	50		
0.104	9.77	19.6	19.6
0.104 - 0.053	11.19	22.4	42.0
0.053 - 0.043	4.15	8.3	50.3
- 0.043	24.88	49.7	100

Table 2 (c)

SAMPLE D			
Fraction (mm)	Weight	Weight (%)	Accum. (%)
Ungraded	50		
0.104	24.86	49.7	49.7
0.104 - 0.053	14.47	28.9	78.6
0.053 - 0.043	3.49	7.0	85.6
- 0.043	7.17	14.4	100

Table 2 (d)

The particle size analyses indicate that samples A and B are quite similar but sample C has a finer grain size, less than 43 µm (49.7%). Sample D is the coarsest, approximately 50% is greater than 100 µm.

3.3. Particle Size Fraction at 15 µm.

Particle size fractionations were carried out with wet samples of A, B, C and D at 15 µm. The results are displayed in Table 3.

Sample A	Weight	Weight (%)	Equiv. Magnet. (%)
Ungraded	50	100	8.04
+ 0.015 mm	38.59	77.2	6.04
- 0.015 mm	11.41	22.8	0.0
Losses	1.21		

Sample B	Weight	Weight (%)	Equiv. Magnet. (%)
Ungraded	50	100	8.04
+ 0.015 mm	37.83 (39.53)	79.1	6.07
- 0.015 mm	10.02 (10.47)	20.9	1.51
Losses	2.15		

Sample C	Weight	Weight (%)	Equiv. Magnet. (%)
Ungraded	50	100	8.04
+ 0.015 mm	30.25 (30.27)	60.5	5.62
- 0.015 mm	19.71 (19.73)	39.5	0.0
Losses	0.04		

Sample D	Weight	Weight (%)	Equiv. Magnet. (%)
Ungraded	50	100	8.04
+ 0.015 mm	43.30 (46.6)	93.3	7.58
- 0.015 mm	3.12 (3.36)	6.7	3.56
Losses	3.58		

Table 3. Particle fractions at 15 µm in samples A, B, C and D.

These analyses show that samples A and B are similar, with 20% of their total being less than 15 μm. Sample C has finer particles of less than 15 μm. Sample D has 90% of particles greater than 15 μm.

3.4. Chemical Analysis

The results of analysis by X-ray fluorescence are shown in Table 4 (a, b, c and d).

The analyses of the samples were carried out using a Philips model PW 1404 XR sequential spectrometer. This equipment is provided with a Rh anode X-ray tube and with the analysing crystals necessary for testing elements between Na and U.

The quantitative analysis was carried out using the program UNIQUANT. This is a program which uses the fundamental parameters such as mass absorption coefficients, spectrum of the tube used, fluorescence performance, line overlapping factors, etc. The samples to be tested may have different physical presentations (compact tablets, pearls, metallic specimens, loose dust, fibres).

	Sample A		Fraction + 15 μm	Fraction - 15 μm	Washed Sample
	Ungraded	Reconst.Ung.	77.2%	22.8%	97.9%
Fe	44.44	44.79	49.25	29.67	44.52
Na_2O	0.4	0.22		0.97	0.48
MgO	1.77	2.46	2.93	0.9	1.71
Al_2O_3	2.72	2.70	2.66	2.83	2.84
SiO_2	7.35	8.25	9.15	5.24	7.27
P	0.072	0.072	0.071	0.077	0.073
S	1.43	0.93	0.64	1.9	1.43
Cl	1.43	0.49		2.14	1.05
K_2O	2.14	0.95	0.2	3.51	1.64
CaO	15.40	14.92	11.91	25.11	15.38
Ti	0.087	0.085	0.081	0.100	0.088
Cr	0.028	0.027	0.03	0.015	0.024
MnO	0.39	0.037	0.38	0.33	0.39
Co	0.021	0.021	0.022	0.018	0.020
Ni	0.021	0.021	0.025	0.008	0.021
Zn	0.019	0.028	0.023	0.049	0.028
Pb	0.28	0.28	0.089	0.92	0.28

Table 4 (a). XRF analysis of sample A.

	Sample B		Fraction + 15 µm	Fraction - 15 µm	Washed Sample
	Ungraded	Reconst.Ung.	79.1%	20.9%	99%
Fe	43.59	45.56	47.92	36.61	44.22
Na_2O	0.32	0.20		0.97	0.22
MgO	1.99	2.96	3.48	1.01	1.95
Al_2O_3	2.83	2.88	2.74	3.39	3.00
SiO_2	7.58	9.11	9.91	6.09	7.47
P	0.073	0.071	0.066	0.091	0.073
S	1.50	0.62	0.48	1.16	1.48
Cl	1.18	0.52		2.53	1.94
K_2O	2.11	0.75	0.19	2.87	1.79
CaO	16.35	15.00	12.18	25.66	16.12
Ti	0.092	0.089	0.084	0.11	0.091
Cr	0.031	0.032	0.022	0.07	0.030
MnO	0.36	0.36	0.34	0.43	0.35
Co	0.020	0.020	0.020	0.019	0.020
Ni	0.024	0.026	0.033		0.022
Zn	0.013	0.040	0.009	0.16	0.014
Pb	0.27	0.27	0.073	1.02	0.27

Table 4 (b). XRF analysis of sample B.

	Sample C		Fraction + 15 µm	Fraction - 15 µm	Washed Sample
	Ungraded	Reconst.Ung.	60.5%	39.5%	96%
Fe	41.41	41.93	50.25	29.21	42.23
Na_2O	1.06	0.58		1.46	0.55
MgO	1.48	2.14	2.96	0.89	1.55
Al_2O_3	2.50	2.53	2.51	2.57	2.75
SiO_2	6.55	7.2	8.75	4.85	6.68
P	0.065	0.064	0.062	0.068	0.066
S	1.52	0.92	0.39	1.74	1.23
Cl	2.93	1.47		3.73	1.74
K_2O	3.46	1.99	0.19	4.75	2.23
CaO	16.41	16.41	11.53	23.89	18.95
Ti	0.086	0.084	0.076	0.095	0.088
Cr	0.024	0.021	0.025	0.016	0.024
MnO	0.35	0.34	0.34	0.34	0.38
Co	0.019	0.020	0.022	0.017	0.021
Ni	0.015		0.023		0.014
Zn	0.022	0.032	0.010	0.064	0.022
Pb	0.68	0.63	0.16	1.35	0.72

Table 4 (c). XRF analysis of sample C.

	Sample D		Fraction + 15 µm	Fraction - 15 µm	Washed Sample
	Ungraded	Reconst.Ung.	93.3%	6.7%	93%
Fe	37.52	48.47	49.62	32.60	46.28
Na_2O	2.25			0.60	
MgO	2.12	3.05	3.05	3.07	3.43
Al_2O_3	2.90	3.08	2.93	5.14	3.42
SiO_2	6.70	10.65	10.86	7.72	9.96
P	0.041	0.062	0.062	0.075	0.058
S	1.30	0.47	0.44	0.85	0.83
Cl	9.09			3.81	1.33
K_2O	6.55	0.37	0.19	2.91	1.12
CaO	12.08	9.97	8.99	23.60	10.80
Ti	0.10	0.11	0.11	0.12	0.11
Cr	0.008	0.13	0.013	0.019	0.011
MnO	0.62	0.76	0.76	0.74	0.75
Co	0.017	0.025	0.025	0.022	0.019
Zn	0.017	0.26	0.27	0.16	0.044
Ba	0.021	0.016	0.016	0.024	0.016
Pb	0.22	0.28	0.14	2.27	0.19

Table 4 (d). XRF analysis of sample D.

3.5. Analysis by Electron Microscopy

For the analysis of these samples, use was made of an electron microprobe unit, which permits analysis by energy dispersive and wavelength dispersive X-ray spectrometry (XRS).

3.5.1. Sample A.

Photo 1 shows a set of particles in sample A. The morphology of the particles varies considerably. It is possible to see particles with round forms at approximately 100 to 150 µm and others with long forms at approximately 200 µm. Energy dispersive XRS spectrum (EDS) 1 shows the general composition of a broad zone. The particles of white tonality are somewhat porous and correspond to Fe compounds. EDS 2 presents the composition of these particles. EDS 3 corresponds to the composition of the dark particles, in this case in the form of magnesium silicate. Globular particles of Ca are also seen, which are in the form of CaO.

Photo 2 shows another set of particles in an image of retrodispersed electrons. The white particles correspond to compounds constituted by heavy elements (Fe compounds) and the dark particles correspond to light elements (silicates). Some dark particles are detected, some of which are carbonaceous (EDS 4) and others of complex silicates as seen in EDS 5.

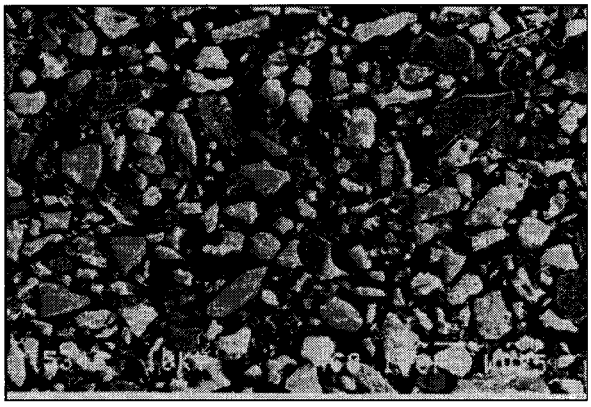

Photo 1

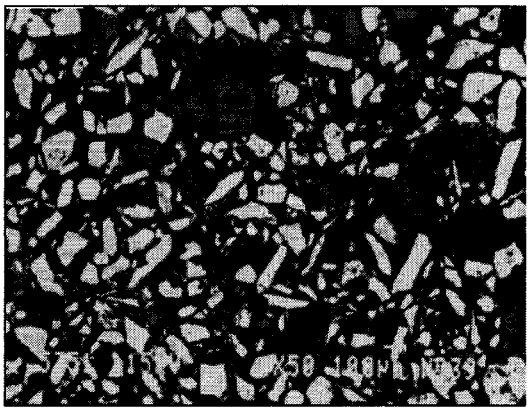

Photo 2

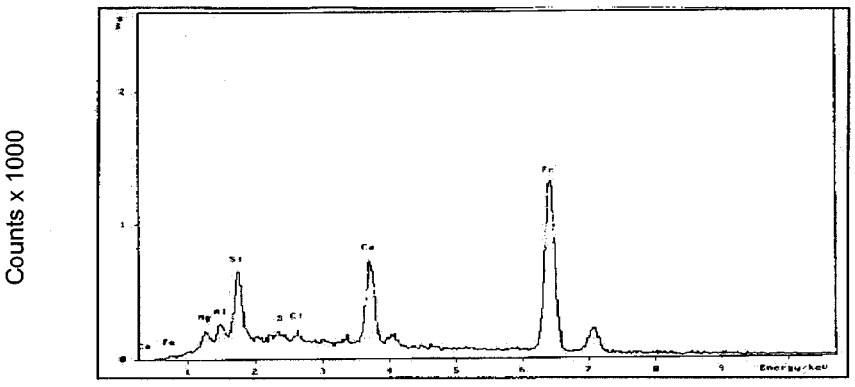

E.D.S. 1

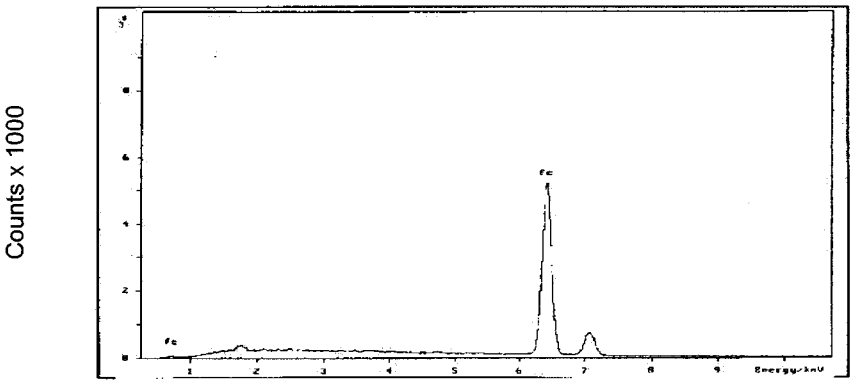

E.D.S. 2

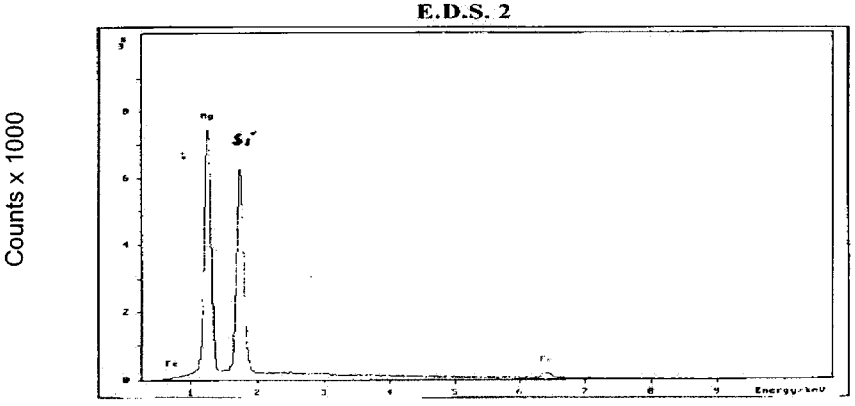

E.D.S. 3

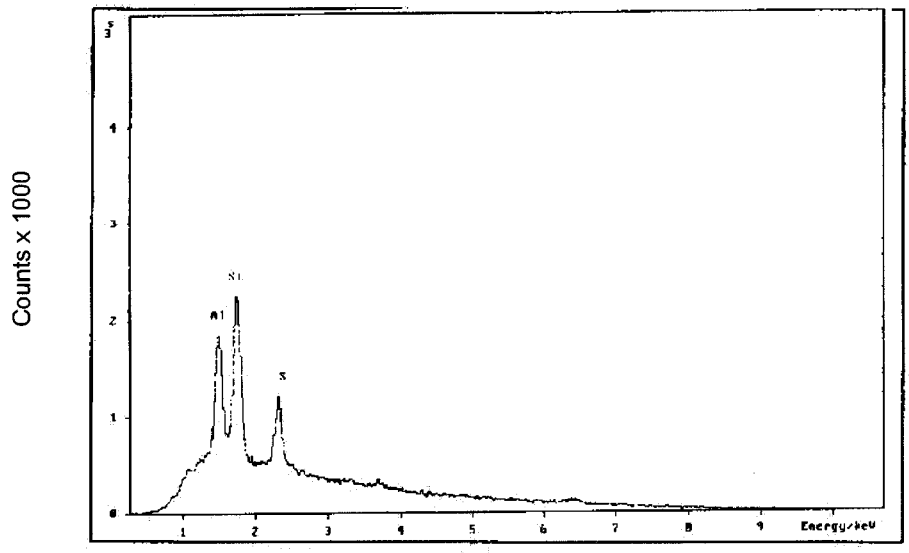

E.D.S.4.

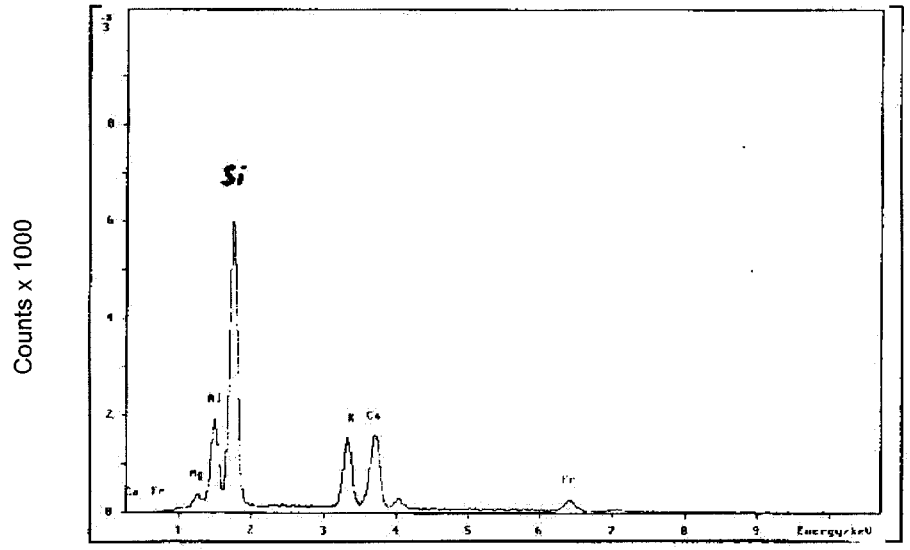

E.D.S. 5

3.5.2. Sample B.

Sample B is similar to sample A. Photo 3 shows a set of particles. These particles do not exactly have globular forms, they have the form of pebbles. The particle size varies, approximately from 10 to 150 µm, with the predomination of sizes between 100-150 µm. EDS 6 shows the general composition of a broad zone. The majority elements are Fe-Ca-Si-Mag-Al. EDS 7 shows the composition of the white particles, constituted by Fe compounds. EDS 8 presents the composition of the dark zone of a mixed particle and EDS 9 the composition of the light zone of a mixed particle.

In photo 4 the particles can be seen in greater detail. Particles are detected of Si in the form of SiO_2, of CaO and associations of Mg-Si and Fe. Globular particles of calcium ferrites are also seen.

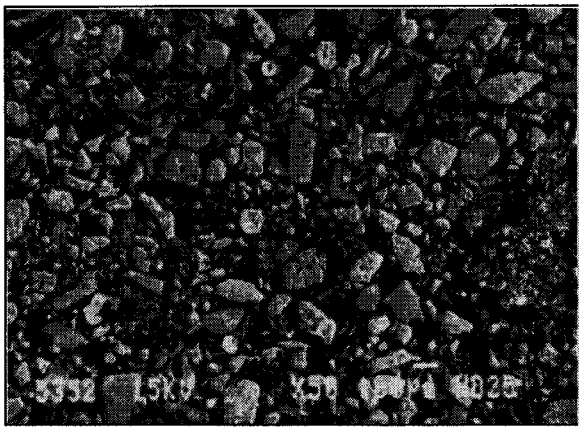

Photo 3.

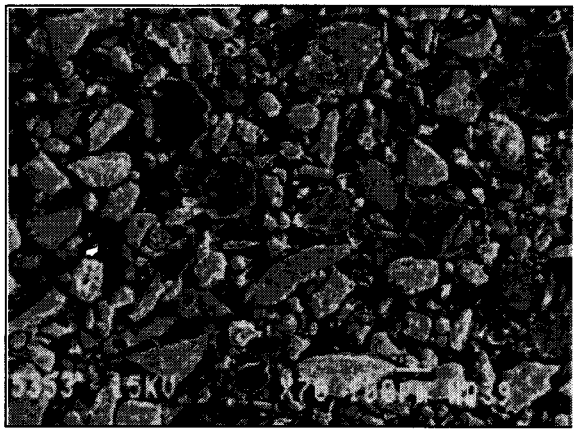

Photo 4.

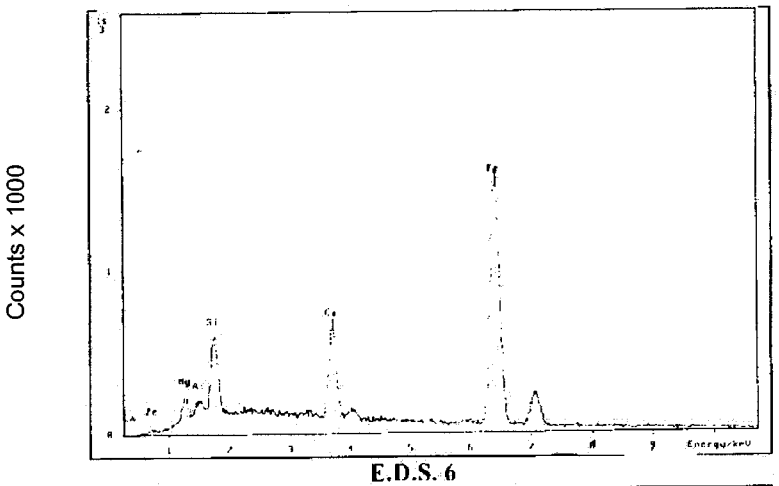

E.D.S. 6

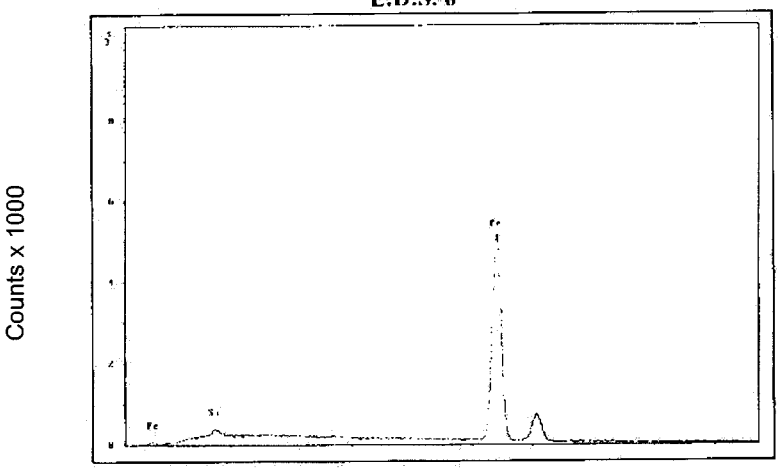

E.D.S. 7

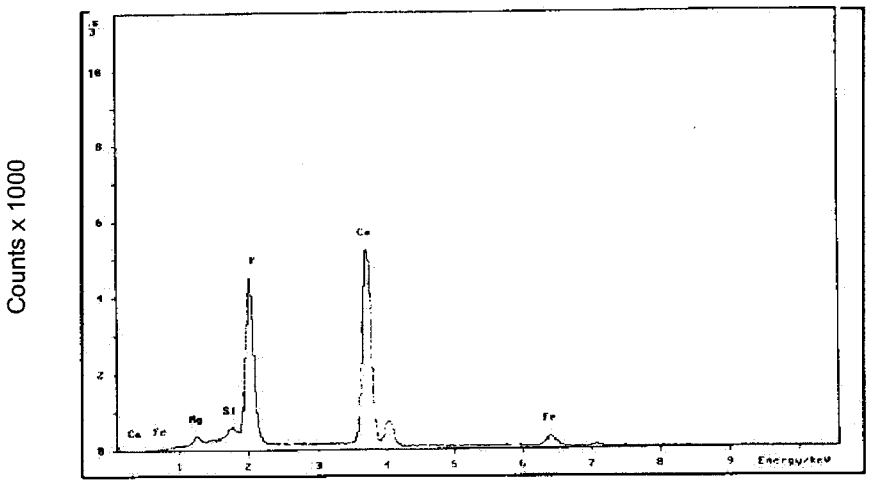

E.D.S. 8

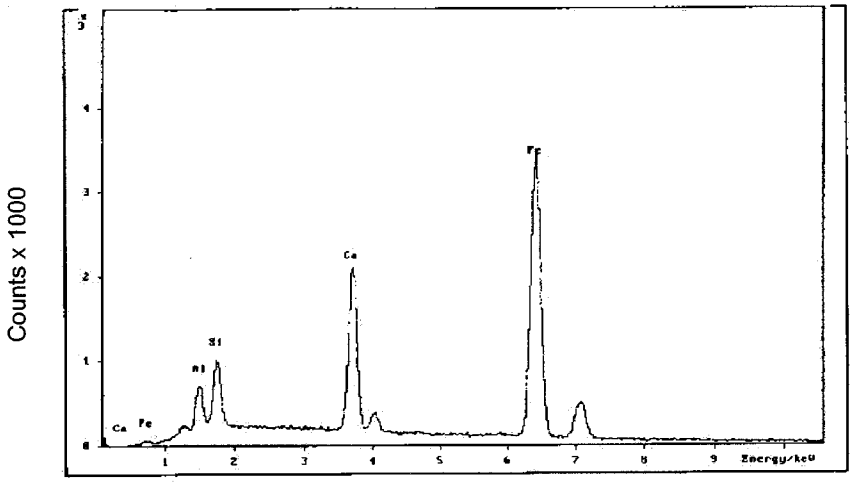

E.D.S. 9

3.5.3. Sample C

In terms of particle size, sample C is different from A and B, approximately 50% being smaller than 50 µm. This confirms the result of the particle size analysis which gave 49.7% smaller than 43 µm.

Photo 5 shows the general appearance of the sample, in which dark carbonaceous and silicate particles are detected. It is also possible to see the predomination of white particles which correspond to Fe compounds. EDS 10 presents the majority components of the sample.

Photo 6 shows another zone of sample C. In terms of composition, the particles are similar to those contained in samples A and B.

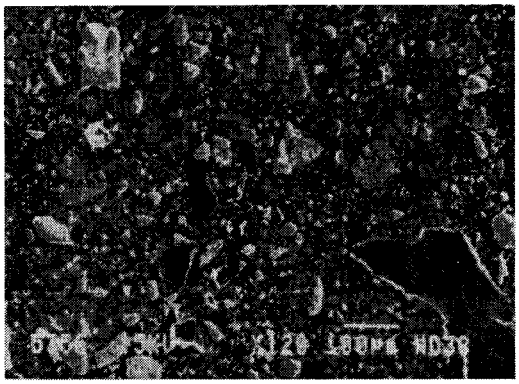

Photo 5

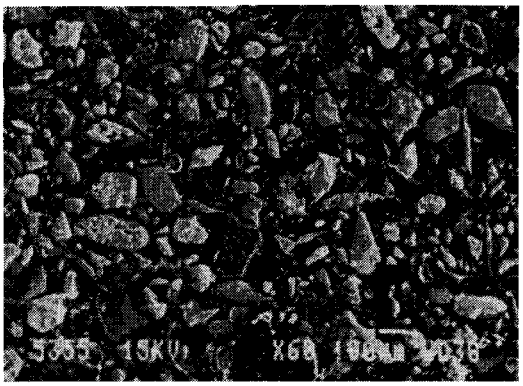

Photo 6

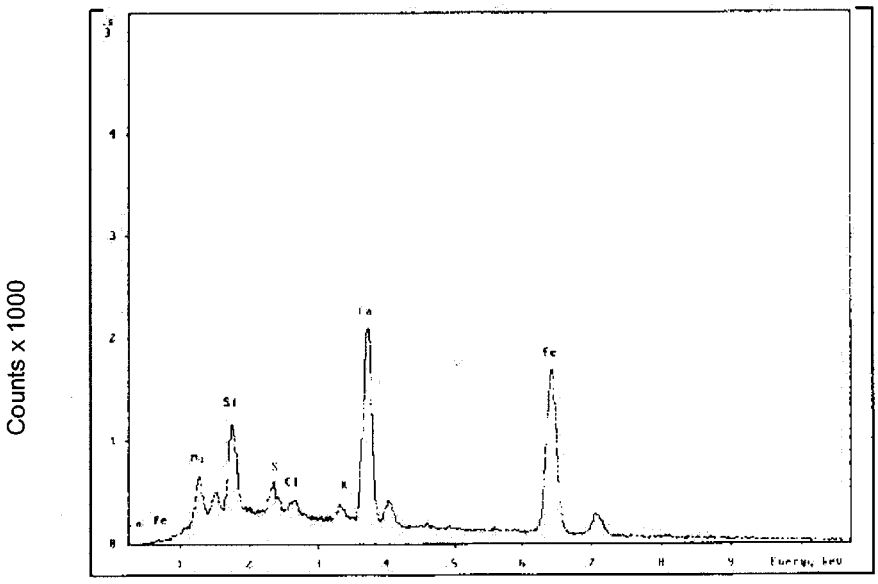

E.D.S. 10

3.5.4. Sample D.

Photo 7 shows the general appearance of these particles. The particle size is between 1 and 0.5 mm. The form of the particles is varied, with the predomination of particles with round forms. The composition of these particles varies according to their tonality, with white particles of Fe compounds and dark particles corresponding to the presence of silicates and other light compounds. K and Cl are associated with very small particles (20 µm) of Fe-Ca-Si. Fe particles are porous and of different forms. Ca-Mg associations are also detected. EDS 11 shows the composition of a broad zone.

Photo 7. General appearance of sample D.

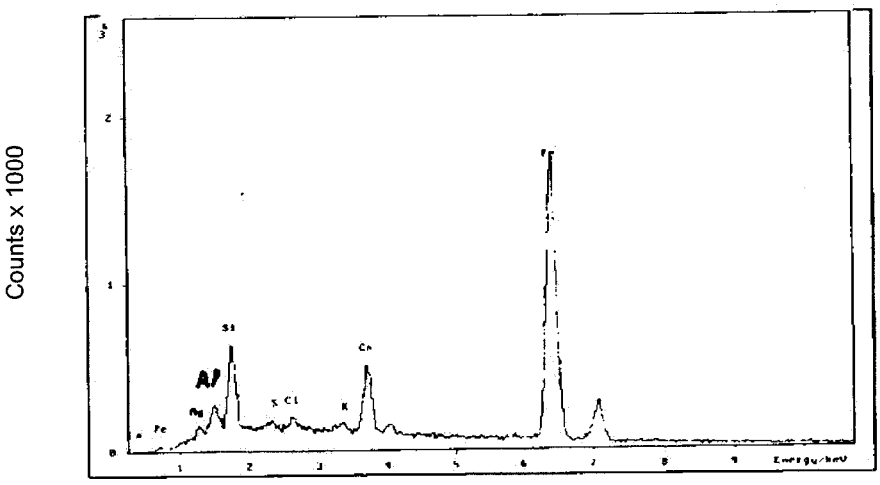

E.D.S. 11. Composición general de la muestra D.

3.6. Characterisation of Samples from CSI Planos (Avilés)

A second sample of ESP dust was received from CSI Planos for microstructural and physical-chemical characterisation.

3.6.1. Particle Size Analysis

These analyses were carried out in order to know the particle size distribution of the sample received. Subsequently a chemical analysis of each one of the fractions was carried out in order to determine possible segregations of the constituent elements. A determination was also made of the equivalent magnetite in the ungraded sample and in each fraction. Table 5 displays the size analysis between the fractions 0.981 to -0.104 mm. These analyses indicate that 60 % of the sample is smaller than 100 µm.

Fraction (mm)	Weight (g)	Weight (%)	Accum. (%)	Equiv. Mag.
Ungraded	200.00			5.55
+ 0.981	3.37	1.7	1.7	9.09
0.981 - 0.104	75.22	37.6	39.3	6.74
- 0.104	121.41	60.7	100	3.36

Table 5. Particle Size Analysis of the ESP Dust.

3.6.2. Chemical Analysis

Chemical analysis was carried out using X-ray fluorescence. Table 6 gives the results of the analysis.

	ELECTROFILTER DUST	Fraction + 0.981 mm	Fraction + 0.104 mm	Fraction - 0.104 mm
Fe	42.70	46.04	49.31	41.51
Na_2O	0.76	--	--	0.85
MgO	1.07	4.06	1.78	1.04
Al_2O_3	2.70	2.33	2.42	2.76
SiO_2	5.28	12.62	6.86	5.19
P	0.045	0.042	0.047	0.041
S	1.31	0.19	0.65	1.41
Cl	5.14	0.53	1.84	5.47
K_2O	5.35	0.63	2.04	5.76
CaO	13.92	12.49	11.66	14.62
Ti	0.068	0.056	0.066	0.070
Cr	0.010	0.023	0.012	0.010
MnO	0.54	0.51	0.56	0.52
Co	0.020	0.021	0.018	0.022
Zn	0.020	0.015	0.012	0.018
Ba	0.026	0.030	0.023	0.027
Pb	0.29	0.032	0.11	0.31

Table 6. Analysis of the ESP dust (ungraded) and size fractions.

3.6.3. Analysis by Electron Microscopy.

Photo 8 shows the general appearance of the ESP dust. The forms of the particles are varied, with the predomination of pebble or rounded forms. The particle size varies between 100-150 µm. The white particles correspond to Fe compounds and the dark particles to light compounds (silicates). Photo 9 shows another zone of the sample, where the predomination of white particles can be seen. EDS 12 presents the general composition of the sample, which is constituted by Fe-Ca-Si-Al-Mg-K-Cl-S.

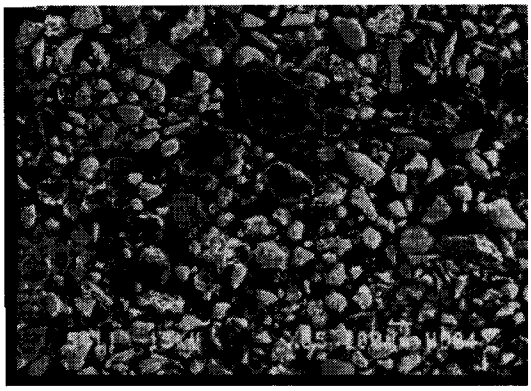

Photo 8

Photo 9

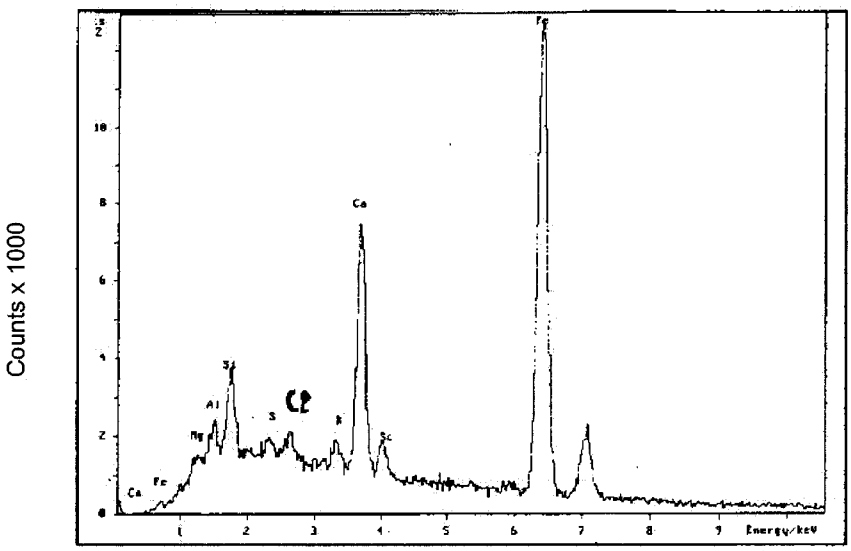

E.D.S. 12

APPENDIX 5

SUMMARY OF ACTIVITIES WITH THE MESH TEST UNIT

The following is an abbreviated description of the work by the Iberian partners aimed at operating a mesh test unit in simulated industrial conditions, to determine optimal performance in terms of filtration velocity, pulse cleaning arrangements and mesh size. Many problems were encountered in this work and the objectives were not realized. Indeed it might be argued in hindsight that the objectives were unrealistic for the equipment and techniques available, especially in view of the lack of familiarity of the personnel involved with the technical aspects of filtration. However, because the performance of the main test filter in the UK proved substantially insensitive to variations in mesh size, dust properties etc., achievement of the major objectives was not prejudiced. A lengthy treatise of the Iberian work is therefore unwarranted, but the following should enable an appreciation to be gained of the investigations involved.

A5.1 Initial Experiments

A series of experiments at the sinter pot facilities both at CSI (Aviles) and CENIM (Madrid) were conducted, to gain information on whether simulation of industrial wind main conditions might be possible.

At Aviles, isokinetic dust sampling from the gas stream before the main fan serving the sinter pot gave dust concentrations of only around 32 mg/m^3. These levels, much lower than would be expected in industrial wind mains, were attributed to the relatively low flows employed to enable the tests to be of reasonable duration. In other test runs (seven in all), dust was collected on a sheet of mineral wool placed in the flow stream between sinter box and fan. As well as the filtered dust, wind box dust was also collected and separated into major fractions. This material was split, quite consistently into the following bands:

>0.246 µm	70 – 80%
0.246 – 0.125 µm	10 – 12%
0.125 – 0.043 µm	7 – 16 %
<0.043 µm	~ 3%

CENIM considered that the dust caught by the filter and the < 0.043 µm fraction of the wind box dust, taken together, could represent the fume in an industrial wind main. The corresponding range of dust concentrations in these tests was approximately 35–500 mg/m^3 (stp).

These were regarded as somewhat low by industrial standards, and tests were made at CENIM (Madrid) to generate increased concentrations by injecting sintering dust from a Macawber dispenser. In these cold tests, use of the dispenser with ESP dust from Aviles allowed a range of higher concentrations to be achieved. Wind box dust was found to be problematic in that it tended to agglomerate and block the feeder. To limit the injected amount to required levels, it was necessary to split the dispenser flow, approximately 10% to the sinter pot and 90% to a specially constructed dust filter box containing mineral wool. What was not clear was whether the injected dust would be useful in hot tests (it might be trapped by the sinter bed) or could be useful only in cold tests, where the dust would be presented straight to the filter in conveying air.

In view of the reasonable possibility of being able to provide dust concentrations representative of industrial levels, and the ability at least to provide concentrations in hot tests at the lower end of the industrial range, design of a small trial filter proceeded. The design, outlined in Fig. A5.1, was developed in conjunction with Parftec Ltd., who also supplied the mesh screens. It incorporated two screen cylinders 1220 mm long by 190 mm diameter. The unit was constructed and installed at Aviles, and three sets of screens (100, 130 and 170 mesh) were provided. To complete the installation, the Macawber dispensing equipment was transferred from Madrid, and a flow diverter module, designed to sit in place of the sinter pot between the combustion hood and wind box, was constructed. PCME tribological dust monitoring equipment was ordered to facilitate on-line continuous assessment of dust concentration.

The experimental arrangements are shown schematically in Fig. A5.2, and the filter and flow diverter are illustrated in Fig. A5.3.

Three series of cold tests were conducted, all with 170 mesh screens, aimed at establishing conditions for filter cake formation. In these tests, dried ESP dust from Aviles was fed to the diverter module.

In the first series, progressively reduced wind box suctions (430, 220 and 110 mm water gauge) were employed, but no cake building (as judged by pressure drop across the filter unit) could be observed. There was, however, some evidence of retained dust on inspection of the screens after the third test. There was also a major problem of dust emission from the chimney and the tests had to be curtailed.

It was concluded that conditions for cake building would be improved if the filtration area were reduced. Accordingly, the second series of tests was performed with about 2/3 of the screen obscured by tape. In the first test, cake formation began after 10 minutes, and on termination after 25 minutes a 3–4 mm layer had been established. It became progressively easier to build a cake thereafter (confirming experience with the larger unit in the UK).

In these tests, the dust concentration presented to the filter screens was much higher than in industrial conditions, at about 15 g/m^3. The filtration velocity (flow/filter area), at ~ 6 m/min, was also higher than envisaged for full scale operation. Particle size analysis of the captured dust showed a preponderance in the 50 – 200 μm region.

A further series of tests established the pressure of the pulse cleaning air needed to clean the screens.

Again, in the second and third series of tests, emission of dust from the chimney was a considerable problem.

In the light of experience from the above tests, several modifications were made to the equipment, including improved access and viewing arrangements.

A5.2 Resiting and Modifying the Equipment

At this time, because of company restructuring, plans were revealed to to close the M-5 sinter strand at Aviles, and to move it, together with the pilot sintering facilities, to Gijon (Veriña). Some further tests were performed prior to the resiting, but these were limited to establishing some measurement techniques. Difficulties were experienced with the continuous dust monitor.

In order to allow tests to continue, the mesh test unit was transferred to CENIM in Madrid, causing considerable delays. After reinstallation, the dust monitor again showed problems in logging operational data, and further problems were experienced following a breakdown in the main power supply, which led to damage to several items of equipment, including some of the required instrumentation. Whilst repairs were underway, a second tribological dust monitor was ordered. Also, since the tests at Aviles had employed dust loadings higher than would be encountered with real sintering off-gas, the experimental facility was further modified to allow long term tests at around $1g/m^3$ by the addition of a flow splitter after the injector outlet and a dust recycling filter. The modified arrangements are shown in Fig. A5.4. Additional instrumentation was also designed and fitted at this stage since the low flows required were outside the range of the standard equipment at the sinter pot facility.

A5.3 Tests at CENIM

Several tests with the revised configuration were carried out. Although it was found possible to form a filter cake in some of these (at relatively high inlet dust loadings), attempts to operate the unit were frustrated by excessive dust deposition in the flow circuit. This led to widely varying dust concentrations being presented to the screens, and it was impossible to achieve the steady, reproducible operation, necessary for a meaningful campaign of trials.

At this stage, management at Aceralia expressed an interest in a secondary gas cleaning configuration. It was believed that a metallic filter placed in series with a conventional electrostatic precipitator might give a very clean outlet gas, whilst reducing the load on the filter. It was therefore decided to to attempt to simulate the conditions for such a configuration. This required low dust concentrations, as the bulk of the dust would be removed by the ESP. The Macawber dispenser was incapable of providing appropriately low feed rates, so a feeder capable of 600–1200 g/h was constructed (Fig. A5.5).

A number of tests with this equipment feeding the filter in place of the Macawber dispenser failed to achieve a filtration layer, even in tests of 4 h duration. This failure to build a cake was ascribed to the unsteady nature of the dust feeding, and once again to deposition within the flow circuit of dust which should have been presented to the filter. In retrospect, it is likely that ESP dust is not fully representative of wind main dust, since some agglomeration will have taken place during precipitation and collection. The agglomerated particles will therefore be larger and heavier and so more liable to sedimentation. A check using the Macawber unit at higher injection rates allowed a cake to be built.

The deposition of dust in the flow circuit and filter housing led to consideration of a pre-separation cyclone. This configuration had already been thought of as a full scale option. Such a unit was designed (though not built) and since the design principles may be of interest in the future, they are reproduced in Appendix 9.

Also at this time, because of the difficulties in building a filtration layer, consideration was given by CENIM personnel to the use of deliberately induced electric charge to enhance particle capture. The results of a survey are given in Appendix 10, since this approach remains a future possibility. It was concluded that, whilst various (generally small scale) devices employ this principle, and such an enhancement might be possible, the effects are complex and considerable experimental effort would be required to apply the principles effectively, with no guarantee of success. In addition, the main pilot filter appeared to operate quite well without such a strategy.

By this stage it had become apparent that the simulation of industrial gas conditions in a sinter pot facility is almost impossible. In cold tests with injected dust, the configuration of the flow circuit using sinter pot equipment was far from ideal for the carriage of consistent dust concentrations. Hot tests (which would be preferable) could only be of a duration less than that shown in the UK tests to be necessary to form a filter cake, and the batch nature of the process means that gas conditions vary with time.

It was believed that the best possibility of gaining useful information from the mesh test unit would be by transferring the equipment to an industrial sinter plant and using real wind main gas, with no time constraints on its availability.

A5.4 Tests at Gijon

After agreeing the transfer with management, the equipment was moved to the Gijon B sinter plant wind main. It was originally intended to test filtration both before and after the electrostatic precipitator, but time constraints precluded this, and the most convenient site was about 1/3 of the length of the wind main from the sinter discharge end of the plant (20 wind boxes out of 30 from the charge end). Figure A5.6 illustrates the siting. This position had the potential advantage of allowing tests at relatively high temperatures, since the wind main gas temperature at this position was higher than that of the fully combined gas in the tests at Scunthorpe. The arrangement, including a new 10 kW fan, is shown in Fig. A5.7. The offtake from and return to the wind main were about 7 m apart. The filter was provided with instrumentation to measure temperature, gas flow and pressure drop, and the tribological dust monitors were fitted in the inlet and outlet. Figure A5.8 shows the unit in place.

The main objective of the subsequent tests was to determine the optimum filtration velocity for good filtration at minimum investment cost, i.e. the smallest filtration area per unit flow consistent with reasonable pressure drop. In the event, this was not achieved. Three series of tests (one with each of the three mesh sizes) were carried out at a flow of about 16 m^3/min. This corresponded to a velocity in the 150 mm connecting pipework of about 15 m/s (presumably chosen initially to avoid dust deposition). At the filter screens (1.43 m^2) this is equivalent to a filtration velocity of 11 m/min, which is considerably higher than that employed on the pilot filter in the UK (2.3 m/min). It proved impossible with the control arrangements to reduce the flow to the lower levels (~3 - 4 m^3/min) consistent with filtration velocities around 2 m/min. This problem was attributed to flow being driven by pressure differences in the wind main between the offtake and return positions.

In all the tests condensation was a major problem. The long duct runs (~ 10 m) and high surface:volume ratio of the small diameter ductwork meant that heat losses were high, and consequently the filter operated at well below condensation temperature. This moisture, allied with excessively wet compressed air available for pulse cleaning, meant that the screens were very difficult to clean.

Some promising results were obtained. Despite the high filtration velocity, several of the pressure drop versus time traces indicated cake formation. An example is given in Fig. A5.9. The rise to 25 mbar pressure drop across the filter, compared with 12 – 15 mbar on the larger unit at Scunthorpe, is a consequence of the high flow. The dust monitor readings reported for this test suggested about 95% filtration efficiency, although their accuracy may be suspect in a wet environment. This level (if correct) is not acceptable for emission abatement, but is surprisingly good for such a high filtration velocity. There appeared to be no difference in the performance of the different screens.

All that can be concluded from these tests is that cake building and filtration can take place even at filtration velocities 5 times higher than would normally be designed for, and with considerable free moisture in the gas stream. Conventional fabrics would almost certainly have become unusable in these conditions.

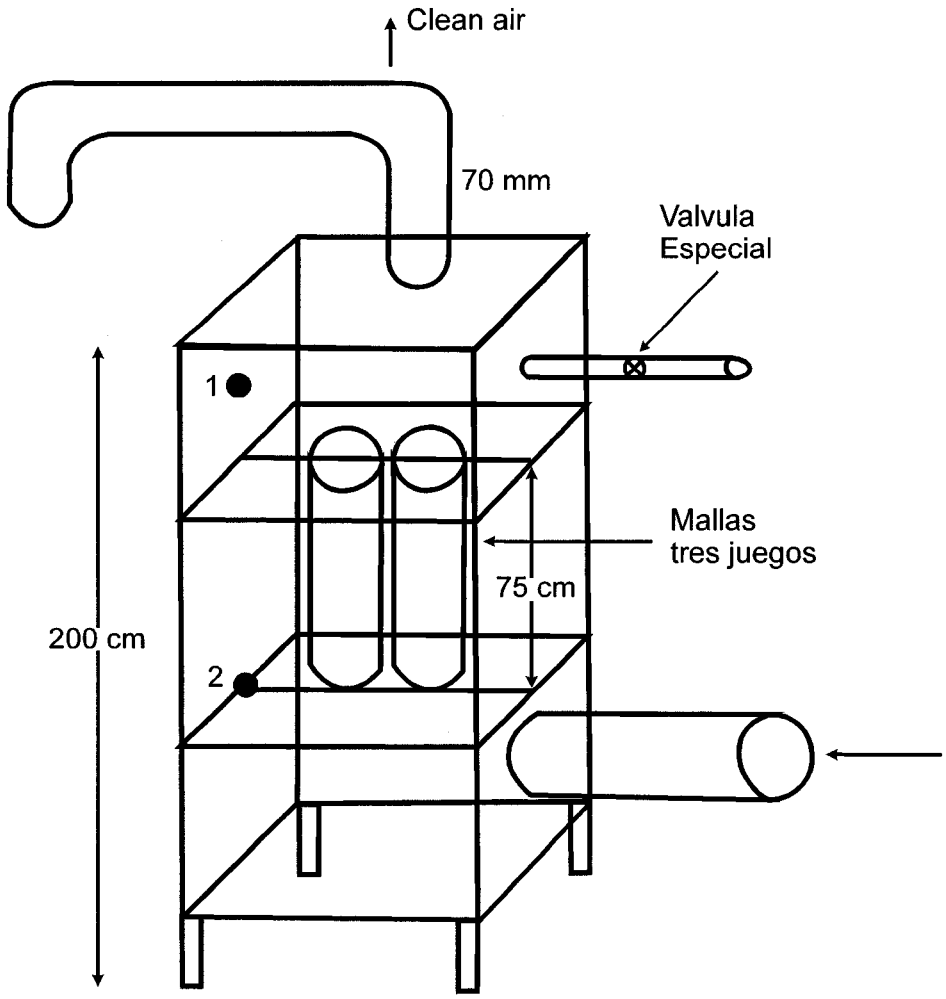

1 y 2 tomas de presión

FIG. A5.1 FILTER MESH TESTING MODULE (D0231J16)

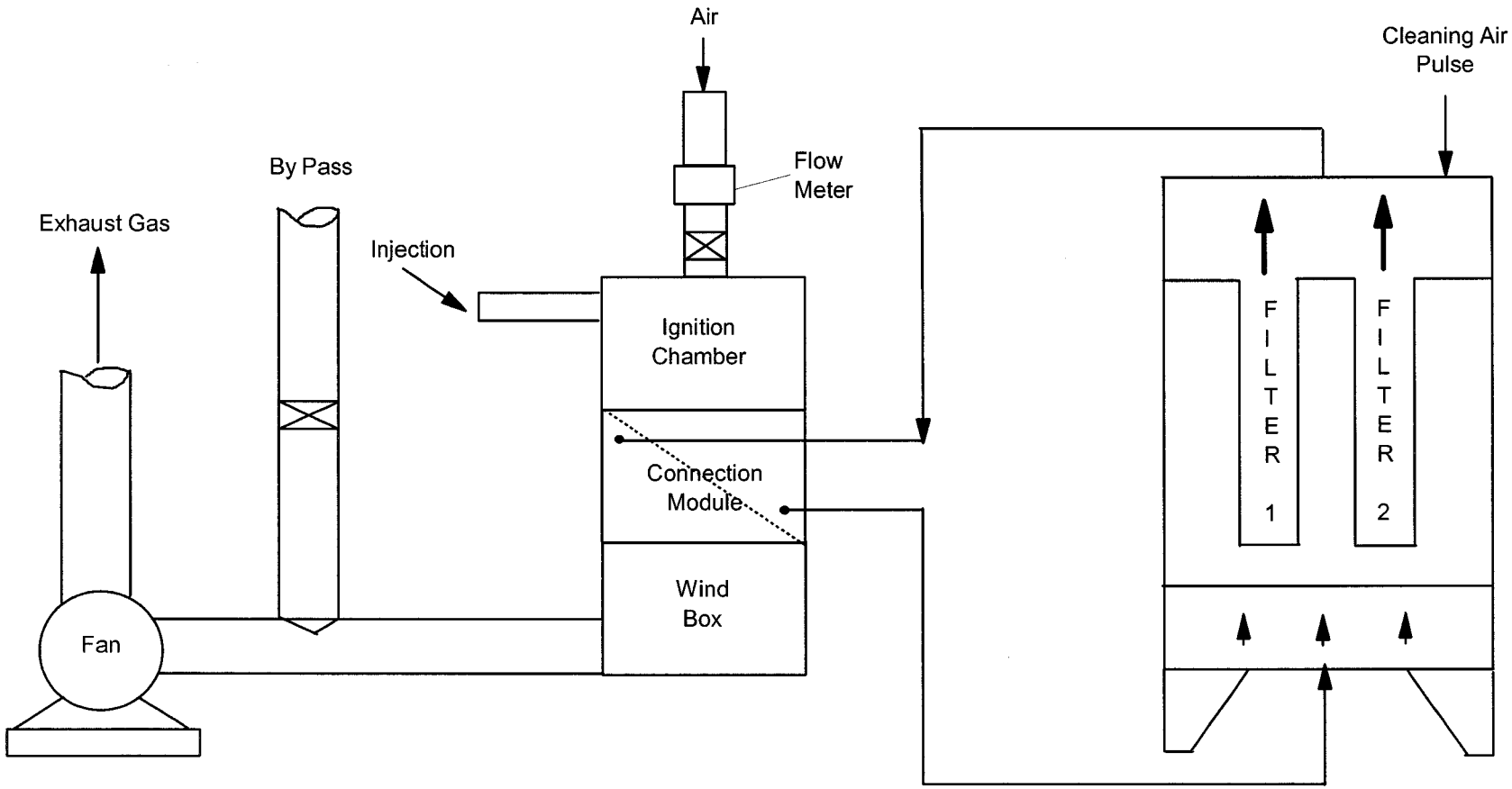

FIG. A5.2 **SCHEMATIC OF FILTER TEST FACILITY** **(D0231J17)**

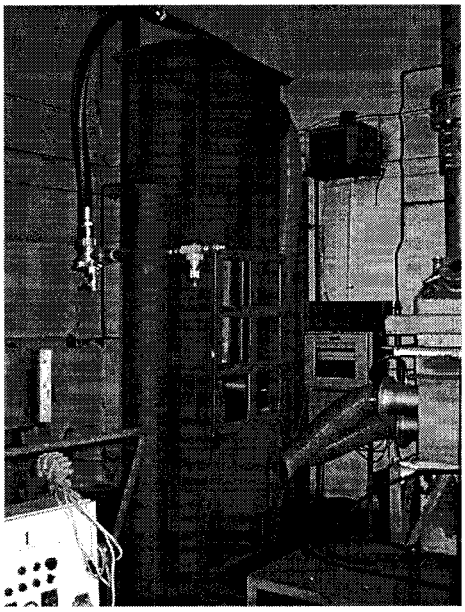

General View

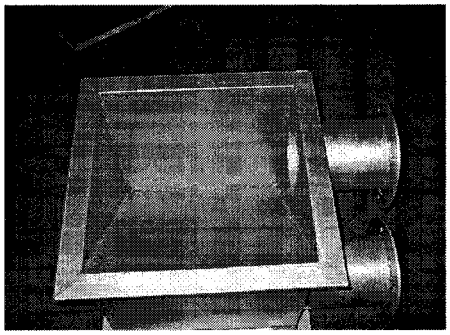

Flow Diverter Module

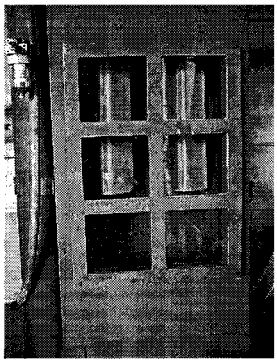

Screens Inside Filter

FIG. A5.3 IMAGES OF MESH TEST UNIT (D0231J16)

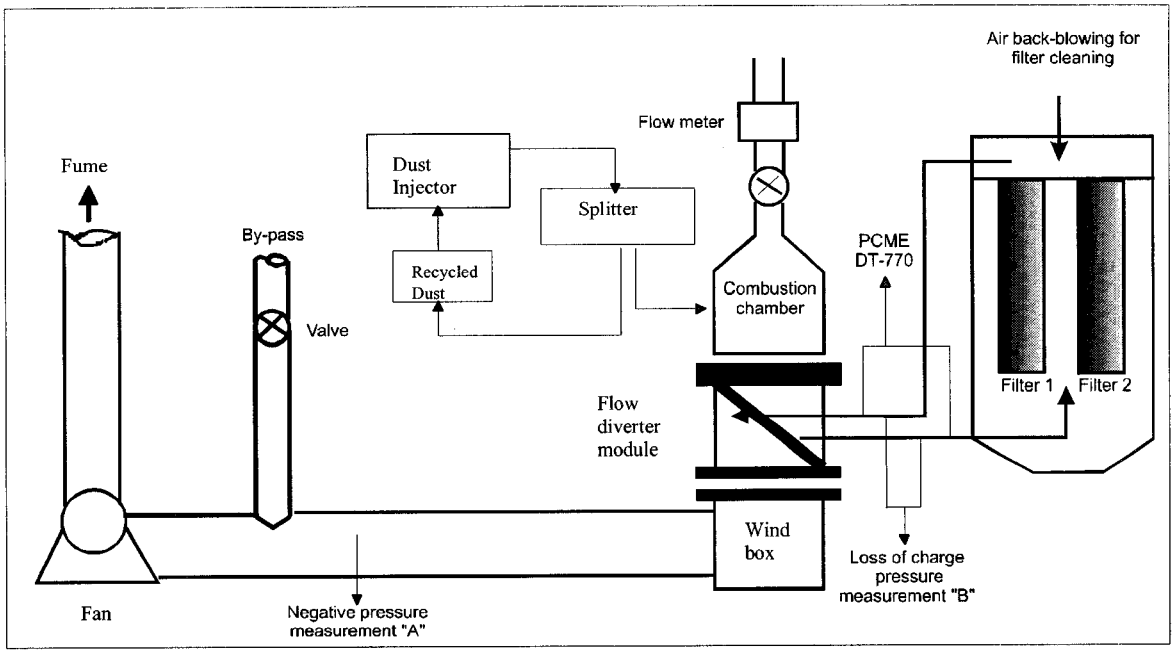

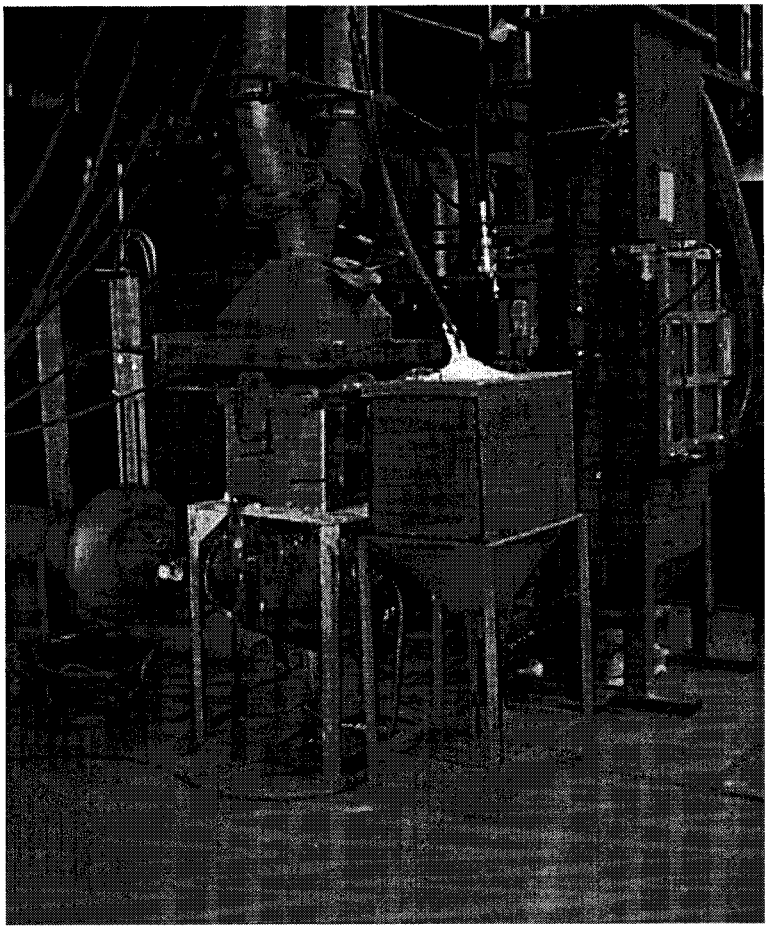

FIG. A5.4 **SKETCH AND PHOTOGRAPH OF MODIFIED ARRANGEMENT** **(D0231J16)**

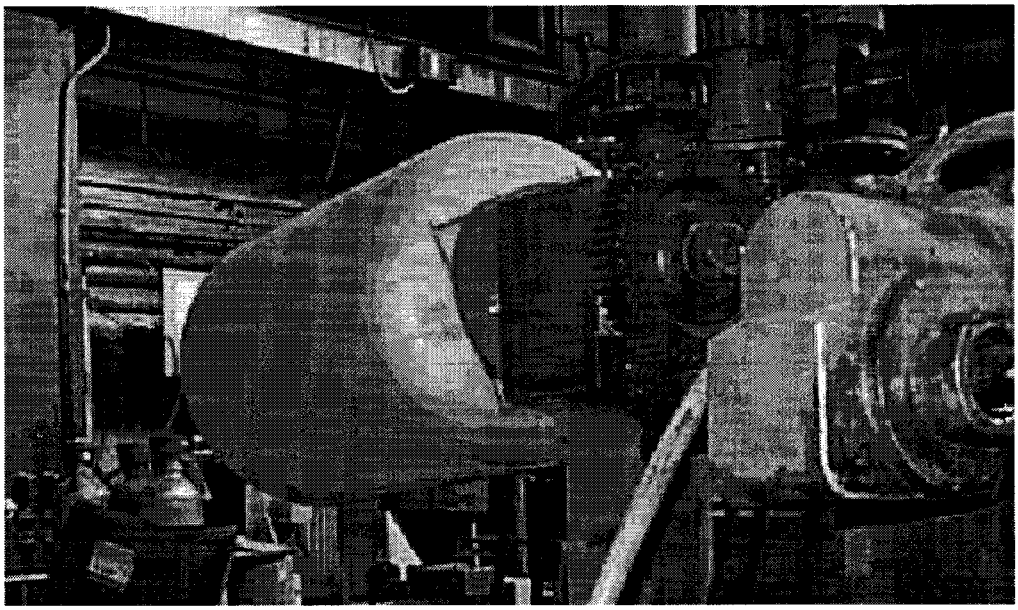

FIG. A5.5 **DUST FEEDING APARATUS** **(D0231J16)**

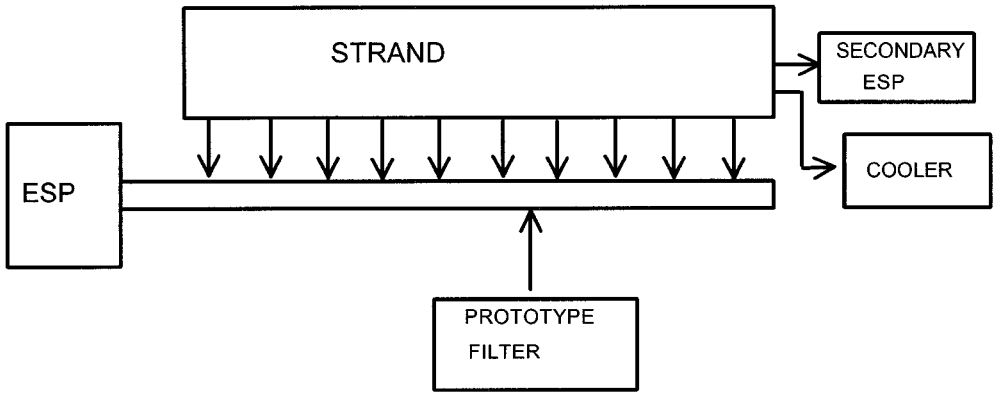

FIG. A5.6 **LOCATION OF PROTOTYPE FILTER AT ACERALIA** **(D0231J16)**

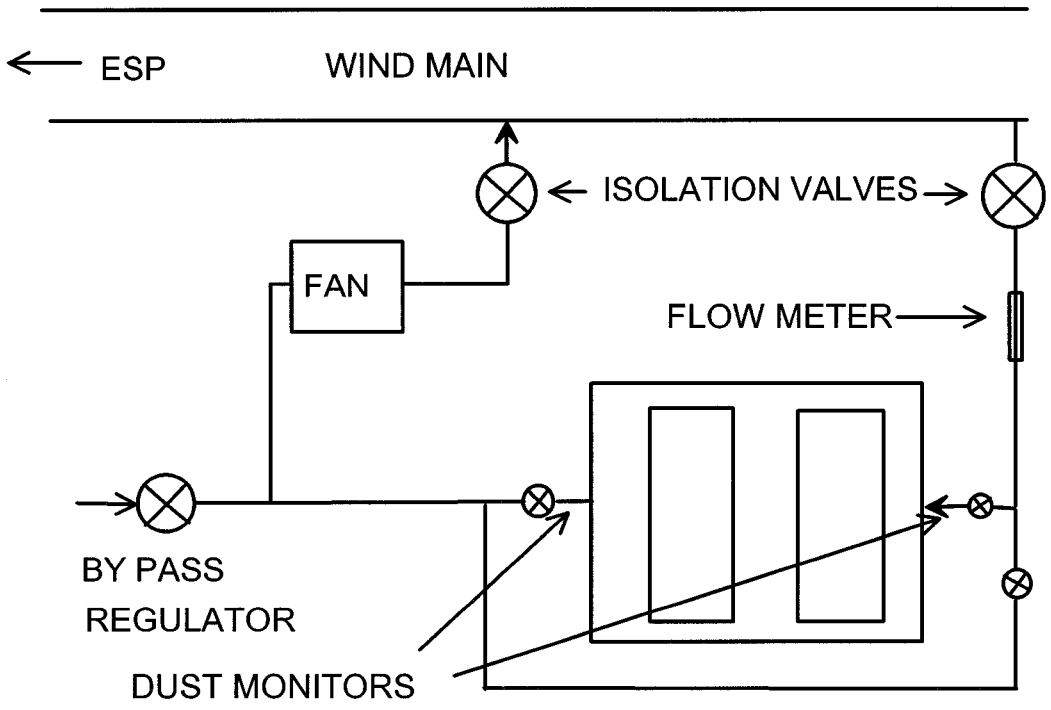

FIG. A5.7 **ARRANGEMENT OF FILTER** **(D0231J16)**

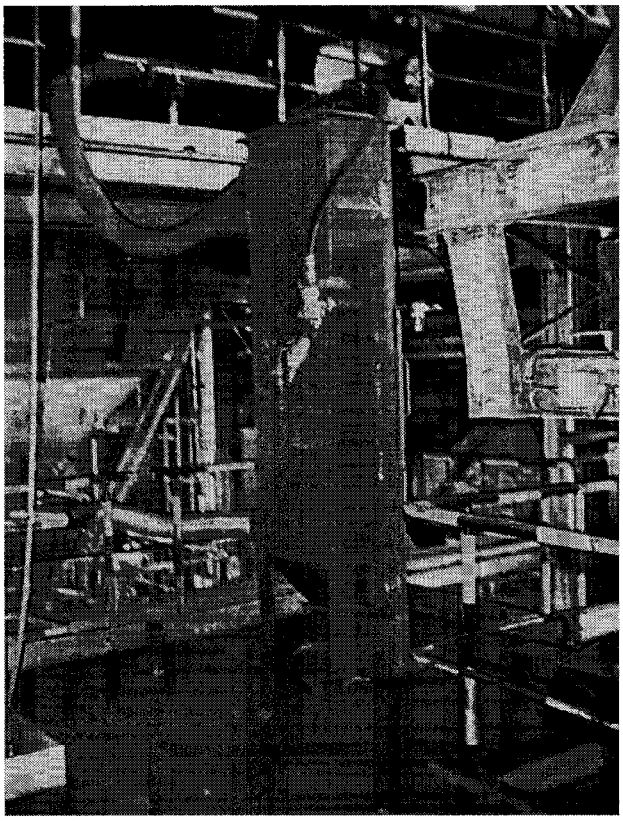

FIG. A5.8 MESH TEST UNIT INSTALLED AT GIJON (D0231J16)

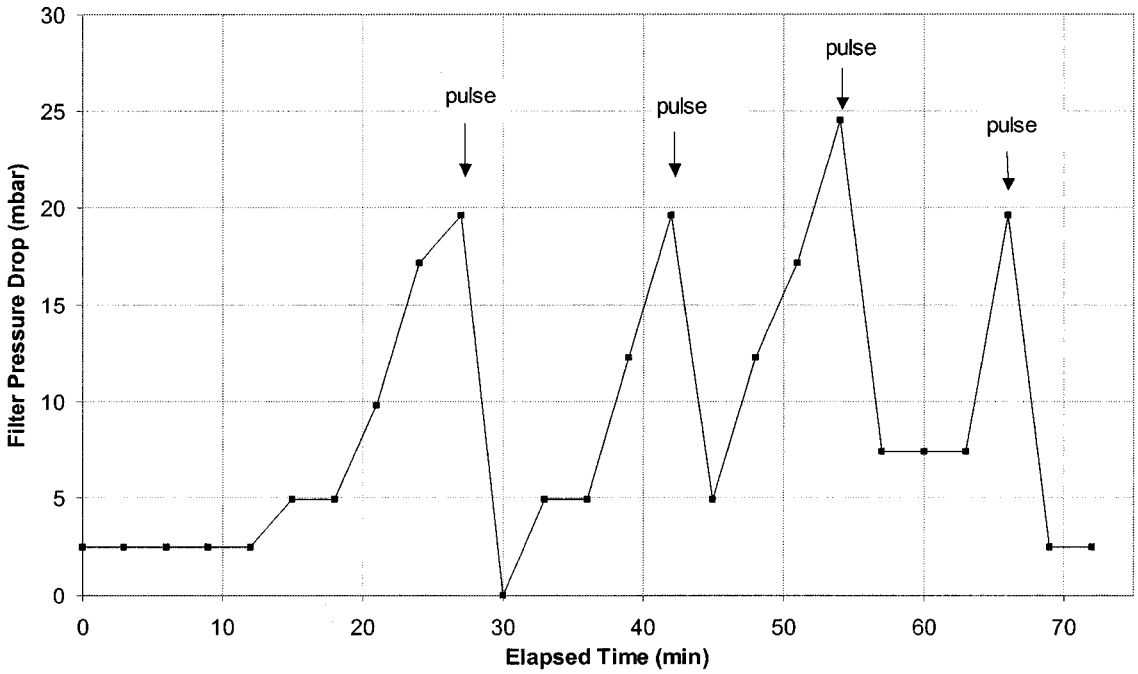

FIG. A5.9 MESH TEST UNIT PRESSURE DROP DURING GIJON TESTS (D0231J16)

APPENDIX 6

MEASUREMENTS ON THE PILOT FILTER – EAF TESTS

The list below summarises the measurement locations and methods employed. The locations are also shown in Fig. A1.1.

Location	Measurement	Method
Direct extraction duct	Gas temperature	Type K thermocouple
Inlet flow position	Gas temperature Gas velocity Dust loading (gravimetric) Dust loading (continuous)	Type K thermocouple Pitot-static tube and pressure transducer In-house pot system (results indicative) PCME DT270
Filter inlet	Gas temperature Gas velocity	Type K thermocouple Pitot-static tube and pressure transducer
Filter outlet	Gas temperature Gas velocity	Type K thermocouple Pitot-static tube and pressure transducer
Outlet flow position	Gas temperature Gas velocity Dust loading (gravimetric) Dust loading (continuous)	Type K thermocouple Pitot-static tube and pressure transducer 25 mm Gelman head and GF/A filters (~ half of tests to BS3405) PCME DT270 (low temperature probe)
Filter	Filter pressure drop	Built-in tappings and pressure transducer
Overall	Data recording	Grant Squirrel datalogger

Waste gas velocity and temperature were measured at the filter inlet and outlet together with the overall filter pressure drop. Attempts were also made to provide a continuous indication of the dust loading at the filter inlet and outlet using the PCME DT 270 dust emission monitoring system. A system including high temperature probes and purge blocks was installed at each location. Towards the end of the monitoring period a low temperature PCME probe was installed at the outlet measurement position.

Gravimetric dust loadings were undertaken at both inlet and outlet. The measurement of inlet dust loading was achieved using an in-house pot system (a system developed for use in small ducts where dust loadings are high). These results are only indicative because it was not possible to sample for the requisite length of time at four positions to comply fully with BS 3405 because of the high inlet loadings. At the filter outlet a 25 mm Gelman head and Whatman GF/A glass microfibre filter papers were used. About half of the gravimetric tests were over a relatively short sample duration (< 12 min) and were designed to provide data to calibrate the outlet PCME dust emission monitor and consequently do not fully comply with BS 3405. The remaining tests, however, used four sample positions on two

traverses and the sampling duration was a minimum of three minutes at each position. These tests complied fully with the requirements outlined in BS 3405.

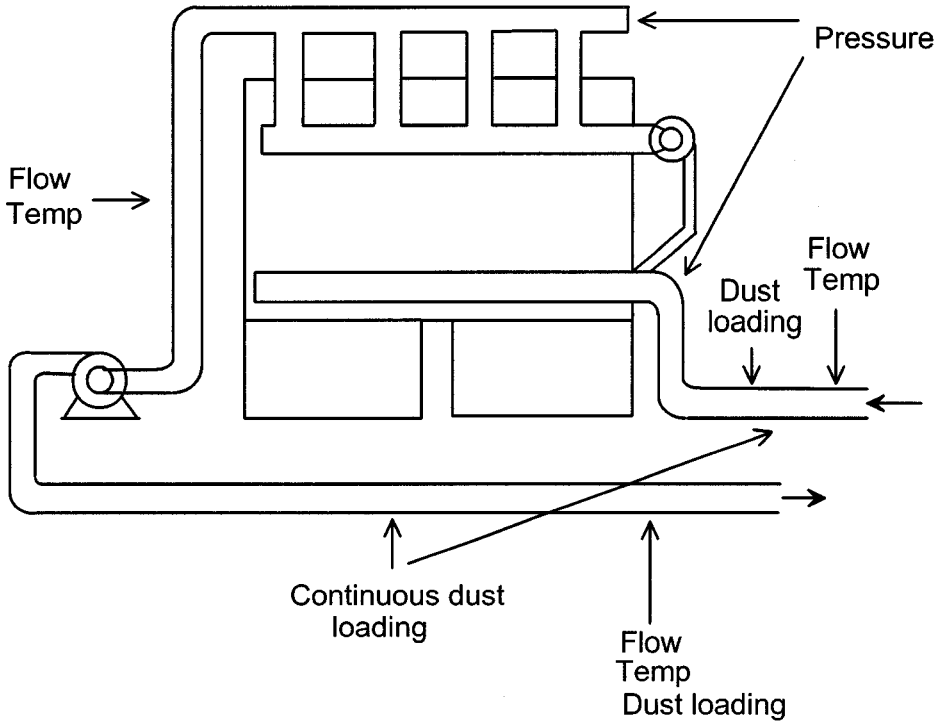

FIG. A6.1 **SCHEMATIC OF MEASUREMENT POSITIONS** **(D0231J18)**

APPENDIX 7

OPERATION AND TESTING OF THE PILOT FILTER ON EAF OFF GAS AT ALDWARKE MELTING SHOP

A7.1 FILTER OPERATION

Initial work was aimed at establishing an operation which gave acceptable outlet dust loadings with the highest possible filtration velocity (corresponding to a reasonable pressure drop). This phase was protracted owing to difficulties in calibrating the continuous dust monitors necessitating the use of gravimetric methods. The alterable parameters were inlet flow, recaking flow and elements of the cleaning/recaking cycle (settling time, pulse duration, chamber pressure drop at the end of recycling etc.).

The initial cleaning cycle is outlined below, so that changes can be seen in context.

1. Compartment changeover.

2. 120 s delay.

3. Pulse first of the two tube banks in the off-line compartment.

4. 40 s delay to allow pressure recovery in the pulse air manifold.

5. Pulse second tube bank.

6. 20 s delay (dust settling time).

7. Start recirculation fan for cake rebuilding.

8. Stop recirculation fan when pressure drop across recaking compartment reaches set point (6.2 mbar initially), or after 30 s, whichever is larger.

9. Bring newly conditioned compartment back on-line and take next compartment off-line.

In the first tests it was evident that cake formation with EAF dust was very rapid, and pressure drop quickly became excessive at flows approaching the design flow of 1.5 m^3/s. Flow was reduced to give a workable pressure drop, and changes were made to the cleaning cycle. In order to reduce average pressure drop, it was believed necessary to reduce the cleaning cycle so that newly conditioned compartments were available as soon as possible. Accordingly, the delay (2) was reduced to 20 s, and the delay between pulsing the two sets of screens (4) was eliminated.

This gave some improvement, but outlet dust loadings appeared to be highest when a newly conditioned compartment came back on line having undergone a rapid recaking phase. This occurred at times when the inlet dust loadings were high and a newly pulsed compartment was undergoing recaking. Reduction of recirculation flow, and a minimum recirculation time of 4 min eliminated visible outlet emissions, although pressure drop was still high. Dust measurements gave good results with this operation.

Tests with longer cleaning pulse durations (500 ms and 1 s) gave no noticeable improvements, but it was audibly evident that there were two distinct pulses. The setting of delay (4) to zero had given sequential rather than simultaneous pulses, which resulted in reduced second pulse pressure, and therefore less effective cleaning for the second tube set. Visual examination of the tube surfaces confirmed this.

After modification of the PLC program to give truly simultaneous pulses, screen cleaning appeared to improve substantially, as evidenced by a marked decrease in pressure drop for similar inlet flows. There was no apparent deterioration in outlet dust loadings.

The final tests were designed to investigate the pressure/flow characteristic of the unit over the maximum possible range, to determine whether operational characteristics were typical of fabric filters, and to provide starting data for the sinter plant trials.

A7.2 OPERATING RESULTS

A7.2.1 Inlet and Outlet Gas Temperatures

Typical operating temperatures (after thermal insulation was fitted) are shown in Fig. A7.1. It can be seen, as expected, that gas temperatures in the direct duct peaked at around 500°C. Temperatures at the filter inlet were appreciably lower, generally in the range 150 to 250°C, with a maximum of around 270°C. These values were no higher when the filter was operated continuously for a 24 h period.

Outlet gas temperatures, even after insulating the body of the filter, rarely exceeded 100°C. The large temperature loss across the filter was found to be primarily due to the air ingress employed to form an air curtain around the valve flap which was used to divert the gases either to the outlet manifold or to the recirculation/cake building circuit. This is discussed in more detail below.

A7.2.2 Filter Pressure and Flow

The pressure/flow relationship (and by inference filtration velocity) were investigated in order to establish information for the sinter plant application.

Typical pressure and flow operating conditions for the filter are shown for the two modes of cleaning operation in Figs. A7.2 and A7.3. It can be seen, in both cases, that the inlet flow is 0.6 m^3/s (actual), giving a filtration velocity of 1.4 m/min based on the filtration area of the three on-line compartments. The improvements in pressure drop achieved by simultaneously pulsing both banks of filter screens and extending the pulse duration from 200 ms to 1 s can be seen clearly. Overall filter pressure drop was reduced from between 22 and 28 mbar to between 16 and 22 mbar, which is not atypical of fabric filter operation for EAFs.

The characteristic saw tooth pressure trace is a consequence of compartment changeover and the effect of this on filter inlet flow can be seen to be small.

Further tests were undertaken, over a limited range of filtration velocities (1.5 to 3 m/min), to establish the relationship between pressure and flow under operating conditions. Under these conditions increasing the inlet flow would be expected to increase cake thickness, particularly as the predominant trigger for compartment change over was time (minimum

recaking time 4 min). Theory suggests that under these conditions the pressure drop should be a function of the square of the filtration velocity.

The relationship established using linear regression on these data, as shown in Fig. A7.4, is:-

$$Q = 0.0078.(P.T)^{0.5}$$

where Q = gas flow, m^3/s actual;
P = pressure drop, mbar;
and T = gas temperature, K.

The data used in the determination of this relationship cover a limited range of inlet temperatures from 180 to 240°C. However, the equation can be used to estimate the likely pressure drop at different inlet flows and gas temperatures under broadly similar operating conditions.

In addition to these operating data, the pressure/flow characteristic across an established cake of constant thickness has also been investigated. These tests were carried out when the furnace was off in order to ensure that no additional dust was added to the filter cake produced at the end of the previous day's normal operation. These data are presented graphically in Fig. A7.5. The linear relationship between actual flow and filter pressure drop confirms theory in that a laminar flow regime must pertain at the filter tube surface. The relationship established for this particular filter cake is:-

$$Q = 0.0438.P + 0.0308$$

where Q = flow, m^3/s actual;
and P = pressure drop, mbar.

The intercept is small and at zero pressure drop relates to a measured velocity head of less than 0.001 mbar which is within the limits of experimental error.

Because pressure drop attributable to geometrical factors (restrictions, bends etc.) is related to the square of velocity, this linear relationship indicates good filter design since the pressure loss is almost all caused by the filter cake itself.

A7.2.3 Inleakage

The low outlet gas temperatures, typically less than 80°C at inlet temperatures of 200°C (after insulation of the filter body), suggested some air inleakage into the filter. Simultaneous measurements of inlet and outlet flow under working conditions indicated that this was indeed the case with air ingress accounting for typically around 50% of the inlet flow (see Fig. A2.6). This dilution accounts for more than half of the gas temperature loss across the filter and also reduces the outlet dust loadings by dilution.

To determine the source of this inleakage gas flows were measured, during a furnace non-productive period, at the filter inlet, fan inlet and fan outlet. The results showed that most of the inleakage occurred across the filter (34% of inlet flow) with only a relatively small amount (5%) across the fan. This level of air ingress into the filter is higher than anticipated at the start of the tests. Further tests demonstrated that when the hollow shafts driving the diverter blades were blocked the inleakage across the filter was reduced to 6% or less of the inlet flow.

Air is induced (by design) through the hollow drive shafts and outlet diverter blades by the normal system suction. This air flows out through slots around the edges of the blade producing an air curtain which opposes fume leakage across the blade to housing gap as illustrated in Fig. 5 of the main text.

These results suggest that the air ingress through the total open area of the shafts is approximately 0.15 m^3/s equating to an average velocity of about 25 m/s. This was confirmed by measurement of the velocity across the open end of each shaft using a pipe-shrouded pitot-static tube and a hot wire anemometer. This experimental design feature, therefore, whilst very desirable from a maintenance viewpoint, has implications with respect to operation, and for the basis on which the outlet emissions should be reported. In this Appendix the outlet dust loadings are presented as measured, with no adjustment for the air dilution.

This phenomenon should not be over emphasised. With the valve design as tested, the proportion of indrawn air would reduce considerably with increase in filter size. Also, the design has not been optimised, and tighter clearances would almost certainly allow operation with reduced air curtain flows.

During this work simple attempts were made to investigate the effect of reduced flow with the existing design by blocking the open ends of the diverter shafts whilst leaving the linkage end open. Flow measurements indicated that the inleakage across the filter reduced to about 21% of the inlet flow with the flow through the valve shafts being reduced to approximately 0.08 m^3/s. However the effect of this flow reduction on the velocity distribution around the edges of the diverter plate is unknown. The effect on performance was to increase outlet loadings but levels were still acceptable (see next Section).

A7.2.4 Inlet and Outlet Dust Loadings

Initially 31 outlet gravimetric tests were performed with T furnace operating and the filter cleaning cycle as outlined in Section A7.1. At this time the cleaning pulse was of 200 ms duration and the two tube banks were not pulsed simultaneously. The pulse pressure was about 2.4 bar (gauge) for the first tube bank.

Inlet dust loadings were not always measured at the same time as outlet levels but the results obtained showed a range between 4.1 and 12.4 g/m^3 stp with a mean of approximately 8 g/m^3 stp, i.e. about a thousand times greater than those expected after the filter.

Some of the outlet tests were designed to provide information to calibrate the outlet dust emission monitor and consequently do not conform fully to BS 3405 in respect to four measurement points and the required sampling duration at each point. About 45% of the tests conformed fully to BS 3405 whilst the rest had sampling durations of 10 min (39%) or less (16%). However, the mean values of each of these data sets are all very similar being in the range 9 to 11 mg/m^3 stp compared with the overall mean of 9.6 mg/m^3. The range of outlet loadings obtained can be seen in Fig. A7.7 which shows that 87% of the tests gave less than 20 mg/m^3 stp. If no inleakage occurred across the filter (and provided that the same amount of dust was passed) the outlet loadings would be proportionally higher and the mean for this data set would be increased to 14.4 mg/m^3 stp and the proportion less than 20 mg/m^3 stp would reduce to 81%.

In addition to the relatively short duration gravimetric tests two measurements were undertaken which covered complete furnace operating cycles of 101 and 75 min. During one of these the open end of the diverter valve shaft was blocked to reduce air inleakage and thus air flow to the diverter valve seal. Outlet loadings of 3 and 10 mg/m^3 stp were obtained with the lower value obtained with the open valve shafts.

A further series of outlet dust loadings was undertaken with true simultaneous pulsing of both tube banks and with pulse durations increased to 500 ms and 1 s. These results are similar to those obtained in the initial tests having a range between 5.4 and 13.3 mg/m^3 stp, with a mean value of 9.5 mg/m^3 stp, and show that the modifications made to the pulse cleaning arrangements (giving lower filter operating pressure drop) did not adversely affect outlet emissions. It is also worthy of note that, even allowing for inleakage, these results are all less than 20 mg/m^3 stp.

The initial attempts to provide information regarding continuous inlet and outlet dust loadings, using high temperature DT 270 triboelectric probes made by PCME, were unsuccessful. However, later tests using a low temperature probe at the fan outlet position provided a range of results that enabled a calibration to be produced. A linear regression has been used to relate the PCME signal to dust loading in mg/m^3 stp and this has been used to provide an almost continuous trace of outlet dust loading which is of particular interest at compartment changeover and pulse cleaning periods (see Fig. A7.8). In most cases a peak was detected by the continuous dust monitor at compartment changeover followed 20 s later by another peak which coincided with the cleaning pulse of the compartment just taken off line. During these periods the output from the continuous monitor often reached its maximum value which was equivalent to 266 mg/m^3 stp. However, it must be noted that this signal is a 3 s average and the average level during compartment changeover and pulsing may be better reflected by the 30 s average values stored in the instrument memory (compartment change and pulse takes approximately 30 s). The maximum of these 30 s averages ranged from 50 to 100 mg/m^3 stp. It should also be noted that the outlet dust concentration profile for a conventional filter is believed to exhibit a similar profile. Data on such continuous measurements are not readily available in the literature.

It is likely that the amount of dust bleed-through on compartment changeover is to a large degree determined by the condition of the newly established cake. No systematic study was made of the effect on cake stability of the recirculation flow. Neither was any attempt made to set the changeover pressure level to approximate that of the on-line compartments after changeover. This strategy would have minimised the instantaneous velocity change through the newly formed cake. It is therefore believed that optimisation of recoating parameters should give improved performance. Indeed, the filtration performance might be regarded as surprisingly good in view of the lack of optimisation.

A7.2.5 Collection Efficiency

This is defined as the difference between inlet and outlet dust loading expressed as a percentage of the inlet loading. To enable the collection efficiency to be calculated a limited number of simultaneous inlet and outlet tests were undertaken. The results are shown in Table A7.1. Inlet dust loadings varied from about 4 to 12 g/m^3 stp and outlet loadings from 2.4 to 17.5 mg/m^3 stp. The collection efficiency was typically around 99.9%.

TABLE A7.1
COLLECTION EFFICIENCY (EAF TESTS)

Furnace State	Inlet Dust Loading (g/m^3 (stp))	Outlet Dust Loading (mg/m^3 (stp))	Filter Efficiency (%)
1st Basket Melt	4.1	4.3	99.93
	8.0		
	10.2		
	5.6	2.4	99.97
	7.2		
	8.7		
	9.4	9.0	99.89
	7.1		
	7.3		
	9.1		
	7.0		
	5.2	4.0	99.94
	8.4		
2nd Basket Melt	12.4		
	7.4	17.5	99.77
	8.5		
	7.4		
	8.1	8.4	99.90

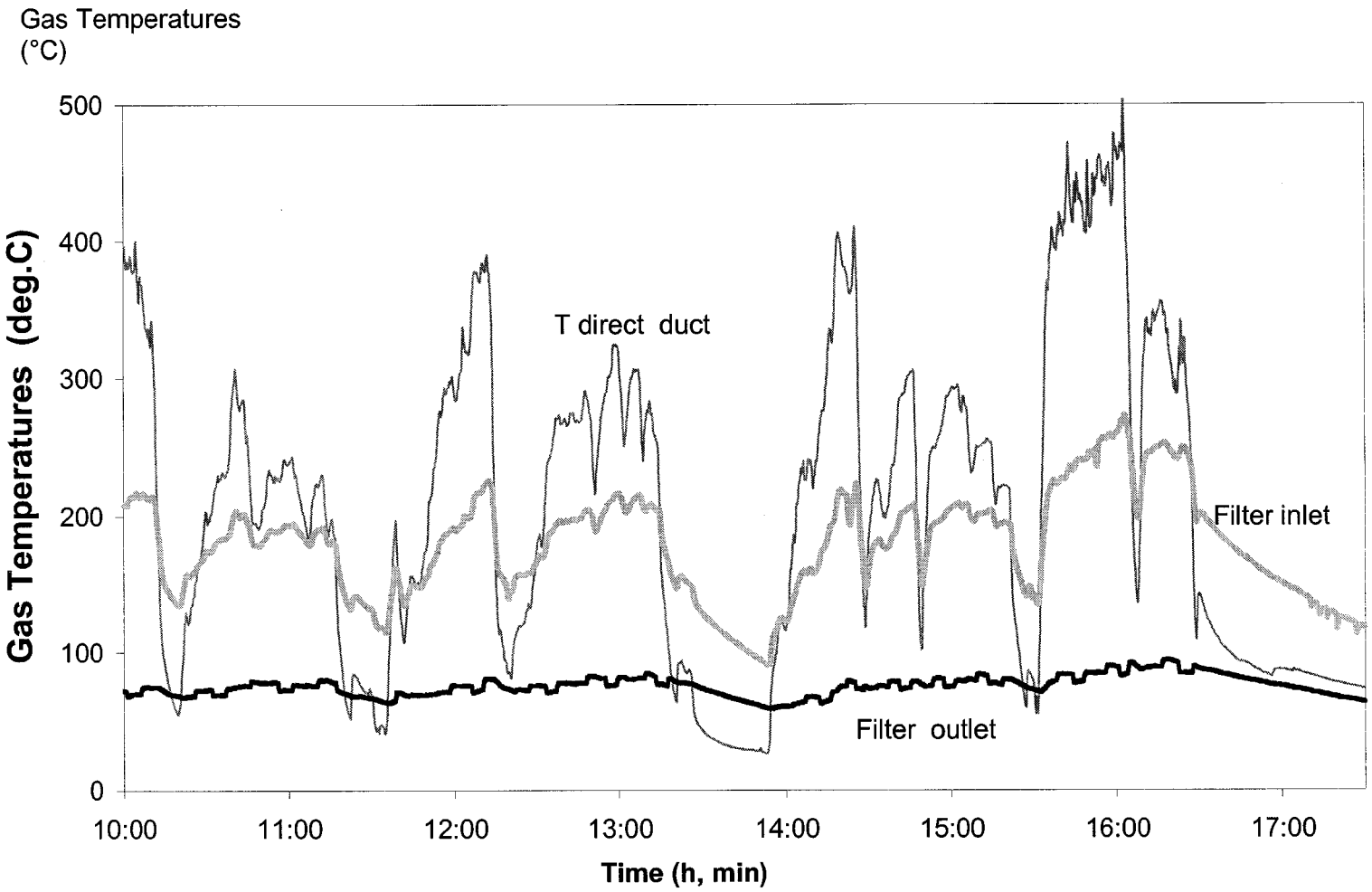

FIG. A7.1 **TRACE OF TYPICAL OPERATING TEMPERATURE** **(D0231J20)**

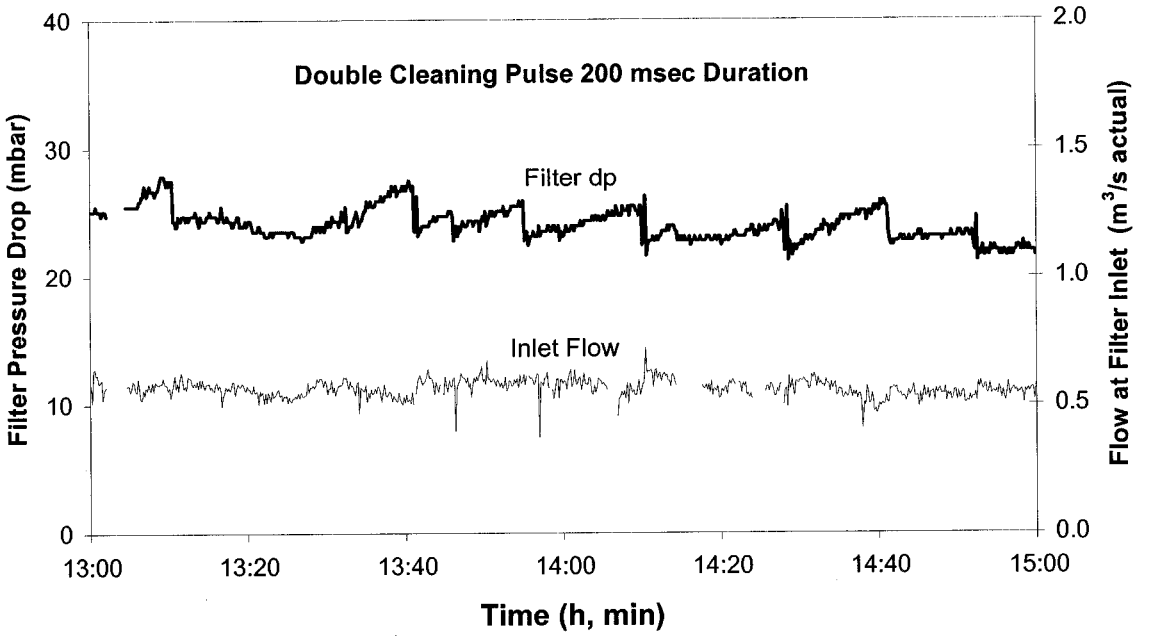

FIG. A7.2 EARLY OPERATION PRESSURE AND FLOW (D0231J21)

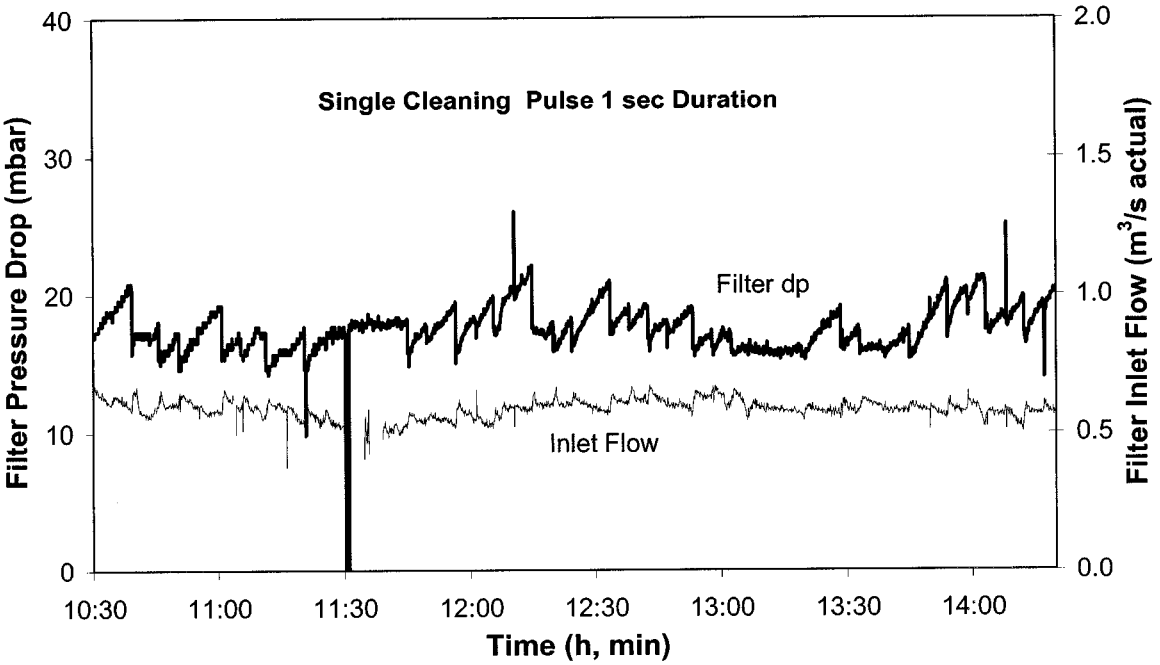

FIG. A7.3 LATER OPERATING PRESSURE AND FLOW (D0231J21)

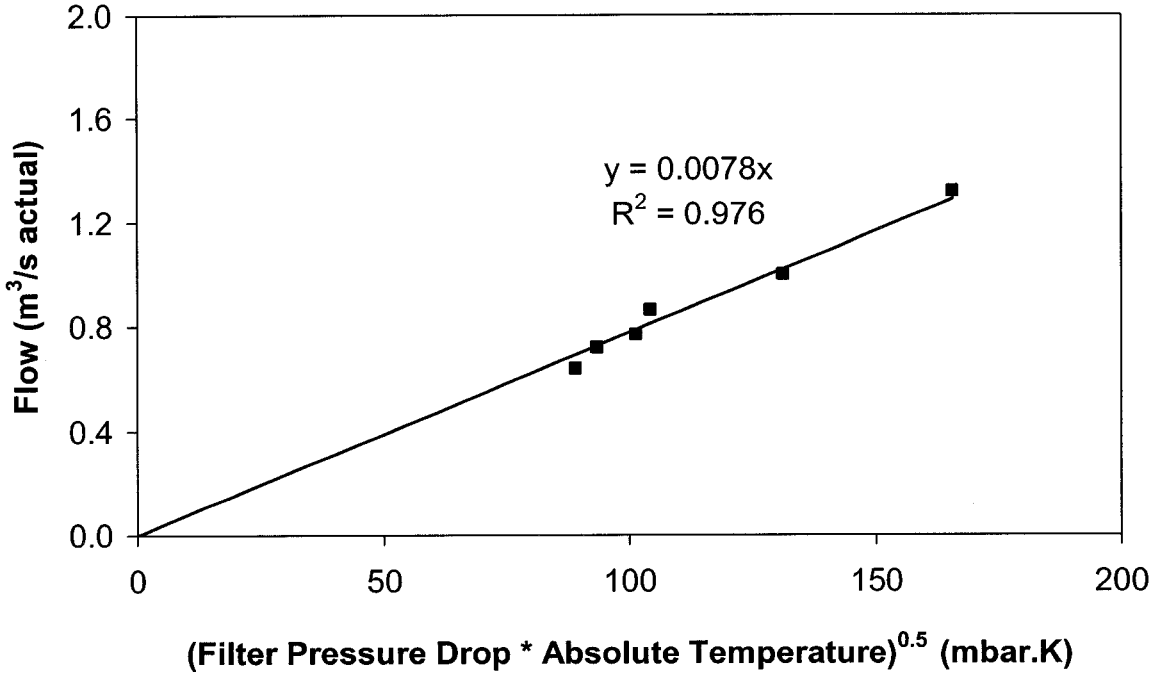

FIG. A7.4 FLOW/PRESSURE RELATIONSHIP FOR NORMAL OPERATION (D0231J21)

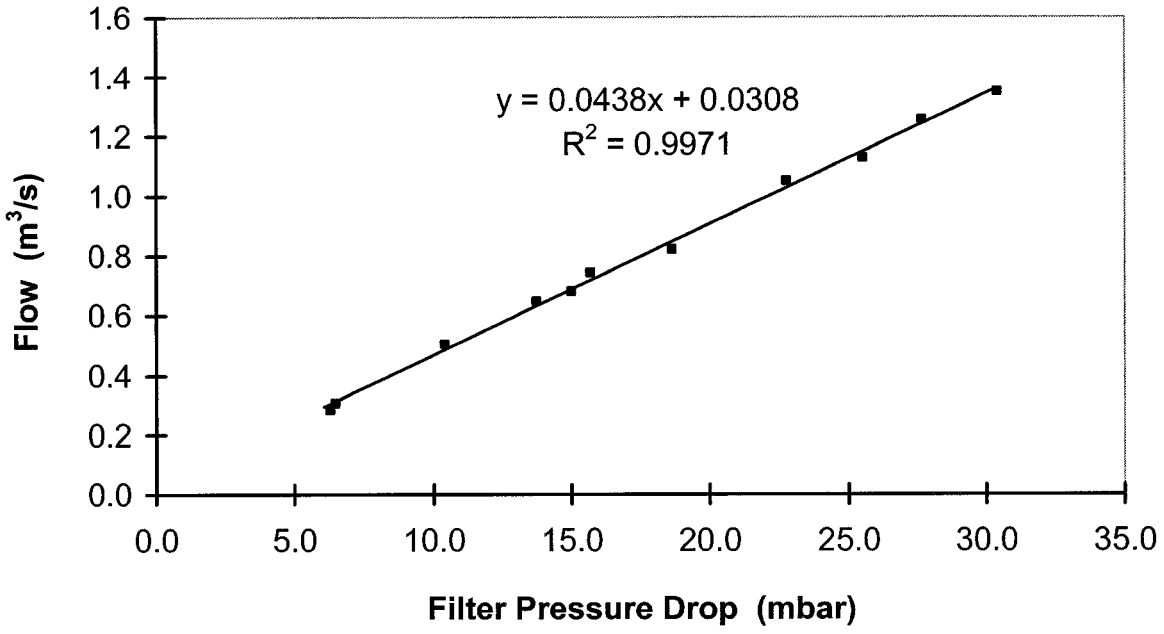

FIG. A7.5 FLOW/PRESSURE RELATIONSHIP FOR CONSTANT CAKE THICKNESS (D0231J21)

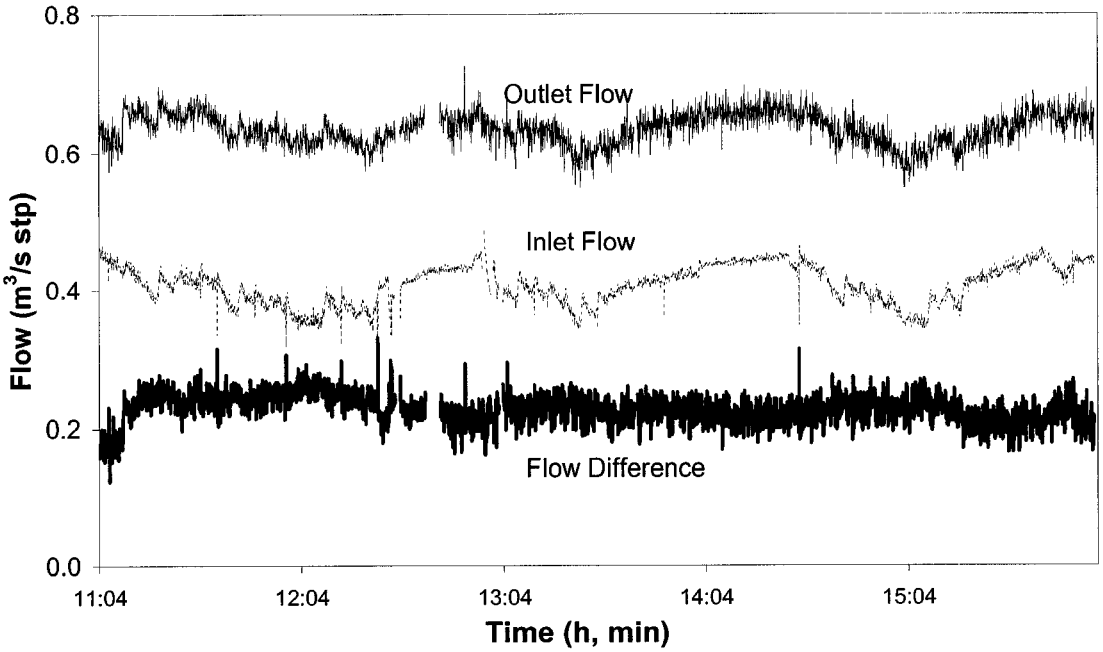

FIG. A7.6 INLEAKAGE (D0231J21)

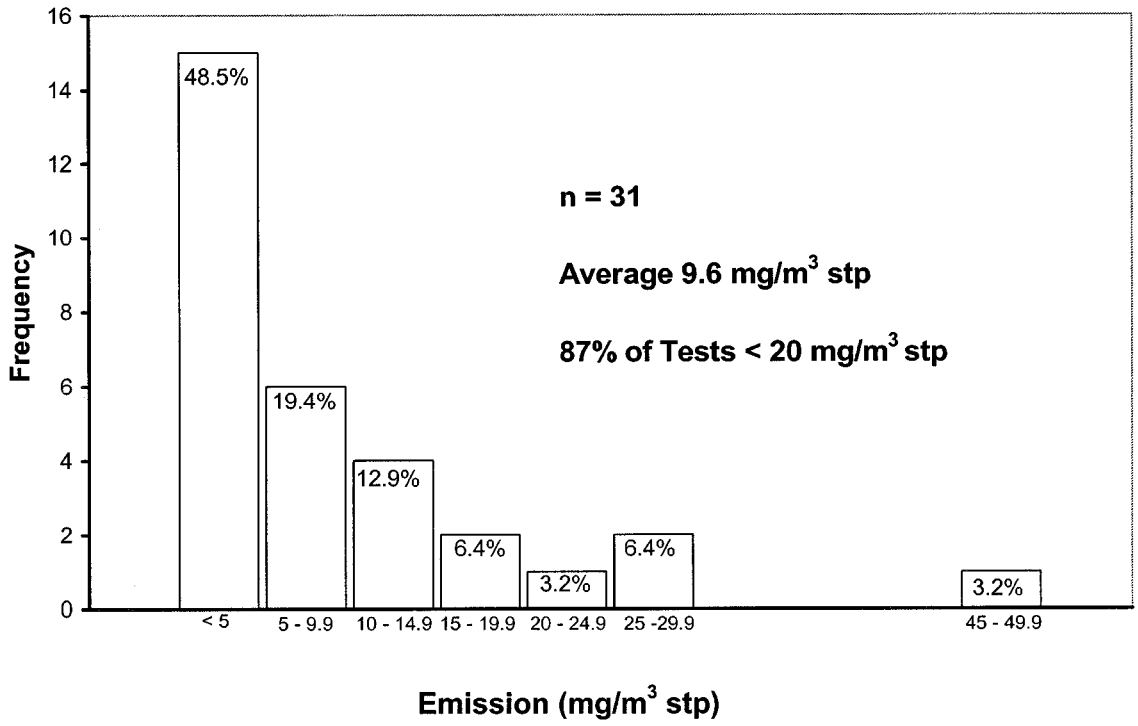

FIG. A7.7 OUTLET EMISSION RESULTS (D0231J21)

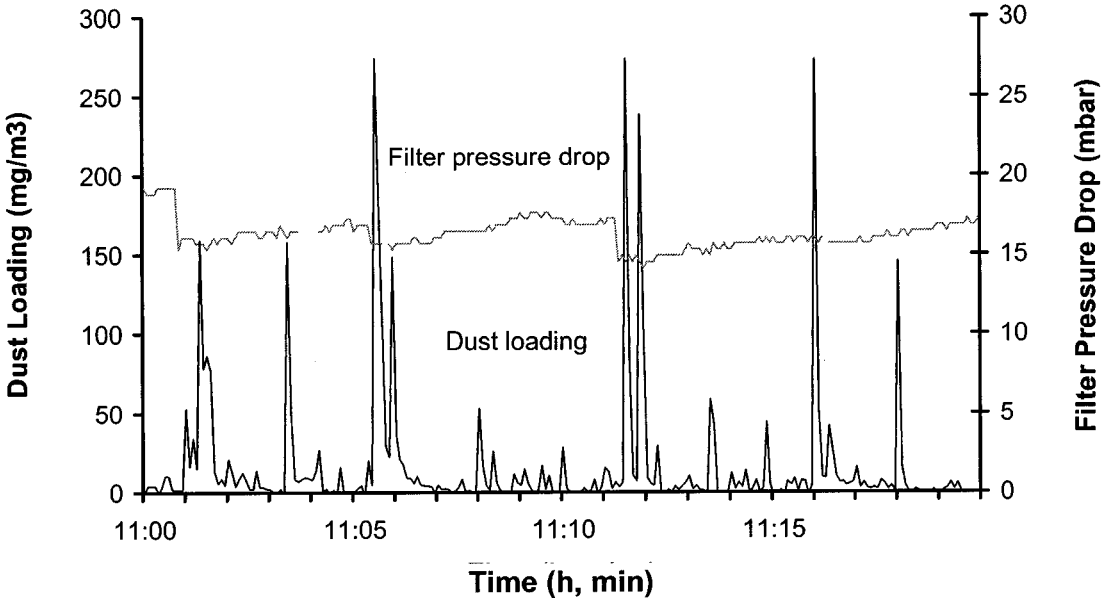

FIG. A7.8 TRIBOLOGICAL DUST MONITORING RESULTS (D0231J21)

APPENDIX 8

SAMPLES OF COLLECTED DUST FROM THE PILOT FILTER

The sources of the samples are shown in Fig. A8.1

Particle size analyses are given in Tables A8.1, A8.2 and A8.3, and illustrated in Fig. A8.2. It can be seen that the dust from Bins A, B and C (Samples 1, 2 and 3) is of a broadly similar size range, the major constituents being in the 124 - 246 μm band, with <10% below 43 μm. Bin D (Sample 4) which is nearest the inlet has more of the smaller fractions and less of the larger, whilst the material collected when the screens in Compartment C (Sample 5) were pulse cleaned has 60% <43 μm and very little above 125 μm. This supports the distribution theory outlined in Section 3.6 of the main text.

Samples for chemical analysis were treated as follows:

Drying to 100°C.
20 g sub-sample heated to 600°C for 1 h and weight loss determined.
Grinding.
XRF analysis.
Magnetite equivalent determination.

Results of the XRF analysis of the dry samples and after heating are listed in Table A8.6. The composition after thermal treatment showed little changed. The stability is confirmed by the magnetite equivalent (indicating presence of Fe^{2+}) before and after heating at 600°C (Table A8.4).

The chemical compositions vary in a similar manner to those in Table 9 of the main text. K, Na, Cl, Pb, Zn and S increase as the proportion of fine material increases, and are highest in the material collected from the screens, confirming the concentration of undesirable components in the finer fractions.

It is interesting that Hg (as expected) and Cd (unexpectedly) were not detected, and that Se, Br and Tl become detectable as the smaller fractions increase. Carbon content remained stable after heating and loss of weight was small (Table A8.5).

All the above supports the proposition that pre-separation of larger particles by a sedimentation chamber or cyclone, followed by filtration, could be an effective combination for separating readily recyclable and undesirable materials.

TABLE A8.1
PARTICLE SIZE ANALYSIS OF DRY SAMPLES 1 AND 2

Size (mm)	Sample 1			Sample 2		
	Weight (g)	%	% Acum	Weight (g)	%	% Acum
>0.495	0.95	6.2	6.2	0.18	1.2	1.2
00495-0.246	2.34	15.4	21.6	2.26	14.9	16.1
0.246-0.124	8.03	52.8	74.4	7.49	49.5	65.6
0.124-0.063	3.15	20.7	95.1	3.78	25.0	90.6
0.063-0.043	0.52	3.4	98.5	0.81	5.4	96.0
<0.043	0.23	1.5	100.0	0.61	4.0	100.0
Total	15.22	100.0		15.13	100.0	

TABLE A8.2
PARTICLE SIZE ANALYSIS OF DRY SAMPLES 3 AND 4

Size (mm)	Sample 1			Sample 2		
	Weight (g)	%	% Acum	Weight (g)	%	% Acum
>0.495	0.99	6.6	6.6	0.99	6.7	6.7
0.495-0.246	5.13	34.2	40.8	2.37	16.1	22.8
0.246-0.124	5.85	39.1	79.9	2.56	17.4	40.2
0.124-0.063	1.40	9.3	89.2	2.66	18.1	58.3
0.063-0.043	0.53	3.5	92.7	1.41	9.6	67.9
<0.043	1.09	7.7	100.0	4.73	32.1	100.0
Total	14.99	100.0		14.72	100.0	

TABLE A8.3
PARTICLE SIZE ANALYSIS OF DRY SAMPLE 5

Size (mm)	Sample 1		
	Weight (g)	%	% Acum
>0.495	0.09	0.6	0.6
0.495-0.246	0.09	0.6	1.2
0.246-0.124	0.69	4.7	5.9
0.124-0.063	2.72	18.4	24.3
0.063-0.043	2.40	16.3	40.6
<0.043	8.77	59.4	100.0
TOTAL	14.76	100.0	

TABLE A8.4
MAGNETITE EQUIVALENT CONTENT

Sample	Dried Sample Before Calcination	After Calcination
1	8.05	7.64
2	6.64	6.57
3	8.18	8.01
4	5.10	-
5	3.30	-

TABLE A8.5
CARBON CONTENT AND WEIGHT LOSS AFTER HEATING

Sample	% C	Ignition Loss of Weight
1*	1.4	0.3
2*	1.9	0.6
3*	1.8	0.6
1**	2.2	

* After heating (600°C, 1 h) ** Dry sample

TABLE A8.6
CHEMICAL COMPOSITION OF DUST SAMPLES

	Dry Samples				
	Sample 1	Sample 2	Sample 3	Sample 4	Sample 5
Na/Na_2O	0.054 / 0.073	0.080 / 0.108	0.276 / 0.372	0.523 / 0.705	1.28 / 1.73
Mg/MgO	2.61 / 4.32	1.95 / 3.23	2.04 / 3.39	0.982 / 1.63	0.627 / 1.04
Al/Al_2O_3	1.12 / 2.12	1.22 / 2.31	1.23 / 2.32	1.20 / 2.27	1.34 / 2.52
Si/SiO_2	4.44 / 9.50	4.00 / 8.55	3.86 / 8.27	3.03 / 6.49	2.68 / 5.73
P/P_2O_5	0.0548 / 0.0548	0.0618 / 0.0618	0.0579 / 0.0579	0.0640 / 0.0640	0.0590 / 0.0590
Sx/SO_3	0.539 / 1.35	1.40 / 3.50	1.79 / 4.48	5.44 / 13.59	5.43 / 13.56
Cl/Cl	0.179 / 0.179	0.443 / 0.443	0.933 / 0.933	2.35 / 2.35	4.46 / 4.46
K/K_2O	0.0776 / 0.0936	0.212 / 0.256	0.592 / 0.713	1.46 / 1.76	3.50 / 4.22
Ca/CaO	5.61 / 7.85	7.03 / 9.83	7.47 / 10.45	9.95 / 13.91	11.39 / 15.93
Ti/TiO_2	0.0556 / 0.0927	0.0624 / 0.104	0.0648 / 0.108	0.0643 / 0.107	0.0747 / 0.125
Cr/Cr_2O_3	0.0186 / 0.0272	0.0179 / 0.0261	0.0189 / 0.0276	0.0288 / 0.0421	0.0257 / 0.0376
Mn/MnO	0.241 / 0.311	0.256 / 0.331	0.281 / 0.363	0.305 / 0.394	0.268 / 0.346
Fe/Fe_2O_3	51.54 / 73.69	49.54 / 70.84	47.58 / 68.03	38.59 / 55.18	33.58 / 48.01
Co/Co_3O_4	0.0322 / 0.0410	0.0350 / 0.0445	0.0316 / 0.0402	0.0299 / 0.0381	0.0267 / 0.0340
Ni/NiO	0.0337 / 0.0429	0.0320 / 0.0407	0.0270 / 0.0344	0.0310 / 0.0395	0.0193 / 0.0245
Cu/CuO	-	-	-	0.0297 / 0.0372	0.0455 / 0.0570
Zn/ZnO	0.0091 / 0.0113	0.0187 / 0.0233	0.0325 / 0.0404	0.114 / 0.142	0.115 / 0.143
Se/SeO_2	-	-	0.0099 / 0.0139	0.0400 / 0.0562	0.0588 / 0.0827
Rb/Rb	-	-	-	0.0147 / 0.0161	0.0361 / 0.0395
Br/Br	-	0.0094 / 0.0111	0.0245 / 0.0245	0.0873 / 0.0873	0.160 / 0.160
Sr/SrO	-	-	0.0116 / 0.0137	0.0142 / 0.0168	0.0163 / 0.0193
W/WO_3	-	-	-	-	-
Re/Re_2O_7	0.0115 / 0.0149	0.0129 / 0.0168	-	-	-
Tl/Tl_2O_3	-	-	-	0.0123 / 0.0138	0.0216 / 0.0241
Pb/PbO	-	0.0298 / 0.0321	0.0985 / 0.106	0.395 / 0.426	0.714 / 0.769
	Calcined Samples				
Na/Na_2O	0.055 / 0.074	0.083 / 0.112	0.123 / 0.166	-	-
Mg/MgO	2.51 / 4.16	2.43 / 4.03	2.33 / 3.87	-	-
Al/Al_2O_3	1.03 / 1.95	1.11 / 2.10	1.19 / 2.26	-	-
Si/SiO_2	4.59 / 9.82	4.35 / 9.30	4.11 / 8.79	-	-
P/P_2O_5	0.0533 / -	0.0550 / 0.0550	0.0611 / 0.0611	-	-
Sx/SO_3	0.495 / 1.24	0.939 / 2.35	1.50 / 3.73	-	-
Cl/Cl	0.143 / 0.143	0.328 / 0.328	0.781 / 0.781	-	-
K/K_2O	0.0697 / 0.0840	0.168 / 0.203	0.482 / 0.581	-	-
Ca/CaO	5.26 / 7.36	5.96 / 8.33	6.83 / 9.55	-	-
Ti/TiO_2	0.0516 / 0.0861	0.592 / 0.0988	0.0585 / 0.0976	-	-
Cr/Cr_2O_3	0.0124 / 0.0181	0.0169 / 0.0247	0.0143 / 0.0209	-	-
Mn/MnO	0.231 / 0.298	0.251 / 0.324	0.263 / 0.340	-	-
Fe/Fe_2O_3	50.97 / 72.87	49.30 / 70.49	47.19 / 67.47	-	-
Co/Co_3O_4	0.0350 / 0.0445	0.0333 / 0.0424	0.0325 / 0.0413	-	-
Ni/NiO	0.0332 / 0.0422	0.0265 / 0.0337	0.0271/ 0.0345	-	-
Cu/CuO	-	-	0.0081 / 0.0101	-	-
Zn/ZnO	0.0138 / 0.0172	0.0202 / 0.251	0.0306 / 0.0381	-	-
Se/SeO_2	-	-	0.0085 / 0.0120	-	-
Br/Br	-	-	0.0230 / 0.0230	-	-
Sr/SrO	0.0088 / 0.0104	-	0.0100 / 0.0118	-	-
W/WO_3	0.0396 / 0.0500	0.0286 / 0.0361	0.0178 / 0.0225	-	-
Re/Re_2O_7	0.0132 / 0.0172	-	-	-	-
Pb/PbO	-	0.0236 / 0.0254	0.0874 / 0.0941	-	-

APPENDIX 9

PARTICLE SEGREGATION AND CYCLONE DESIGN

A9. 1 SEGREGATION IN THE TEST UNIT

In the mesh test unit (during test involving the injection of ESP dust) the formation of deposits was observed, particularly on flat horizontal surfaces such as the ledge of the observation window in the interior of the metallic filters' housing. These were taken as an indication of particle drag problems, and prompted an investigation of the segregation.

Particle size analyses were carried out on the dust deposited in the filters, in the filter housing, and on the ledge inside the filter casing. A dust sample was also collected after the cleaning of the filters and filter circuit.

The analysis resulted in the distributions shown in Fig. A9.1

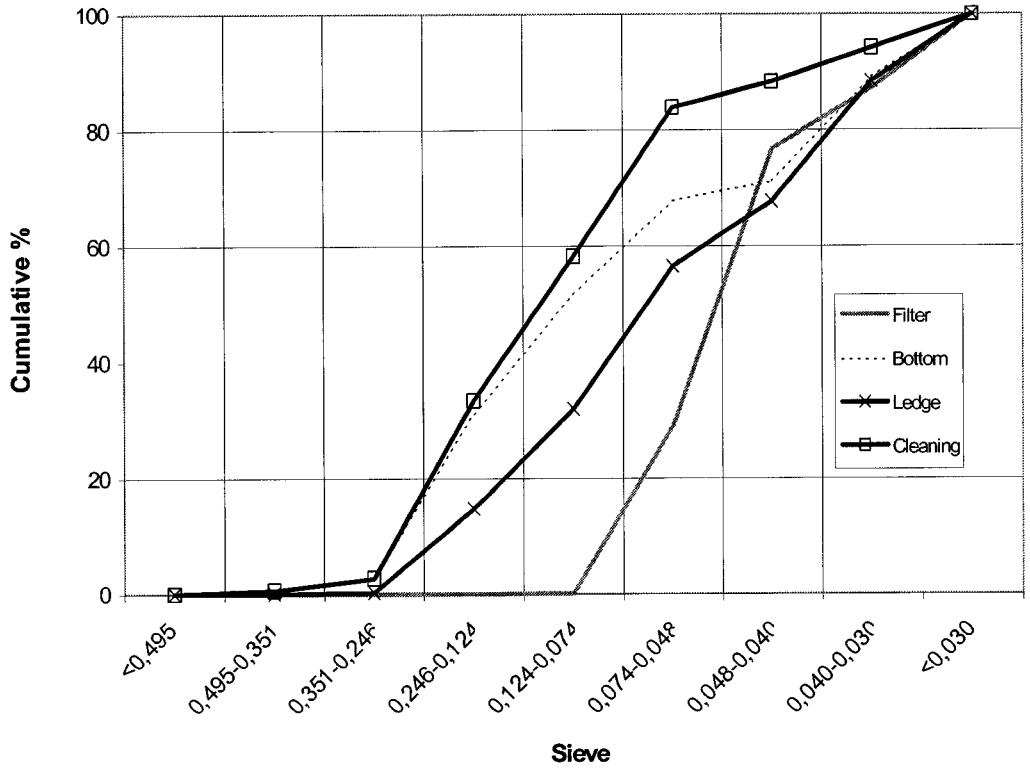

FIG. A9. 1 SIZE DISTRIBUTION OF DUST SAMPLES

As can be seen in the graph, the dust denominated "cleaning" is the coarsest, leading to the belief that this is the dust which is less subject to drag due to its size and which settles throughout the filtering circuit.

When the dust sample denominated "ledge" was collected it was observed that the dust was deposited by particle size, from smaller to greater.

These observations led to consideration of the design of a cyclone as a pre-separator of the coarse dust.

A9. 2. CYCLONE DESIGN

The following takes as an example the design of a cyclone for the mesh tests unit, but the method is applicable to industrial scale equipment.

Works cited are:

Perry J H Chemical Engineers Handbook, 4th Edition, McGraw-Hill, USA.

Lapple C E Air Pollution Eng. Manual, USA Dept. of Health, Education and Welfare. Pub 999, Ap40, 1967 USA.

Industrial ventilation. A Manual of Recommended Practice, 1980. Committee on Industrial Ventilation. American Conference of Governmental Industrial Hygienists, USA.

Current conditions of the gas input duct:.

D = 15 cm = 0.15 m.

Pipe cross sectional area: $A = \frac{\Pi D^2}{4} = \frac{\Pi 0.15^2}{4} = 0.0177 m^2$

Gas flow at 25°C: $Q_{25} = 1.8 \frac{m^3}{min} \cdot \frac{1}{60} = 0.03 \frac{m^3}{sec}$

Velocity at 25°C: $V_{25} = \frac{Q_{25}}{A} = \frac{0.03}{0.0177} \cong 1.7 m/s$

Gas flow at 300°C:

$$Q_{300} = Q_{25} \cdot \frac{273 + 300}{273 + 25} = 0.03.(573/298) = 0.058 m^3/s$$

Ducting for a cyclone.

When designing a cyclone it is necessary to take into account the limitations relating to pressure drops which may exist in the system in which the cyclone is to work. The limitations of the fan commonly lead to a maximum permissible ΔP value corresponding to a gas input velocity to the cyclone within the range 6 to 21 m/s. Consequently, cyclones are frequently designed with input velocities close to 15 m/s.

On the other hand, the "Industrial Ventilation Manual" recommends, for transportation in suction-based ventilation systems, velocities of 17.7 to 20.3 m/s for avoiding drop out of "Average Industrial Dust."

17.7 m/s is a sufficient velocity for transportation and feed to the cyclone (Vc).

The required duct area, working at 300°C is:

$$A = \frac{Q_{300}}{V_c} = \frac{0.058 m^3/s}{17.7 m/s} = 0.0328 m^2 \quad \text{and} \quad D = \sqrt{\frac{4x0.0328}{\Pi}} = 0.065 m$$

Cyclone Design.

On the basis of the calculated duct diameter a high efficiency cyclone will be designed following the standards noted in this respect by Perry J H and Lapple C E (see previous references).

The most widespread design is that corresponding to Lapple, which is shown in Fig. A9.2, in which all the characteristic dimensions of the cyclone are expressed in relation to the diameter D_c of the cylindrical body of the equipment.

The pressure drop through the cyclone can be expressed as a function of the velocity pressure (kinetic energy) of the gas upon entering the cyclone. The area of the cyclone input duct, which is of rectangular section (see figure), is:

$$A_c=B_c.H_c$$

and the gas flow velocity on entering the cyclone (input velocity) is:

$$Vc = \frac{Q}{Ac}(m/s)$$

Q = Feed Flow, m^3/s

The gas velocity pressure on entering the cyclone, expressed in mm water gauge, is obtained by applying the following expression:

$$Pc = 10^3 \frac{Vc^2}{2g} \frac{\rho}{\rho w}$$

Pc = Gas velocity pressure at input, mmH_2O.
Vc = Input velocity, m/s
g = 9.81 m/s^2
ρ = Gas density, kg/m^3
ρ_w= Water density, kg/m^3

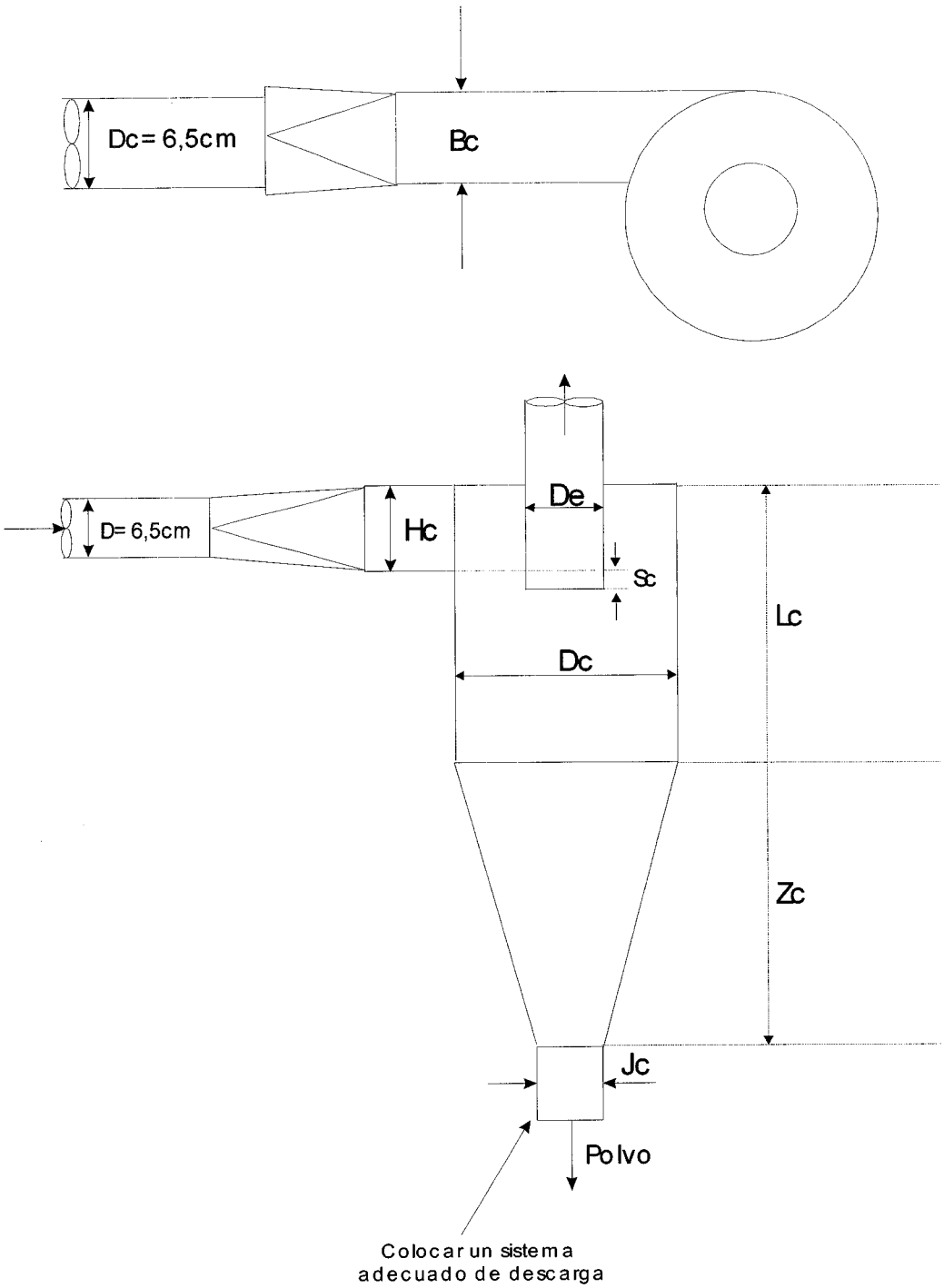

Where:
B_c= Dc/4; H_c= Dc/2; D_e=Dc/2; L_c=2Dc; Z_c=LDc; S_c=Dc/8; J_c= Dc/4 (Arbitrary value)

FIG. A9.2 **CYCLONE LAYOUT**

Taking for water at standard conditions (20°C) a density of 998 kg/m^3, the above equation gives:

$$Pc = 10^3 \frac{Vc^2}{2x9.81} x \frac{\rho}{998}$$

$$Pc = 0.051\rho\ Vc^2\ (mm\ H_2O)$$

From this value it is deduced that the pressure drop which the gas undergoes when passing through the cyclone is:

$$\Delta Pc = 0.38\rho Vc^2\ \ (mm\ H_2O)$$

Efficiency of separation.

The particle diameter for which the separation efficiency of the cyclone is 50% is known as the cut-off diameter, *dc*. This means that 50% of the particles of this size which enter with the gas are separated in the equipment. The most satisfactory empirical equation for calculating the cut-off diameter was developed by Lapple:

$$dc = \sqrt{\frac{9\mu Bc}{\Pi NcVc(\rho s - \rho)}}$$

Where

d_c= Cut-off diameter, cm.
μ = Gas viscosity, g/cm s
ρ = Gas density, g/cm^3
ρ_s= Solid density, g/cm^3
B_c= width of cyclone input, cm
N_c= number of turns made by the particle in the cyclone. Lapple recommends values for Nc= 4 to 5.

Setting B_c as a function of D_c (see figure) and operating, the above equation can be written as follows:

$$dc = 0.85\sqrt{\frac{\mu Dc}{NcVc(\rho s - \rho)}}$$

The cyclone is designed with an input velocity, V_C=18 m/s.

Input duct area (rectangular):

$$A_C = B_C H_C = Q/V_C$$

$$Q = Q_{300} = 0.058\ m^3/s$$

$$A_C = \frac{0{,}058 m^3/s}{18 m/s} = 0.00322 m^2$$

$$B_C H_C = 0.0322\ m_2$$

As $H_C = 2B_C$ (see figure), $2B_C^2 = 0.00322$; $B_C = 0.040m$;

$$H_C = 2B_C = 0.08\ m;$$

$D_C=2H_C=0.16$ m

$Lc = Zc = 2Dc = 0.32m$

$$De = \frac{Dc}{2} = \frac{0.16}{2} = 0.080m$$

$$Sc = \frac{Dc}{8} = \frac{0.16}{8} = 0.02m$$

$$Jc = \frac{Dc}{4} = \frac{0.16}{4} = 0.04m$$

Pressure drop in the cyclone:

$\Delta P_C=0.8\delta V_C^2$

$V_C=18$ m/s

ρ = Gas density at 300°C

ρ (25°C) = 1. (g/l)

$$\rho(300°C) = 1.1x\frac{273+25}{273+300} = 1.1x\frac{298}{573} = 0.572g/l$$

$$\rho(300°c) = 0.572kg/m^3$$

$$\Delta Pc = 0.38x0.572x18^2 = 70.5mmH_2O$$

Cut-off diameter:

$$dc = 0.85\sqrt{\frac{\mu Dc}{NcVc(\rho s - \rho)}}$$

μ = gas viscosity $\cong 0.00020$ (estimated on the basis of air viscosity)
$\rho s = 4.5$ g/cm^3
$\rho = 0.0572$ kg/m^3 = 0.572 g/l = 0.000572 g/cm^3
$N_C = 4$ (Lapple)
$D_C = 0.16$ m, Vc = 18 m/s = 1800 cm/s

$$dc = 0.85\sqrt{\frac{0.00020x16}{4x1800(4.5-0.000572)}} = 2.7x10^{-4}cm \cong 3\mu m$$

A9.3. TRANSPORTATION VELOCITY AS A FUNCTION OF PARTICLE SIZE AND DENSITY

To study how velocity required for the transportation of the particles varies as a function of their size and density, the following equation may be applied:

(*) $V = 15.6\rho s^{0.37} dp^{0.26}$ (homogeneous units)

In which:

V = transportation velocity, m/s

ρs = density of solid particles, g/cm^3

dp = Particle diameter, mm

This equation is derived from that published in the work "Instalaciones de ventilación localizada: velocidad mínima de transporte". R. Pocovi et al. Revista de Ingeniería Química (Madrid), No. 254, May 1990.

In this an empirical equation is found for the *minimum velocity* for dust transportation. The equation (*) is written considering a safety factor f=3.

1. <u>For solid of ρ=4</u>

1. dp = 0.20 mm

   $V = 15.6 \times 4.5^{0.37} \times 0.20^{0.26} = 15.6 \times 1.74 \times 0.66 = 17.9$ m/s

2. dp = 0.15 mm

   $V = 15.6 \times 1.74 \times 0.15^{0.26} = 16.5$ m/s

3. dp = 0.10 mm

   $V = 15.6 \times 1.74 \times 0.10^{0.26} = 14.9$ m/s

4. dp = 0.05 mm

   $V = 15.6 \times 1.74 \times 0.05^{0.26} = 12.4$ m/s

5. dp = 0.020 mm

   $V = 15.6 \times 1.74 \times 0.020^{0.26} = 9.8$ m/s

2. <u>For solid of ρ=1.2 (e.g. coal)</u>

Similarly,

for dp = 0.20 mm, V = 11.0 m/s,

for dp = 0.15 mm, V = 10.2 m/s,

for dp = 0.10 mm, V = 9.2 m/s,

for dp = 0,05 mm, V = 7.7 m/s

for dp = 0,020 mm, V = 6.0 m/s

It should be noted that the calculated velocities here are not minimum transportation velocities (at which the solid transported starts to sediment), but are transportation velocities recommendable for ventilation installations using a safety factor of 3.

From the equation (*) it would be possible to draw curves representing V=f(dp) for different densities (Fig. A9.3).

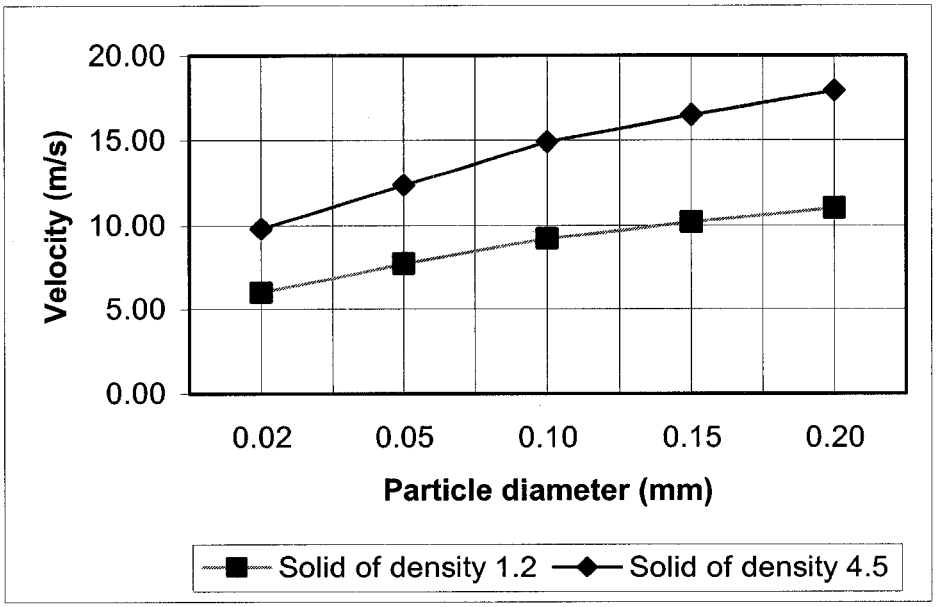

FIG. A9.3 TRANSPORTATION VELOCITY RELATED TO SIZE AND DENSITY

A9. 4 EXTRAPOLATION OF THE TRANSPORTATION VELOCITY EQUATION FOR APPLICATION AT HIGH TEMPERATURES.

The aforementioned equation for calculating the velocity required for the transportation of particles was obtained working experimentally with air at room temperature (20°C). This equation is:

$$\otimes \quad v = 15.6\ \rho s^{0.37}\ dp^{0.26} \text{ (non homogeneous units)}$$

It may be accepted that v corresponds to a certain value of the dynamic drag force exercised by the gas on the particles, which is determining for their transportation.

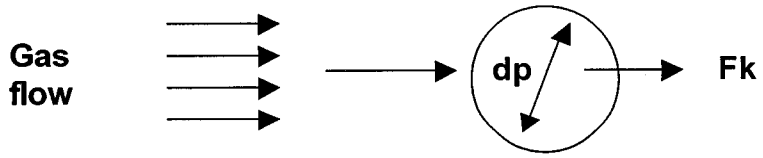

Fk = dynamic drag force (N).

Bird, Steward & Lightfoot (Transportation phenomena) define this force as

$$Fk = C_D . K . A.$$

C_D = Proportionality coefficient (dimensionless) known as the drag coefficient or friction factor.
K = kinetic energy of the unit of volume of gas, Nm/m^3.
A = impact area (situated on a plane perpendicular to the flow).

So:

$$K = \rho \frac{v^2}{Z} \left(\frac{kg}{m^3} \frac{Nm}{kg} = \frac{Nm}{m^3} \right)$$

$$A = \frac{Tdp^2}{4} (m^2)$$

$$Fk = C_D \rho \frac{v^2}{Z} \frac{\pi Tdp^2}{4} = \frac{\pi C_D \rho v^2 dp^2}{8}$$

If Fk is the value of the force required for the transportation of the particles, the transportation velocity will be:

$$v^2 = \frac{8Fk}{\pi C_D \rho dp^2}$$

$$v = 1{,}60 \sqrt{\frac{Fk}{C_D \rho dp^2}}$$

For ρ_o the gas density at room temperature, (T_o = 298 K), with corresponding value C_{Do} of the drag coefficient (which is a function of the Reynolds No.), the corresponding transportation velocity will be:

$$v_o = 1{,}60 \sqrt{\frac{Fk}{C_{Do} \rho_o dp^2}} (m/s) \quad (A9.1)$$

At the operating temperature T (e.g. T = 300 + 273 = 573 K), to maintain the same value of the force, Fk, required for transportation, the corresponding velocity (v_T) will be:

$$v_T = 1{,}60\sqrt{\frac{Fk}{C_{DT}\rho_T dp^2}}\,(m/s) \qquad (A9.2)$$

Relating (A9.1) and (A9.2) we obtain:

$$\frac{V_T}{V_o}\,1{,}60\left(\frac{C_{Do}\rho_o dp^2}{CD_T\rho_T dp^2}\right)^{1/2} = \left(\frac{C_{Do}\rho_o}{CD_T\rho_T}\right) \qquad (A9.3)$$

The density at the working temperature (T) as a function of ρ_o is:

$$\rho_T = \rho_o \frac{T_o}{T}$$

$$\frac{\rho_o}{\rho_T} = \frac{T_o}{T} \qquad (A9.4)$$

With regard to the drag coefficient C_D, this is a function of the Reynolds number, defined as:
$R = (dp.\ \rho.\ v)/\ \mu$

For instance (using homogeneous units):

dp = particle diameter, cm.
ρ = gas density, g/cm^3.
v = velocity, cm/s.
μ = viscosity, poise (g/cm s).

The values of $C_D = f(R)$ are given in "Perry, 4th De., Chemical Eng. Handbook, pp. 5-60".

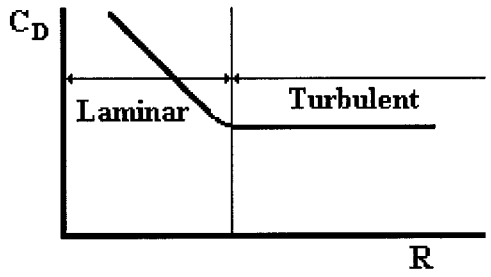

It can be seen that for alternately turbulent flow, as in the case of the problem under study, $C_D \approx$ cte., i.e. without much error it can be accepted that

$$C_{Do} = C_{DT} = \text{cte} \qquad (A9.5)$$

Replacing (A9.4) and (A9.5) in Equation (A9.3) gives

$$\frac{v_T}{v_o} = \left(\frac{T}{T_o}\right)^{1.2}$$

$$v_T = v_o \left(\frac{T}{T_o} \right)^{1/2}$$

For instance, for a particle of dp = 0.10 mm. and ρ_s = 4.5 g/cm^3,

$$v = 15.6\ \rho s^{0.37}\ dp^{0.26}$$

$$v_o = 15.6 \times 1.74 \times 0.55 = 14.9 \text{ m/s.}$$

This is the velocity obtained from Equation (A9.6) (used in the plotting of the v curves = f(dp,ρ_s).

When the gas temperature is varied to 300°C, i.e. T = 573 K, the required transportation velocity would be:

$$v_T = 14.9\ (573/293) = 14.9 \times 1.40 = 20.8 \text{ m/s.}$$

On this basis, the equation ⊗ used, obtained for room temperature, can be generalized as

$$v_T = 15{,}6\ _s^{0,37}\ dp^{0,26} \left(\frac{T}{T_o} \right)^{0,5}$$

This equation is only approximate due to the simplifying suppositions established in it:

1. Spherical particles.
2. It is assumed that C_D is constant when the temperature varies.
3. Law of perfect gases for calculating densities (of little importance).
5. Consideration not made of viscous forces acting (Stokes equation).
6. The phenomenon of transportation and sedimentation of the particles is highly complex.

APPENDIX 10

CONSIDERATION OF IMPROVEMENTS IN FILTRATION PERFORMANCE BY USE OF ELECTRICAL CHARGES – INDICATIONS FROM THE LITERATURE

In order to assess the potential for the use of deliberately induced electric charge to improve filtration efficiency, it is first necessary to understand the mechanisms of particle capture.

The effect of particle size on penetration for a simple textile filter is indicated below.

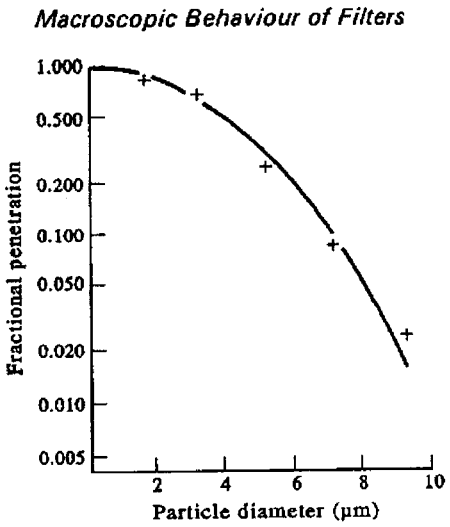

Penetration of monodisperse particles through a simple filter as a function of particle size, illustrating lower capture efficiency of small particles.

In a filter of metallic mesh, the formation of a dust layer is very important because the size of mesh is much greater than the fume particles, so penetration may be much easier. Below is a magnified illustration of a simple wire mesh matrix as used in the metallic filter.

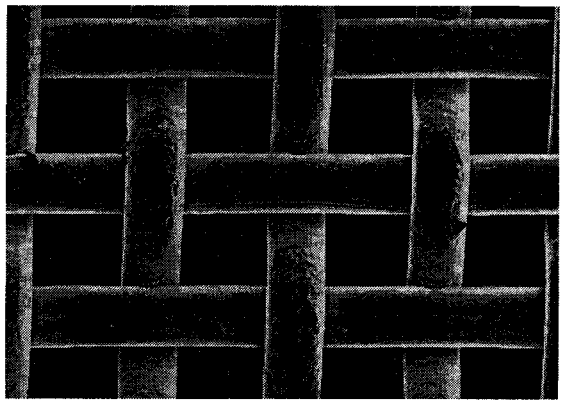

Electron micrograph of fine sieve material

In the formation of a filtration layer, it is probable that there are several steps:

1. Some particles are captured by the metallic wire.

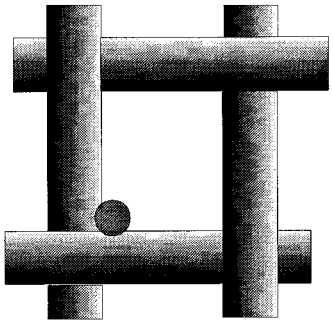

2. A permeable bridging matrix is built in form of a first membrane:

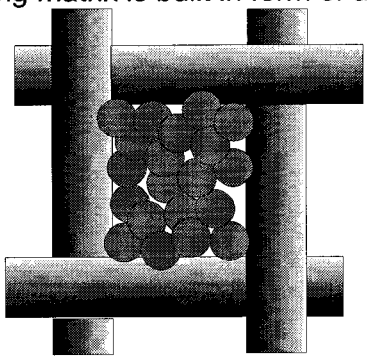

3. Further material is deposited on the bridge.

When the cake is built, a mesh of around 100 µm can filter (low penetration) particles as small as1-10 µm.

In the first and second steps, the mechanisms of capture of particles are important and also, it seems, the electrical charges on particles and fibres/wires.

The basic capture mechanisms, interception, inertial impaction and diffusional deposition, are shown schematically in the following diagram.

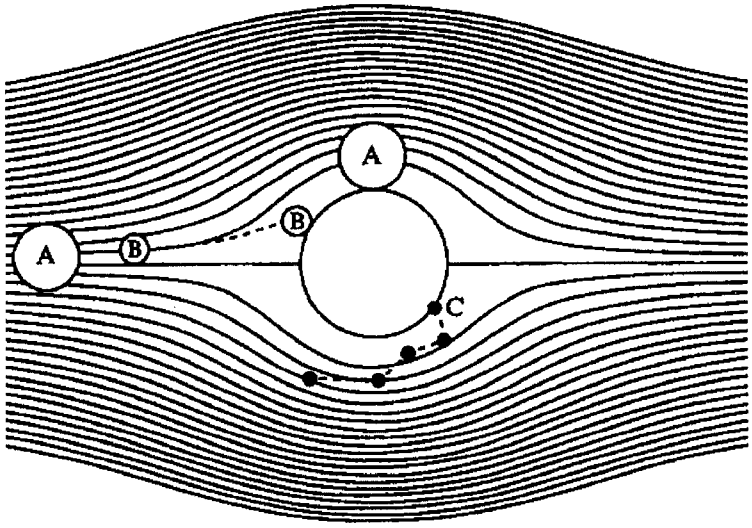

Particle capture mechanisms: A, particle capture by interception; B, particle captured by inertial impaction; C, particle captured by diffusional deposition.

These mechanisms may be enhanced by electrically charged particles and/or filter material.

Electrically charged filter material has a history of several decades; in fact the first such material was used for a period of years before its mechanism of action was understood. The advantage of materials of this type is that the charge on the fibres considerably augments the filtration efficiency without making any contribution to the airflow resistance. Several materials carrying permanent electric charge now exist, finding wide use in situations where a high efficiency is required along with a low resistance, such as in respirator filters.

It is known that the single-fibre capture efficiency, by interception, of micron-sized particles by a 20 μm diameter fibre (a typical size for animal or vegetable fibres, or for synthetic fibres that can be processed with normal textile equipment) is extremely low; and an example of this low efficiency is shown as curve 1 in the following figure. The efficiency of the same material, with a level of charge on the fibres or wires typical of electrically charged material, is considerable, as shown in curve 2.

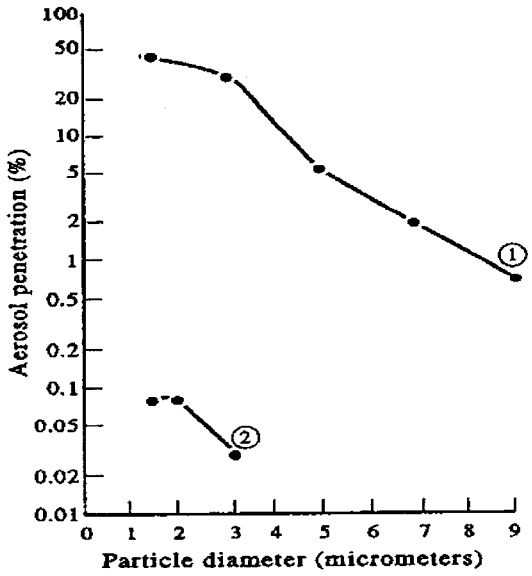

Illustration of the capture of neutral (1) and charged (2) particles by a charged filter fibre.

Electrically charged fibres attract both charged and neutral particles. The mechanism of action is illustrated in the subsequent diagram. The capture of oppositely charged particles by coulomb forces is self-evident. The capture of neutral particles comes about by the action of polarization forces. The electric field of the fibre induces a dipole in a neutral particle, or indeed a charged one, and then attracts it. The strength of the induced dipole depends upon the volume of the particle and the dielectric constant of its constituent material. The component that is nearer to the fibre experiences an attractive force slightly larger than the repulsive force acting on its counterpart, since the electric field diminishes with distance from the fibre; and this slight imbalance causes the particle to be attracted, whatever the sign of charge on the fibre. The efficiency of this mechanism, and that of the coulomb interaction, depends on the quotient of the drift velocity of the particle under the influence of the electric force tending to attract it to the fibre and the convective velocity of the flow field tending to take it past. All electrostatic filters are, therefore, more efficient at low filtration velocities.

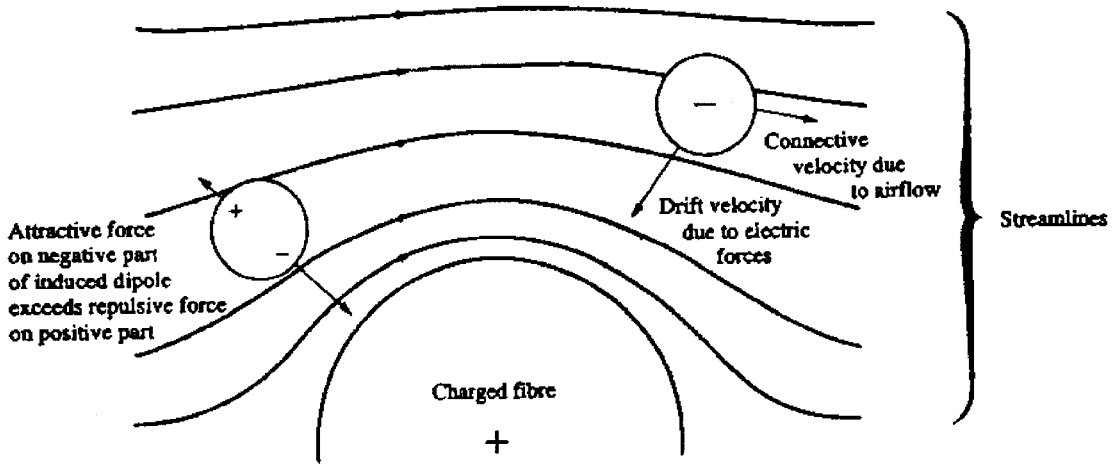

Illustration of the capture of charged and neutral particles by a charged filter fibre.

The exchange of electric charge by friction between two contacting materials is well known, if incompletely understood. On a microscopic level triboelectrification can be used to generate electric charge within a filter. Indeed, it is believed that in fabric filters, especially those employing layers of dissimilar materials, the generation of static electric charge by friction between the gas and the filtration surface contributes to the effectiveness of filtration.

The effect of the quantity of charge held by a filter on its filtration efficiency is quite clear. The greater the charge, the greater will be the electric field produced, and the greater the particle capture efficiency by electric forces.

Charge configuration is equally important, though its significance is not so obvious. If all of the fibres of a filter hold charge of the same sign, the field outside the filter might be very high, but the field between two fibres carrying charge of the same sign may be low, and at points of symmetry it will be zero. The field outside the filter will not contribute to the filtration performance, but dielectric breakdown of the air will limit this field and, therefore, the magnitude of charge in this configuration that the filter could hold. As a result, uniform charge is not of great value in filtration.

At the other extreme is charge that has very rapid spatial variation. A solution of the governing equation indicates that the range of electric field caused by a spatially varying charge is comparable with the period of variation. The extreme case is that of an ionic crystal like sodium chloride, which carries an enormous charge, but in such a way that the equal and opposite charges are separated by atomic distances. The electric field produced will extend no further. An ionic crystal gives no indication, on a macroscopic level, of being electrically charged at all.

To be effective in filtration, electric fields must extend a significant distance beyond the surface of a charged fibre, and so the electric charge must have a spatial variation not much smaller than fibre or inter-fibre dimensions.

Measurement of the configuration of charge on the fibres of a filter in situ is difficult. Furthermore, although electric charge can be eliminated when studying mechanical effects, the reverse is not possible. Experimentation appears to be necessary to determine effective electrical strategies to improve filter performance.

A further effect to be considered is dendrite formation. If a fibre taken from a heavily loaded filter is examined microscopically, branched structures made up of deposited particles are seen which, because of their tree-like appearance, are called dendrites (see photograph below). Dendrite development is best studied with reference to each particle capture mechanism in turn.

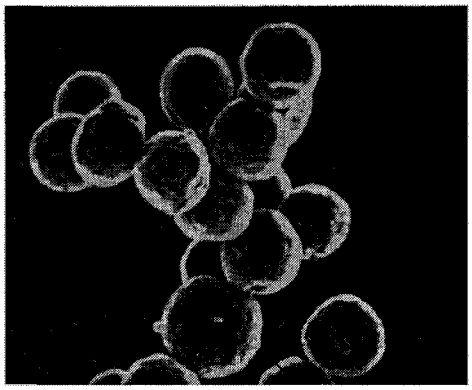

Photograph of a typical dentrite

Typical deposit shapes for each of the three principal mechanical processes are shown below. In practice capture mechanisms may act together, and the deposit itself may change the nature of the capture process.

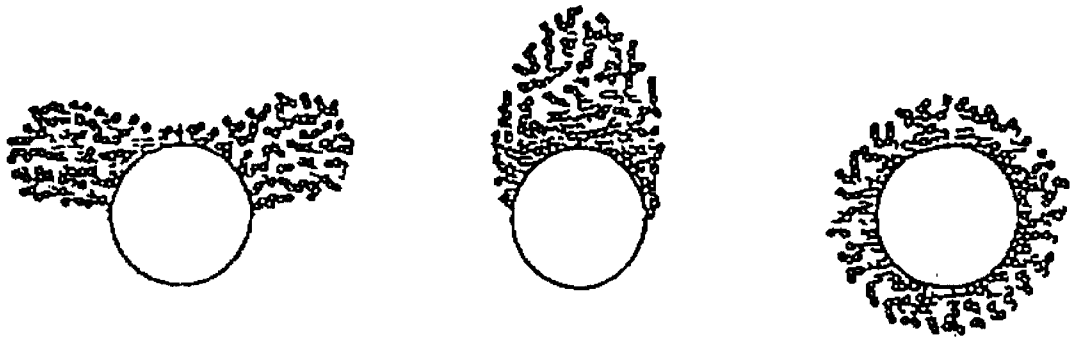

1 2 3

Shape of aerosol deposits: (1) by interception; (2) by inertial impaction; (3) by diffusion.
The simplest approximations to the fibre shape in the cases of interception and impaction deposition are ellipses, the major axis of the ellipse being perpendicular to the flow in the first case and parallel to it in the second.

In the case of dendrite formation by electric forces there is the further complication that electric forces rarely act alone. Particles may, under the influence of electric forces, be captured over the entire fibre surface, and so dendrite formation can be initiated at any point, as it can when dendrites are formed by diffusional deposition. Behaviour peculiar to electric forces is the attraction of captured particles as well as airborne particles to the surface of fibres holding a permanent electric charge, which will encourage the collapse of the dendrites and which may reduce the rate at which loading causes the filter pressure drop to increase.

Filters that have an external electric field differ from permanently charged filters in that the former will have a high (applied) field in their inter-fibre spaces. The effect of this is to cause the particles to form long dendrites with relatively few branches, extending in the direction of the field; and these have been experimentally demonstrated on isolated fibres with an electric field applied perpendicular to both the fibre axis and the flow direction. This implies that the clogging rate of filters with an external electric field should also depend on the field direction.

It can be concluded, therefore, that electric charge on the mesh, on the particles, or both, can be useful in maximising particle capture efficiency. However, the effects are complex, and the magnitude of any improvement and the means of achieving it can be precisely determined only by experiment.

APPENDIX 11

PRELIMINARY ACTIVATED CARBON INJECTION TESTS

A11.1 PROGRAMME

Duplicate tests were carried out both without and with carbon injection over a 4 day period, the first 2 days without injection and the last 2 days with injection. It was not possible to obtain samples of dust collected by the filter at this time because the pilot plant isolation valves had seized, but such samples were retrieved on the first available planned plant stoppage, 10 days after the tests. All the tests were undertaken on the same sinter bed. All samples were analysed for PCDD/Fs, PAHs and PCBs.

A11.2 FILTER OPERATION

The carbon used was a coal-based steam-activated carbon powder (85% less than 75 μm) marketed by CPL Carbons, designated Mesocarb FGT Plus. It was suggested by the supplier that high removal efficiencies for PCDD/F could be achieved with a continuous injection rate of 40 mg/Nm^3. However, according to CPL Carbons, adsorption of PCDD/Fs and heavy metals only occurs on the carbon in the cake formed on the filter medium because the process relies on the ability of the molecules to diffuse into the pore structure of the carbon. Thus contact time is important and ideal times of 0.35 - 0.5 s or longer were suggested. In this application the cake thickness is of the order of a few mm and at the filtration velocity used in these tests (approximately 2.3 m/min) the residence time in the filter cake would be only about 0.05 s. Consequently, higher injection rates were employed (see below).

A11.3 INJECTION TECHNIQUE

Ideally injection of the carbon should take place into each compartment individually, below the screens during the cake building process. This would ensure minimum consumption and effective delivery to the screens. However, the inability to access the filter for modification because of a permanently open isolation valve necessitated single point injection. A simple batch injection technique was therefore employed which utilised the suction in the inlet manifold to induce air and carbon through a tube mounted at the centre of the duct close to the inlet manifold. The method was first tested in the open air employing a compressed air feed regulated to a pressure similar to the suction in the filter inlet duct. The carbon particles appeared to form a well dispersed cloud, and it was judged that the method would be suitable for these initial experiments.

The injection position is marked on the schematic shown in Fig. 32 of the main text. Carbon was fed regularly over the initial cake building stage from a number of containers, each holding approximately 77 g of carbon, with each batch taking about 3 to 4 min to feed. Further batches were fed during the cake rebuilding part of the cycle after each compartment had cleaned although, because the carbon was injected into the inlet manifold, part of this was carried onto the on-line screens. During the two injection tests 1.53 kg and 1.68 kg of carbon were fed over periods of 225 and 248 min respectively giving an overall injection rate of approximately 400 g/h. The filter inlet flow during the tests was 0.94 m^3/s at a temperature of 130°C which is equivalent to 0.64 Nm^3/s. Thus the injection rate averaged around 180 mg/Nm^3 which is about 4 times the rate suggested by the carbon supplier.

A11.4 SAMPLING AND ANALYSIS

Emission samples were collected by the Swinden Technology Centre (STC) Trace Organics Sampling team according to a NAMAS-accredited Operating Procedure. Dust samples were also taken from the collection bins of the filter (see Fig. 32 of the main text). One sample was taken from low down in bin B (sample 1) which was considered to be representative of the fume collected before the carbon injection tests, whilst a second sample, which was expected to be representative of particulates collected during the carbon injection tests, was collected from the top of bin C (sample 2). A further sample (sample 3) was obtained by collecting equal quantities of the dust from the filter screens in compartments B and C.

The samples were analysed for dioxin compounds (polychlorinated dibenzo-p-dioxin [PCDD] and polychlorinated dibenzofuran [PCDF]) in the Trace Organics Analysis Laboratory at STC according to a NAMAS accredited Operating Procedure. The emission samples were also analysed for the sixteen US EPA targeted polycyclic aromatic hydrocarbon (PAH) compounds at STC, and for polychlorinated byphenyl (PCB) compounds by an external NAMAS-accredited contract laboratory (Scientific Analysis Laboratories, Manchester). The dust samples (Samples 1,2 and 3) were also analysed for carbon to give an indication of the degree of drop out of the injected material.

A11.5 RESULTS

A11.5.1 Carbon Content

Samples 1 and 2 (from the bins) contained 3.5 and 3.0% carbon respectively. These levels are similar to those encountered in previous samples of dust from the bins, collected in January 1999 as part of other work not involving injection. Sample 3 (from the screens) contained 13.3% carbon, indicating that a substantial proportion of the injected material reported to the filter cake.

A11.5.2 Results for PCDD/Fs

The PCDD/F outlet emission concentrations obtained with and without carbon injection are shown in Table A11.1 and the concentrations found in the three dust samples are summarised in Table A11.2. It can be seen from Table A11.1 that the concentrations of the 17 targeted PCDD/Fs were reduced from around 0.65 ng I-TEQ/Nm^3 to 0.35 and 0.21 ng I-TEQ/Nm^3 when carbon was injected, a reduction of almost 50% in one case and 68% in the other. The PCDD/F emission concentration of 0.65 ng I-TEQ/Nm^3 recorded at the filter outlet without carbon injection was significantly lower than those typically recorded in the sinter plant stack (0.85-1.5 ng I-TEQ/Nm^3) owing to air inleakage via the diverter valves (a normal feature of operation, as described in previous Technical Reports). Correction for this inleakage gives a mean filter outlet concentration of 0.95 ng I-TEQ/Nm^3 without carbon injection, which is within the normal range for Scunthorpe Sinter Plant. The concentrations of the total tetra- to octa- PCDD/Fs (i.e. both targeted and non-targeted PCDD/Fs) were also reduced by 60 to 74% as may be seen from Table A11.1.

The congener profiles of the emission samples collected during normal operation were typical of those found on sinter stack samples and were dominated by 2,3,4,7,8-PentaCDF which accounted for more than 55% of the overall TEQ. The profiles of samples obtained with and without carbon injection differed significantly in that the concentrations of lower chlorinated PCDD/F homologues (tetra- to hexa- chlorinated PCDD/Fs) were generally

reduced to a greater extent by carbon injection than were the higher chlorinated (hepta- and octa-chlorinated PCDD/Fs) homologues. For example, the concentration of 2,3,7,8-TCDF was reduced from 0.4 to 0.13 ng/Nm^3, a factor of 3, whereas 1,2,3,4,6,7,8-HeptaCDF was reduced from 0.4 to 0.29 ng/Nm^3, a factor of 1.4 and the concentration of OCDF remained the same at 0.9 ng/Nm^3. A similar pattern was observed with the non-targeted PCDD/Fs. The preferential adsorption of lower chlorinated PCDD/Fs is advantageous since these compounds have the highest TEFs and hence make more significant contributions to the overall TEQ of the emission.

The PCDD/F concentrations for the dust (Table A11.2) collected from the filter bins were 69 and 254 ng I-TEQ/kg when the filter was operated without and with carbon injection respectively. In contrast to the emission samples, however, the congener profiles of the dust samples collected with and without carbon injection did not show any marked differences. The concentration on the dust obtained from the filter screens was much higher at around 2730 ng I-TEQ/kg, which is consistent with capture of PCDD/F by the carbon. The PCDD/F concentration of dust collected under normal operation was lower than expected since the concentrations of PCDD/Fs in dust collected in the electrostatic precipitator (ESP) dust at Scunthorpe Sinter Plant are typically in the range 200 to 250 ng I-TEQ/kg. However, PCDD/F concentrations in ESP dust as low as 69 ng I-TEQ/Nm^3 would not be considered outside the normal range for UK sinter plants.

A11.5.3 Results for PAHs

The results for PAHs in the clean gas leaving the filter are summarised in Table A11.3. Under normal operation the concentrations were 73.5 and 85.7 µg/Nm^3, and with carbon injection levels of 25.5 and 26.7 µg/Nm^3 were recorded., where the PAH concentration is expressed as the sum of the 16 US EPA targeted PAHs. A reduction by about two thirds was therefore achieved. The PAH concentration profiles with and without carbon injection are presented in Fig. A11.1. It may be seen that the main PAHs present in the emission were naphthalene and phenanthrene which accounted for approximately 44 and 23% respectively of the total PAH concentration. As may also be seen from Fig. A11.1 the emission concentrations of all 16 targeted PAHs were reduced in roughly the same proportion by injection of carbon.

A11.5.4 Results for PCBs

PCBs were determined in two emission samples, one collected under normal operation and one during carbon injection. The total PCB concentrations were 1342 and 756 ng/Nm^3 for normal operation and with carbon injection, respectively, where the PCB concentration is expressed as the sum of the tri- to hepta-chloro-substituted biphenyls. The results demonstrated the ability of the activated carbon to adsorb PCBs and thereby reduce PCB emissions to atmosphere. Profiles of the targeted PCBs and the sums of the congener groups are presented in Table A11.4. The PCB profile is dominated by the tri- and tetra-chlorinated homologues and almost all the PCB concentrations, with exception of PCB BZ#28 (2,4,4',-trichlorobiphenyl), were reduced when carbon injection was applied.

TABLE A11.1
PILOT FILTER OUTLET PCDD/F RESULTS

Carbon Injection	Measured PCDD/F Concentration (ng I-TEQ/Nm^3)	Measured Total Tetra- to Octa- PCDD/F Concentration (ng/Nm^3)	PCDD/F Concentration (Corrected for Inleakage) (ng I-TEQ/Nm^3)
No	0.66	28.05	0.96
No	0.65	27.34	0.94
Yes	0.34	11.21	0.49
Yes	0.21	7.3	0.3

TABLE A11.2
PILOT FILTER COLLECTED DUST – PCDD/F RESULTS

Sample	PCDD/F Concentration (ng I-TEQ.kg)
1 (Bin - nominally before injection)	68.7
2 (Bin - nominally after injection)	254
3 (Screens - after injection)	2731

TABLE A11.3
SUMMARY OF OUTLET PAH RESULTS

Carbon injection	PAH (US EPA 16) (µg/Nm^3)
No	73.5
No	85.7
Yes	26.7
Yes	25.5

TABLE A11.4
FILTER OUTLET PCBs

Compound	Normal Operation (ng/Nm^3)	Carbon Injection (ng/Nm^3)
Targeted isomers:		
Trichloro, BZ #28	159.41	267
Tetrachloro, BZ #52	13.79	14.18
Pentachloro, BZ #101	10.34	6.68
Pentachloro, BZ #118	2.76	2.88
Hexachloro, BZ #153	2.2	1.75
Hexachloro, BZ #138	1.46	0.83
Heptachloro, BZ #180	0.37	0.04
Total non-targeted isomers		
Trichloro	1,034.04	358.78
Tetrachloro	90.48	79.27
Pentachloro	22.83	16.27
Hexachloro	3.83	6.68
Heptachloro	0.34	1.34
Total PCBs	**1,342**	**756**

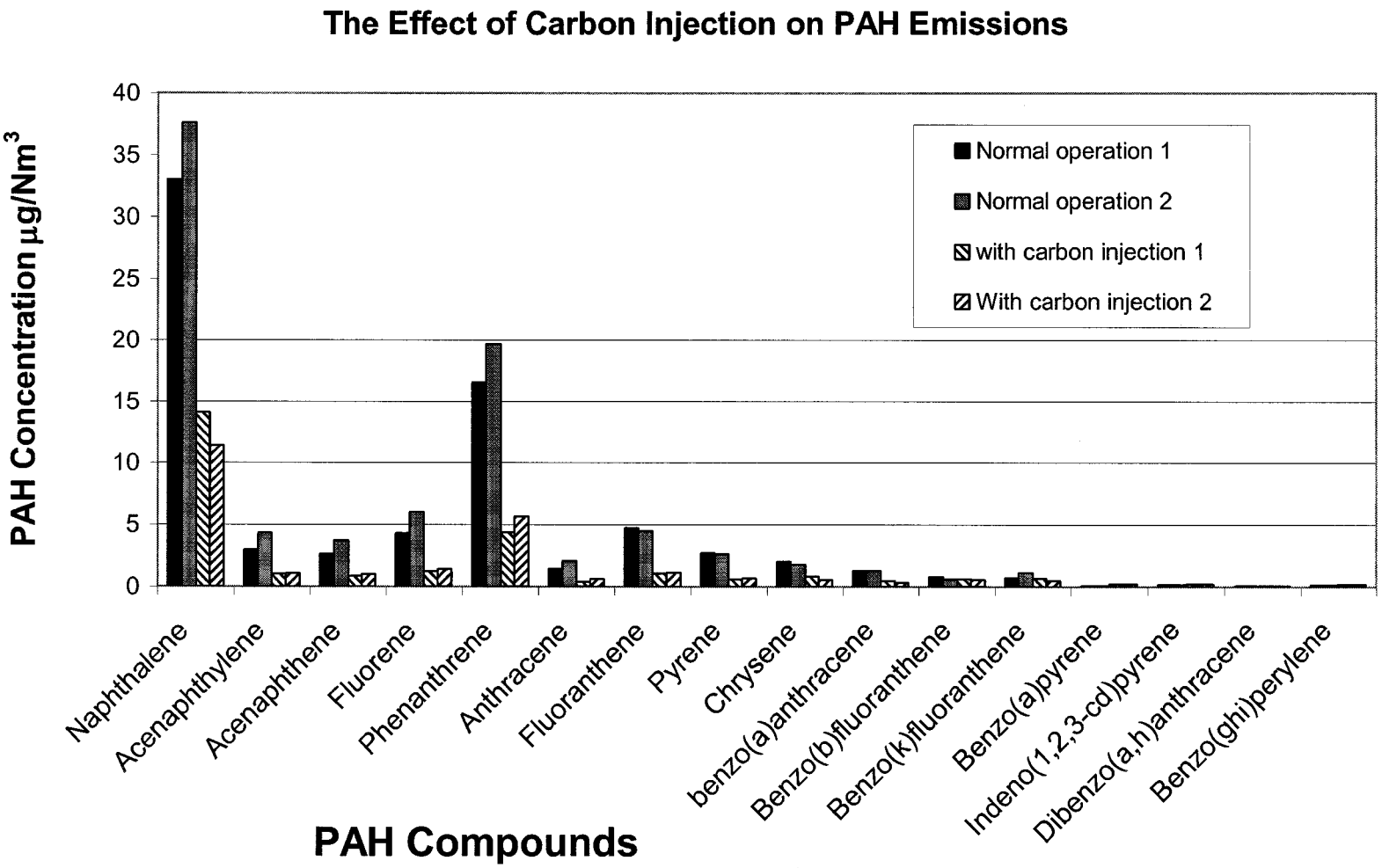

FIG. A11.1 FILTER OUTLET PAH RESULTS (D0231J26)

APPENDIX 12

LIGNITE COKE AND ACTIVATED CARBON INJECTION TESTS

A12.1 EXPERIMENTAL ARRANGEMENTS

The sampling positions were similar to those used for the previous activated carbon injection tests, as were the sampling methods and analytical arrangements, except that in this case PCBs were not studied.

The materials used were steam-activated carbon retained from the previous trial (Appendix 11) and two grades of pulverised lignite coke obtained from Rheinbraun Brennstoff GmbH. These were the 'normal' grade of 63 µm median grain size, and a 'reactivity enhanced' grade of 28 µm median grain size. The bulk densities of the 3 materials (measured at only a ¼ litre scale) were 0.45 g/ml for the reactivity enhanced lignite coke, and 0.52 g/ml for the normal lignite coke and the activated carbon.

In order to ensure consistent and reproducible feed rates, a small screw feeder with an inverter drive controller was employed. Bench calibration tests with the 3 materials showed that reasonably consistent feed rates for given screw rotation rates could be achieved. As mentioned in Appendix 11, the optimum means of injection may well be to inject directly into each compartment during the recirculation/cake building phase, but this would have required 4 injectors or considerable pipework. Single point injection was therefore employed again. To this end a valved injection pipe was manufactured and fitted to the filter inlet manifold. The injection nozzle was made to face the incoming gas flow for best distribution of the powder. The normal suction of the wind main was used to draw the carbonaceous material (fed from the screw feeder) through the injection pipe.

Following commissioning of the system, tests took place over 2 weeks' operation. These comprised base cases (with no injection) at the beginning and end of the tests, and feeding tests at 2, 6 and 10 g/min, approximately equivalent to 50, 150 and 250 mg carbon powder per m^3 stp gas. For the reactivity enhanced lignite coke test at 10 g/min the coke powder was mixed with 25% of alumina powder to improve its feeding characteristics. The activated carbon was not tested at the highest rate because of time constraints.

PCDD/F samples of 80 to 120 min duration were taken from the filter outlet during each test, and an additional sample from the inlet was taken on one day. Because the filter isolation valves had been replaced, allowing complete isolation of the filter from the wind main, it was possible in these tests to take dust samples from the collection bins and screens of each compartment after each test. The screens were pulse cleaned and the collection bins emptied after every test in an attempt to ensure that the next day's test would begin with a clean filter. The dust samples from the filter screens were analysed for carbon to check that the distribution of the injected material was nominally uniform. Filter outlet dust loadings were also taken on most test days.

In all these tests the air inleakage to the filter, at 15%, was considerably less than encountered previously, probably because of some accreted dust around the diverter valve blades reducing the air curtain flow.

A12.2 RESULTS

A12.2.1 Emission Samples

The results from the emission samples, both as measured and adjusted for the 15% inleakage, are summarised in Table 15 of the main text. Figs. A12.1 shows the PCDD/F and PAH concentrations, uncorrected for inleakage, and Fig. A12.2 shows carbon on the screens and the gravimetrically determined dust loadings (averaged where more than one sample was taken), again uncorrected for inleakage. These outlet loadings were derived from 10 min samples generally taken before and after the much longer trace organic samples, and are therefore only snapshots rather than true averages over the test periods.

A12.2.1.1 Outlet Dust Loadings

The outlet dust loadings (Table 15 and Fig. A12.2) indicate that during injection an increase of approximately a factor of 2 occurs. Previous experience had shown normal levels of around 5 - 6 mg/m^3 stp (confirmed in these tests), and the mean of the measurements during injection was 12.3 mg/m^3 stp (uncorrected for inleakage). This is probably because the carbon particles from the small end of the size range can penetrate the cake on the mesh more easily than other particles (see Section A12.2.1.2 below). If carbon injection were to be the practice on a full scale unit it might be necessary to design for a lower filtration velocity. However, a level of 12 mg/Nm^3 still represents good filtration performance compared with ESPs.

A12.2.1.2 Organic Species

It can be seen from Table 15 and Fig. A12.1 that PCDD/F levels in the range 0.12 to 0.34 ng I-TEQ/m^3 stp (0.14 to 0.39 when corrected for inleakage) were achieved during injection of the 3 materials, which represents a major reduction when compared with the normal stack emission of around 1 ng I-TEQ/m^3 stp at this plant. However, there is no consistent pattern of reduction with increasing injection rate of any of the materials. Moreover, the base case levels are also low (~ 0.2 ng I-TEQ/m^3 stp) which was not the case in the previous activated carbon tests. The inlet test, which gave 0.65 ng I-TEQ/m^3 stp, is more closely aligned with previous base case results. Examination of the data for carbon in the dust from the filter screens (Table 15 and Fig. A12.2) offers an explanation, at least in part. The level of carbon is always substantial (even in the first base case test which had been preceded by two days testing the carbon injection equipment), and does not vary systematically with injection rate. It is likely that the normal pulse cleaning of the screens removed only a part of the dust and carbon powder, so that each test had a proportion of powder on the screens from one or more previous tests.

Evaluation is further complicated because the outlet dust loadings are higher during carbon injection, although with the small amount of data available no relationship between injection rate or carbon type and the short term gravimetric dust loading could be established. However, examination of the continuous dust monitor traces over each emission sample period revealed an apparent correlation between the average outlet dust loading over each period and the emission levels of PCDD/Fs as can be seen in Fig. A12.3. These traces also indicated that the general level of particulate emission was higher during injection of the smaller particle size lignite coke compared with the other materials.

These results provide a further explanation as to why little difference was found between the efficiency of removal of trace organics and the feed rate or type of carbon injected. It is

clear that if a small increase in particulate emission takes place during carbon injection and a large part of the increase is carbon, which has already captured some trace organics, then the trace organic emission levels will be increased. It can be calculated that for the difference between the highest and lowest outlet PCCDD/F results to be solely explained by the increase in outlet dust loading, the PCDD/F level on the dust would have to be of the order of 17000 ng I-TEQ/kg. Typically the levels on the screen dust were 2000 ng I-TEQ/kg, and this dust contains about 20% carbon. If almost all the PCDD/F is associated with the carbon, and if all the increased outlet dust were carbon, this would account for about 60% of the difference between the highest and lowest results. This is a large proportion, and would make evaluation of the results difficult in terms of establishing the effects of feed rate and material.

The PCDD/F results therefore can be taken to indicate only that emission levels of around 0.1 - 0.2 ng I-TEQ/m^3 stp can be achieved with injection of the normal lignite coke and steam activated carbon, and that possibly the normal grade is more effective than the finer reactivity enhanced grade because more of the smaller particle size carbon passes through the filter.

The results for PAHs (Table 15 and Fig. A12.1) appear more logical, generally exhibiting a progressive reduction with increasing injection rate. Typically, 20 - 40 µg/m^3 stp (where the PAH concentration is expressed as the sum of the 16 US EPA targeted PAHs) was achieved at the filter outlet, compared with > 100 µg/m^3 stp at the inlet. This progressive reduction with dose rate might be a consequence of adsorption during the time-of-flight of the carbon particles, rather than in the filter cake. Again the normal grade of lignite coke appears to be the most effective material for PAH removal. When correction is made for inleakage across the filter these values increase slightly and are generally in the range 20-50 µg/m^3 stp and are similar to those from the initial SAC injection tests where outlet emissions, after correction for inleakage, were around 35 µg/m^3 stp. Naphthalene and phenanthrene were the main species present at both inlet and outlet, as in the previous tests.

A12.2.1.3 Gaseous Pollutants

Whilst passing the wind main gas through a filter cake (whether carbonaceous sorbents are present or not) would be expected to have little or no effect on CO, SO_2 and NO_x, it was thought prudent to make some check measurements. Therefore, during these injection tests numerous spot measurements of these gases were taken using an analyser employing electrolytic detectors.

The aims were:

(a) to establish whether there was any major difference in levels at the filter outlet compared with the normal values encountered in the main stack, and

(b) to assess any effect of the carbonaceous additives.

The levels at inlet and outlet (the latter adjusted for the small inleakage into the filter) were very similar, with and without injection, and the values obtained were within the typical range for Scunthorpe sinter plant when compared with historical data taken for regulatory purposes.

Typical concentrations were:

CO	0.5 - 0.7 %
SO_2	100 ppm
NO_2	1 - 2 ppm
NO	160 ppm

A12.2.2 Screen Dust And Collection Bin Samples

The PCDD/F concentrations in the samples from the screens and bins are shown in the following table.

Test	Screen Dust		Bin Dust	
	PCDD/Fs (ng I-TEQ/kg)	PAHs Total 16PAHs (µg/kg)	PCDD/Fs (ng I-TEQ/kg)	PAHs Total 16PAHs (µg/kg)
Base Case	1,785	33,045	4.1	250
63 µm LC 6 g/m	1,836	84,527	62.8	2,232
28 µm LC 6 g/m	1,604	156,533	111	9,388
SAC 6 g/m	2,347	182,977	161	12,889

The PCDD/F concentrations for the bin dust collected after the base case test were very low at 4.1 ng I-TEQ/kg. This was much lower than expected since the concentrations of PCDD/Fs in dust collected in the electrostatic precipitator (ESP) dust at Scunthorpe Sinter Plant are typically in the range 200 to 250 ng I-TEQ/kg. This is further confirmed by the results for the bin dusts obtained after carbon injection which show a range of 60 to 160 ng I-TEQ/kg again lower than expected and less than the value obtained in the first injection tests (254 ng I-TEQ/kg). The possibility therefore cannot be discounted that some PCDD/F formation takes place in the dust collected on ESP plates brought about by energy released in corona discharges within the ESP. Work carried out by De Pauw of the University of Liege has suggested that significant PCDD/F formation can take place in this manner.

The PCDD/F levels on the screen dust were in the range 1600 to 2350 ng I-TEQ/kg, indicating good adsorption of these compounds. The base case value of 1785 ng I-TEQ/kg was much higher than expected, probably owing to some retention of carbon on the screens from earlier tests designed to investigate the distribution of injected material throughout the four compartments. The lowest result (1604 ng I-TEQ/kg) was for the lignite coke with the smallest mean particle size and is consistent with the higher background emission levels indicated by the continuous outlet dust monitor. The highest result was from the SAC test where a value of 2347 ng I-TEQ/kg was recorded which is similar to the level of 2731 ng I-TEQ/kg found in the earlier tests.

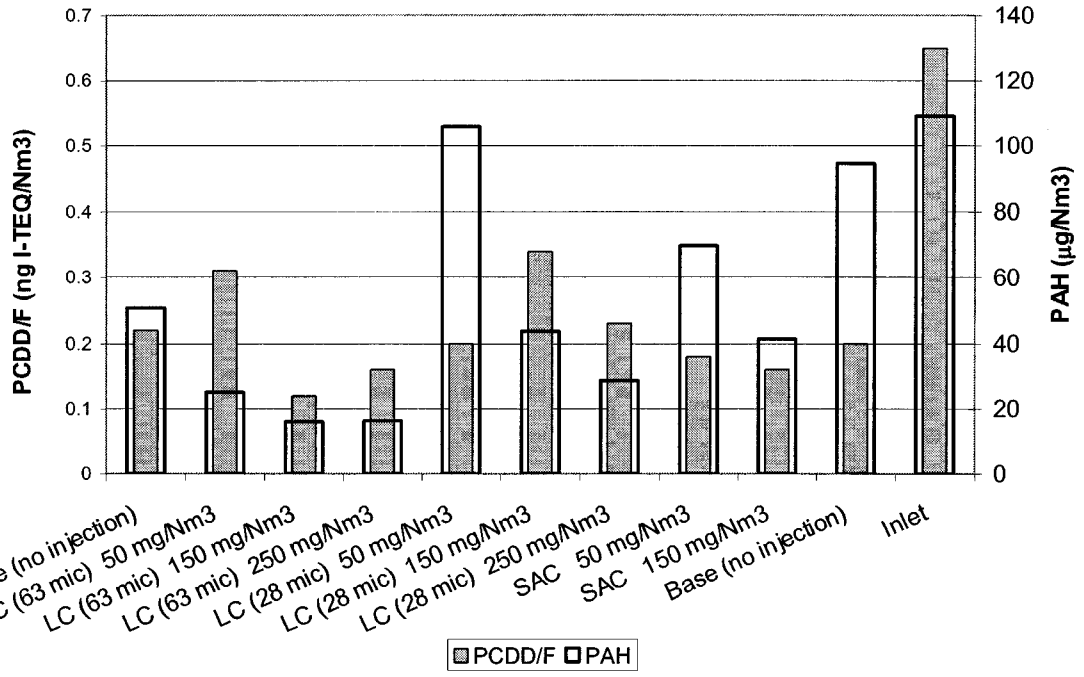

FIG. A12.1 **PCDD/F AND PAH OUTLET CONCENTRATIONS** **(D0231J28)**

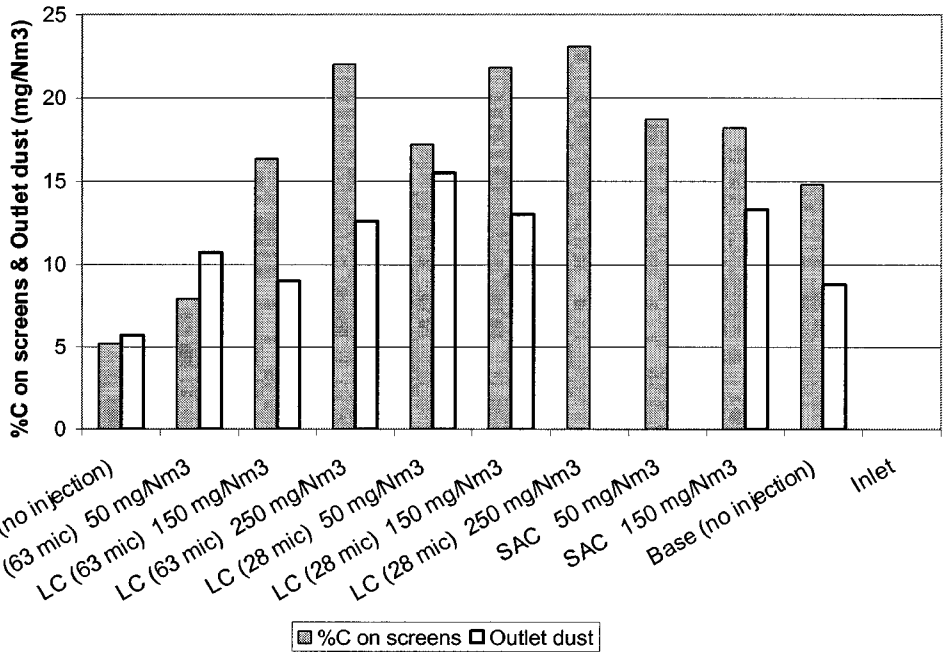

FIG. A12.2 **CARBON ON SCREENS AND OUTLET DUST CONCENTRATIONS** **(D0231J28)**

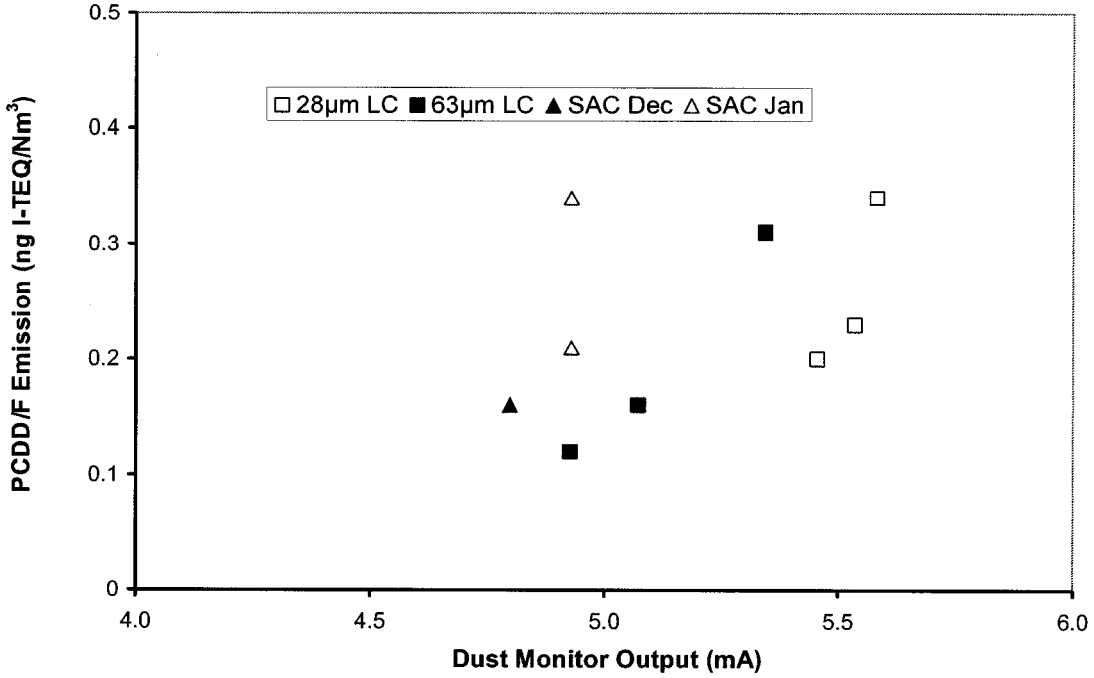

FIG. A12.3 **RELATIONSHIP BETWEEN PCDD/F EMISSIONS AND AVERAGE DUST MONITOR OUTPUT** **(D0231J28)**

European Commission

EUR 21146 — Reduction of iron ores
Reductions in dust and gaseous emissions from sinter strands

A. M. W. Briggs, F. Garcia Carcedo, J. Vega Sedeño, M. A. Estrela

Luxembourg: Office for Official Publications of the European Communities

2004 — 166 pp. — 21 x 29.7 cm

Technical steel research series

ISBN 92-894-8110-2

Price (excluding VAT) in Luxembourg: EUR 25